UNIVERSITÀ
DEGLI STUDI
DI PADOVA

Università degli Studi di Padova

Dipartimento dei Beni Culturali: Archeologia,
Storia dell'Arte, del Cinema e della Musica

Master Degree in
ARCHAEOLOGICAL SCIENCES

Curriculum in
APPLIED SCIENCES TO CULTURAL HERITAGE MATERIALS AND SITES

The Egyptian blue pigment: identification, manufacturing techniques, provenance

Supervisor:

Prof. Gilberto Artioli

Co-supervisor:

Prof. Ivana Angelini

Master Candidate:

Martina Pellegrina

2079345

ACADEMIC YEAR 2023/2024

To whom I love

Blue colour is everlastingly appointed by the deity to be a source of delight. (John Ruskin)
Blue. The only colour we can feel. (Charles Wayland Towne)
Blue is the colour of infinity, the gateway to the sacred. (Yves Klein)

List of Contents

Acknowledgments

First of all, I wanna start mentioning of course my supervisor Prof. Gilberto Artioli and my co-supervisor Prof. Ivana Angelini who gave me not only the possibility to deal with a so multidipliscinary and fascinating topic but also teaching me how to address the argument and followed me step by step during the research thesis.

I am deeply grateful to the scientists Dr. Giovanni Verri of the Art Institute of Chicago, Dr. Giancarlo Sidoti of the ISCR, Dr. Claudio Seccaroni of ENEA, and the conservation scientists Dr. Jørgen Wadum of WATS and Troels Filtenborg of SMK in Copenhagen who understood the importance of this research and placed their trust in me by sending me these precious and unique samples of Egyptian blue without which I would not have been able to write this thesis. Furthermore I want to extend my thanks to Professor Maximilian Martens of Gent university for his helpfulness, kindness and for acting as a go-between for the delivery of the Danish sample.

Thanks also to Koen Janssens for allowing me to use the Raman spectroscopy laboratories at the University of Antwerp and to Dr Gert Nuyts for conducting the Raman analysis on one of the samples.

A cordial thank you to the kind, available and helpful technicians of Geoscience department, Leonardo Tauro who prepared the thick sections of my samples and Caterina Canovaro who not only polished samples for me but taught me also how to use the polarizing microscope and gave precious advises for the thesis.

How can I not mention the PhD student Mauro Veronese who not only spent whole days at the Raman spectrometer with me meticulously investigating the samples, but who also provided valuable advice on both the interpretation of the spectra, literature research and strategies to be undertaken.

Moreover indispensable and invaluable was the help of Raman spectroscope technicians Lisa Santello and SEM technician Federico Zorzi, who patiently followed me in extrapolating and processing the data, working multiple hours with and for me.

A kind acknowledgment goes also to Maria Chiara Dalconi, Gregorio Dal Sasso and Lara Maritan who gave me not only help during the process of using confocal microscope and elaborating data of Raman and SEM but also moral support and company.

I cannot but be grateful to the patient Professor Zoleo for conducting the FTIR analysis on one of the Egyptian blue samples and to Dr Rodler for providing SEM data of other samples for comparison with those analysed in this thesis.

Special thanks also to Gabriele Baldassini who kindly provided me with his master's thesis regarding the Renaissance painter Ortolano.

I am especially grateful for the motivational and emotional support given to me by my brother Marco, my mom and Silvia since without them I would have been lost. Many thanks also to the long-time friends Gabriele, Monica and Giovanni that have always been present during these years of study but also leisure.

A special thought to my master's classmates who coming from all over the world have given a breath of fresh air thanks to their heterogeneous experiences, languages and cultures spurring and giving courage to have new experiences as well as enriching with strength in facing life's challenges.

Last but not least, I also thank myself for never giving up in these long years of university and persevering in achieving this important goal. Thinking back to where and how I started before embarking on my college career, I can say that I have come at least a little closer to my childhood dream of becoming a scientific researcher.

To conclude: everything seems impossible until it is done!

Abstract

Until a few years ago it was believed that the use of the first synthetic pigment in the art history, the Egyptian blue, was limited to antiquity.

Recently its presence was identified in Renaissance artworks, opening new questions about its knowledge and spread.

The aim of this thesis is to understand if the pigment used in Modern Age was re-synthetized or recycled from ancient deposits or works of art.

One fragment from a painting of Ortolano and one from a fresco of Raphael were investigated through spectroscopical (RAMAN) and elemental techniques (SEM) identifying the presence of Egyptian blue.

The investigation of the trace elements correlated with Egyptian blue in the two samples compared with the ancient ones present in literature and the attempt of lead isotopes analysis (LIA) permitted to understand the origin of the pigment solving the long-standing question.

Fino a pochi anni fa si riteneva che l'uso del primo pigmento sintetico nella storia dell'arte, il blu egiziano, fosse limitato all'antichità.

Recentemente la sua presenza è stata individuata in opere d'arte rinascimentali, aprendo nuovi interrogativi sulla sua conoscenza e diffusione.

L'obiettivo di questa tesi è capire se il pigmento utilizzato in età moderna sia stato risintetizzato o riciclato da depositi o opere d'arte antiche.

Un frammento da un dipinto dell'Ortolano e uno da un affresco di Raffaello sono stati indagati attraverso tecniche spettroscopiche (RAMAN) ed elementari (SEM) identificando la presenza del blu egiziano.

L'indagine degli elementi in traccia correlati al blu egiziano nei due campioni confrontati con quelli antichi presenti in letteratura e il tentativo di analisi degli isotopi del piombo (LIA) hanno permesso di comprendere l'origine del pigmento risolvendo l'annosa questione.

Introduction

Colours have always played an important role in human history, having a fascinating aesthetical power and already prehistoric people employed ochres and earths, directly ready-to-use and readily available, for their drawings. Blue among all the other colours represented in all cultures and all times a special and different position (BERKE 2007). The colour blue for the ancient Egyptians assumed a divine, funerary and afterlife meaning, it was the colour of the world of the gods, the sky and the universe (RAGAI 1986; BELLINI 2023).

The well-known painted prehistoric caves of Altamira in Spain and Lascaux in France show the absence of blue colours which were not among the ready available earth colours from the soil (Berke 2007). It is assumed that the limited availability of the precious of lapislazuli present just in Afghanistan or scarce stability of other natural blue pigments such as azurite prompted the creation of artificial blue pigments in different populations all over the world which main ones are listed in Table 1 (BERKE ET AL. 2010).

Name	Composition	Material Type	Time of Appearance
Egyptian blue	$CaCuSi_4O_{10}$	Alkaline-earth copper silicate	3600 BC
Smalt (cobalt blue)	$CoO(SiO_2)_n$	Cobalt oxide in a glass matrix	1000 BC
Chinese (Han) blue	$BaCuSi_4O_{10}$	Alkaline-earth copper silicate	800 BC
Chinese (Han) purple	$BaCuSi_2O_6$	Alkaline-earth copper silicate	800 BC
Artificial ultramarine	$Na_{0.9}[Al_{5.6}Si_{6.4}O_{24}]S_{2.0}$	Sodalite cages filled with S_n^-	800 BC
Maya blue	$(C_{16}H_{10}N_2O_2)_y \cdot [(Mg,Al)_4Si_8(O,OH,H_2O)_{24}]_m \cdot x\ H_2O$	Indigo as a host molecule in white clay	400 BC

Table 1 - List of main synthetic blue and purple pigments produced in antiquity. (Modified after BERKE ET AL. 2010)

The use of colour blue could be considered recent compared to the history of human kind. Although blue along with green is among the most prevalent colours in nature it is absent in the first drawings of the Palaeolithic where black from charcoal or manganese oxide, red and yellow from ochres and white from bones and calcite.

One of the most plausible explanations given by scholars regarding the infrequent use of blue as an art material is of a practical order that is the scarcity of mineral or plant sources that could have been used to produce the blue pigment or dye.

Another, much more fascinating reason, however, concerns the nature of the colour blue itself i.e., how blue was viewed and considered by ancient peoples.

For many millennia blue as concepts seems to be disregarded and in several languages the term blue just does not exist as if initially human beings did not consider it and even used other colours to describe it and even that they did not distinguish the colour because doing so was not essential for survival.

A less credited hypothesis sees blue as a funerary or death-related symbol and therefore not used even when available.

What is certain is that blue fascinated the ancient Egyptians who synthesized it, perhaps by accident, creating the first synthetic pigment in human history moreover, the ancient Chinese also synthesized in parallel a similar pigment called Han blue.

The colour blue the colour blue has continued to fascinate people over the millennia till the invention of International Klein Blue and the most recent synthetic blue called YInMn Blue.

Egyptian blue is one of the most studied pigments and keeps fascinating scientists and onlookers from all over the world. Its use in antiquity is well documented by numerous finds in many parts of the world, however, it is still a mystery as to why its use waned over the centuries from the Middle Ages to the Renaissance and then became a pigment synthesised by commercial manufacturers in contemporary times.

It is precisely the recent new discoveries concerning the Egyptian blue brought new questions about the time extent of its use, production centers and commercial routes.

The analysis made during this research project aimed to try to clarify the composition and the origin of the pigment used on these paintings.

The main mystery is how this complex, non-natural pigment resurfaced after centuries, and how artists knew how to make it.

To try to solve this mystery, a research network called BLUENET (Figure 1) has been set up, involving over 100 researchers from more than 60 institutions worldwide. In particular it aims to investigate the discontinuity in the use of EB over time and the change in its production process and composition. The main goal to determine whether the lack of knowledge about EB is due to insufficient data or to cessation of production. BLUENET plans to non-invasively examine as many artworks as possible to understand the use of EB during the centuries where no traces have been found. The project also aims to determine whether lesser-known artists continued to use EB, which may be obscured by the focus on famous masters. The results are shared at an annual conference, with the aim of resolving outstanding questions about the historical use of EB (SGAMELLOTTI, ANSELMI 2022).

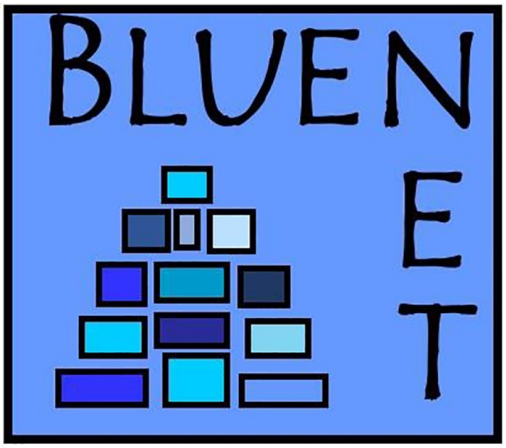

Figure 1 - The BLUENET logo. (SGAMELLOTTI, ANSELMI 2022)

The aim of this thesis is to make a contribution to this research in order to provide new details and insights into the use of Egyptian blue in the Renaissance period and its possible origin using spectroscopic and electron microscopy techniques.

1. Egyptian blue physical-chemical characteristics and related pigments

1.1 EGYPTIAN BLUE DEFINITION

Egyptian blue (EB) is the first synthetic pigment ever produced by humankind. It is a compound mainly constituted by a synthetic calcium copper tetrasilicate called cuprorivaite ($CaCuSi_4O_{10}$) which can be also found in nature as a mineral formed under high pressure and high temperature in the presence of water like the case of Vesuvius in Italy. The natural one was never used as a pigment because it is really rare and only found in minute amounts (ULLRICH 1987; RIEDERER 1997; EASTAUGH ET AL. 2004; NICOLA 2023).

1.2 CHEMICAL COMPOSITION

The main colouring phase constituting Egyptian blue pigment, as already said, is cuprorivaite, but it includes also silicon dioxide (SiO_2) polymorphs such as quartz, cristobalite and tridymite formed during synthesis. When there is an excess of silica and calcium wollastonite ($CaSiO_3$) may form, whereas when copper is in excess cuprite (Cu_2O) or tenorite (CuO) may form (RIEDERER 1997; EASTAUGH ET AL. 2004).

Usually, cuprorivaite is surrounded by a glassy Si matrix containing Ca, Cu, and Na, K, Cl, S respectively from unreacted reagents and fluxes, whereas the presence of As, Sn, Pb and Zn is correlated with impurities in the copper source. Other common elements found in EB samples are Co, Pt, Ni, Mg, Sr, Ba, Sb, Ag, Rb, Y, Zr, Nb, Sc, V, La, Ce, and C (NICOLA ET AL. 2023).

1.3 SYNTHESIS

The synthesis involved to produce EB was quite articulated as it required fixed ratios of ingredients and controlled temperatures. This compound was obtained by combining several ground components into a powder: a calcium compound such as limestone ($CaCO_3$) or calcium hydroxide ($Ca(OH)_2$), a copper source such as copper alloys or copper salts like malachite ($Cu_2(CO_3)(OH)_2$), azurite ($Cu_3(CO_3)_2(OH)_2$) and a silica source generally in the form of sand (SiO_2). The synthesis is called melt-flux or salt-flux since usually a flux stream (above 2% w/w in the final result) of soda ash (Na_2CO_3) or potash ash (K_2CO_3) were used (Figure 2). The mixture is heated to around 800 – 900 °C, that is temperatures that avoid the production of unmelted materials, glass or slags, then the compound is kept at 800 °C for 10-100 hours with the formation of large cuprorivaite crystals

embedded in a silicate glass matrix that can contain copper too. Finally the material can be ground and purified. (RIEDERER 1997, EASTAUGH ET AL. 2004; BERKE 2007; NICOLA ET AL. 2023).

$$\underset{\text{Malachite}}{Cu_2(CO_3)(OH)_2} + 8\ \underset{\text{Sand}}{SiO_2} + 2\ \underset{\text{Lime}}{CaCO_3} \xrightarrow[800-900^{\circ}C]{\text{Flux}} 2\ \underset{\text{Egyptian Blue}}{CaCuSi_4O_{10}} + 3\ CO_2 + H_2O$$

Figure 2 - Example of stochiometric reaction involved in EB synthesis. (BERKE 2007)

When the reacting mass reaches temperatures between 600 °C and 800 °C, the endothermic reaction starts, with weight loss due to calcium carbonate decomposition, and at 800-850 °C there is the formation of EB which is stable up to 1080 °C. After that temperature the decomposition of glass occurs, high temperature silicon polymorphs form and tenorite and cuprite may form if Cu is in excess (RIEDERER 1997).

1.4 CRYSTAL STRUCTURE

Cuprorivaite (Figure 4) is an alkaline-earth copper tetrasilicates, belonging to phyllosilicates and gillespite group and it is part of space group *P4/ncc*, $Z = 4$. It is made up of nano-layers of SiO_4 tetrahedra connected at their corners and linked by coordinated CuO_4 in a square-planar arrangement, through bridging oxygens; each sheet separated by Ca atoms in a distorted cubic geometry (eventually substituted by Ba or Sr in other copper silicates) (Figure 3). The Cu^{2+} ions exhibit square planar coordination, stabilized by the Jahn-Teller effect. Cell parameters of cuprorivaite are: $a = b = 7.30128(4)$ Å and $c = 15.12370(15)$ Å (SGAMELLOTTI AND ANSELMI 2022; NICOLA ET AL. 2023).

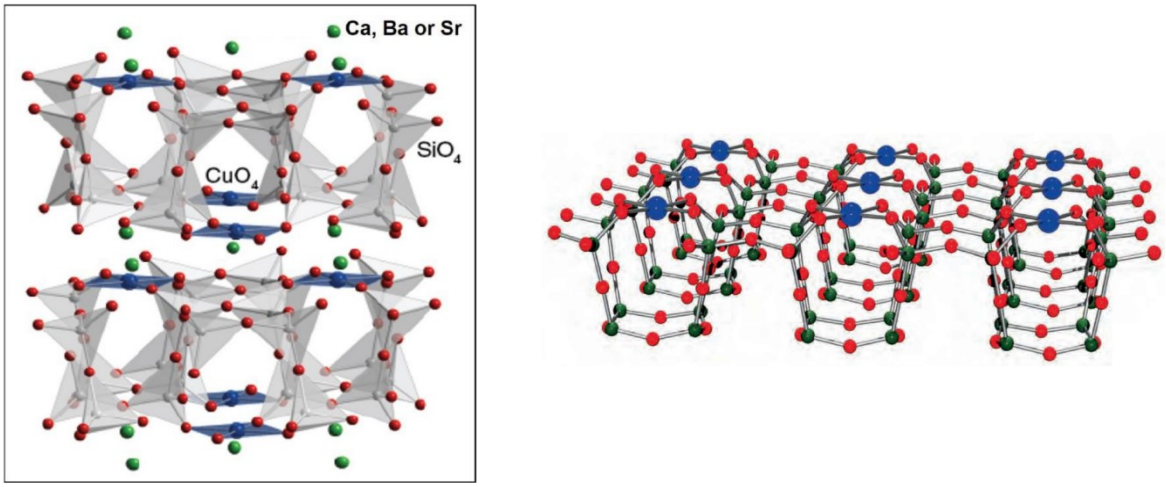

Figure 3 - Two representations of crystal structure of cuprorivaite on the left (SGAMELLOTTI AND ANSELMI 2022) and on the right Cu in blue, Si in green, O in red while Ca is omitted (BERKE ET AL. 2010).

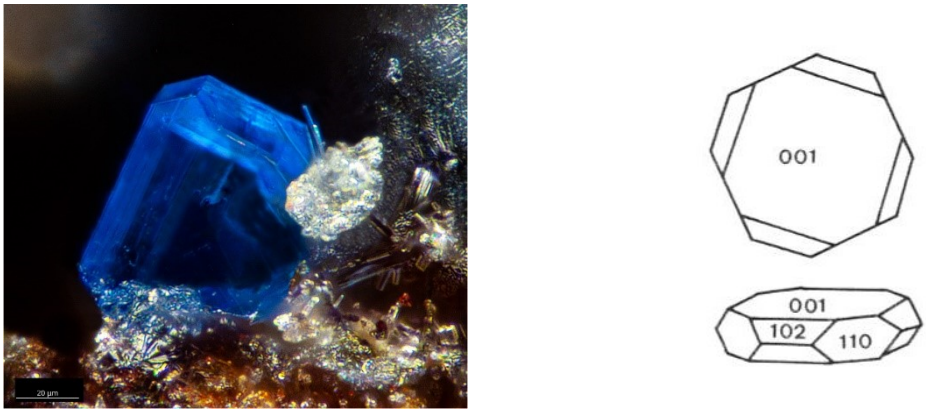

Figure. 4 - On the left photo of a crystal of cuprorivaite from Nickenicher Weinberg, Nickenich, Pellenz, Mayen-Koblenz, Rhineland-Palatine, Germany. Collection of Dieter Nickolay, photo by Volker Heck. (www.mindat.org) On the right representation of ideal morphology of a cuprorivaite crystal (ULLRICH 1987).

1.5 OPTICAL CHARACTERISTICS

Cuprorivaite is a uniaxial mineral that is birefringent, showing high third-order and higher interference colours with low relief. It exhibits dichroism when observed under polarized light in different orientations, displaying an ordinary ray (ω) with a refractive index of 1.636 that results in a deep blue colour, and an extraordinary ray (ε) with a refractive index of 1.591 that appears pale pink to faint lavender (Figure 5). The surface texture of cuprorivaite particles can vary widely, ranging from smooth and glassy to rough, pitted, or spongy. These particles may exhibit anhedral morphologies, irregular angular fractures (not conchoidal), and can have tabular, platy, or euhedral octagonal habits. The size of these particles typically ranges from medium to coarse, with a broad distribution. The colour of the pigment can vary from dark blue to pale whitish as grain size decreases due to differences in light scattering, a property that was also exploited in ancient times (GETTENS AND STOUT 1966; RIEDERER 1997; EASTAUGH ET AL. 2004; NICOLA 2023).

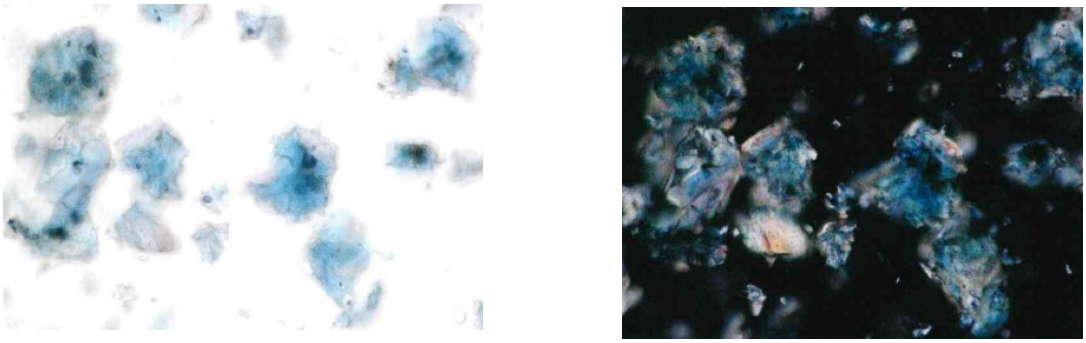

Figure 5 - Crystals of cuprorivaite under plane-polarized light microscope (left) and crossed polars with 40x magnification (Modified after EASTAUGH N. ET AL. 2004).

1.6 COLOUR

The distinctive blue colour of cuprorivaite is due to the presence of Cu^{2+} ions in square-planar coordination and the influence of the crystal's internal electric field. This specific geometry reduces the symmetry from octahedral (O_h) to tetragonal (D_{4h}), which splits the degenerate E_g and T_{2g} orbitals into four distinct energy levels, further energy splitting slightly occurs because of spin-orbit interactions. Three primary broad absorption bands correspond to d-d transitions, two in the visible spectrum and one in the near-infrared (NIR). The blue colour arises because the absorption bands in the visible spectrum are centred in red (630 nm) for the $^2B_{1g} \rightarrow {}^2E_g$ transition, in green (536 nm) for the $^2B_{1g} \rightarrow {}^2A_{1g}$ transition and in NIR (764 nm) for the $^2B_{1g} \rightarrow {}^2B_{2g}$, having a material that reflects blue light (Figure 6) (NICOLA 2023).

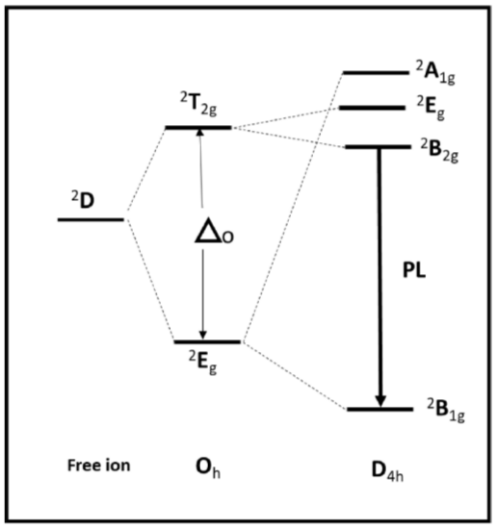

Figure 6 - Scheme of energy level splitting for Cu^{2+} (SGAMELLOTTI AND ANSELMI 2022)

Traditional melt-flux synthesis produces a deep blue colour, whereas if the flux is near zero, the synthesis is based on diffusion laws within a solid-state synthesis, and the temperatures are as high as needed, the resulting quantity of glass is very large, containing just a little copper, and cuprorivaite crystals are small with a general light blue colour. Other possible ways of synthesis are: the hydrothermal synthesis which produces bright blue crystals, and the sol-gel procedure with a variety of blue tones not influenced by grain size (NICOLA ET AL. 2023).

The lack of silica and the excess of copper can lead to incomplete reaction and creation of the unwanted phases (CuO and/or $CaSiO_3$) producing a grey-blackish and whitish colour respectively. The type and grain size of original raw materials used can have effects on final hue too forming peculiar coloured impurities such as NaCl, Fe, Zn and Ca promoting a greenish tone (NICOLA ET AL. 2023).

Other factors influencing the final colour are the duration of the high-temperature production processes and the cooling rate. If the duration of the synthesis is longer and the cooling is slow, the crystal size is larger and the final colour more intense. If the synthesis is short and the cooling is fast of course the crystals are small, faded-coloured crystals and also unreacted reagents are obtained (RIEDERER 1997; NICOLA ET AL. 2023).

1.7 STABILITY

The substantial number of findings of thousands of years old Egyptian blue in optimal conditions testifies its lightfastness and physical-chemical stability. This pigment does not decompose either at temperatures close to freezing or up to 1000°C, and its thermal resistance depends on the presence of Na+ and K+ ions in the glassy matrix due to fluxes. However, if brought to temperatures above 1050 °C it forms a mixture of cupric and cuprous oxides (MAZZOCCHIN ET AL. 2004; WIEDEMANN AND BAYER 1997).

Due to Cu^{2+} ions in square planar coordination and the stable network of SiO_2 tetrahedra is resistant even to hot strong acids like HCl and decomposes just in hydrofluoric acid and nitric acid if a soda flux is used. (PABST 1959; RIEDERER 1997; NICOLA ET AL. 2023) Exposure of EB for thousands of years in harsh environments due to humidity, acids or salts, can lead to copper chloride alteration with the formation of green basic copper chlorides, which are connected to the devitrification of the glass phase, potentially caused by washout or to fungi and bacteria attack. Other changes in macroscopical colour appearance can be the consequence of binders alteration (NICOLA ET AL. 2023).

In alkaline conditions, like in fresco painting, it resists well and decompose just at high temperatures under soda or potash fluxes (RIEDERER 1997). Cuprorivaite is stable also in oxidizing environments and colour resistant under X-ray irradiation even if some scholars have observed some case of discoloration under high-intensity laser irradiation, potentially due to CuO formation (NICOLA ET AL. 2023).

1.8 COMPATIBILITY

Given its chemical composition, reactivity with other pigments or constituent materials of cultural property is almost non-existent (RIEDERER 1997).

During centuries it was used in thin layers often alternated with other pigments or mixed with colours and organic dyes to obtain a variety of hues and shades (NICOLA ET AL. 2023).

1.9 VISIBLE INDUCED LUMINESCENCE (VIL)

Visible induced luminescence (VIL) is a property of a material to emit radiation if excited by a light source, both with specific wavelengths. When EB is hit by green (540.5 nm), red (625 nm) or IR (780 nm) light it emits a broad spectrum centred at 950 nm. Experimentally, visible, UV LEDs sources or fluorescent light source can be used to stimulate light emission of EB in the IR range (800-1000 nm), which can be recorded with a digital camera equipped with a cut-on IR filter (ACCORSI ET AL. 2009; VERRI 2009).

This peculiar feature is attributed to Cu^{2+} ions electronic transitions ($^2B_{1g} \rightarrow {}^2B_{2g}$, ^2E_g and $^2A_{1g}$) and the maximum emission at 910 nm is connected with the transition $^2B_{2g} \rightarrow 2B_{1g}$ (Figure 7).Thanks to its long luminescence lifetime and intense IR emission, the presence of cuprorivaite on all the materials can be visually easily detected, because of its excited-state lifetime of 107 µs and the high quantum efficiency (10.8%) (ACCORSI ET AL. 2009).

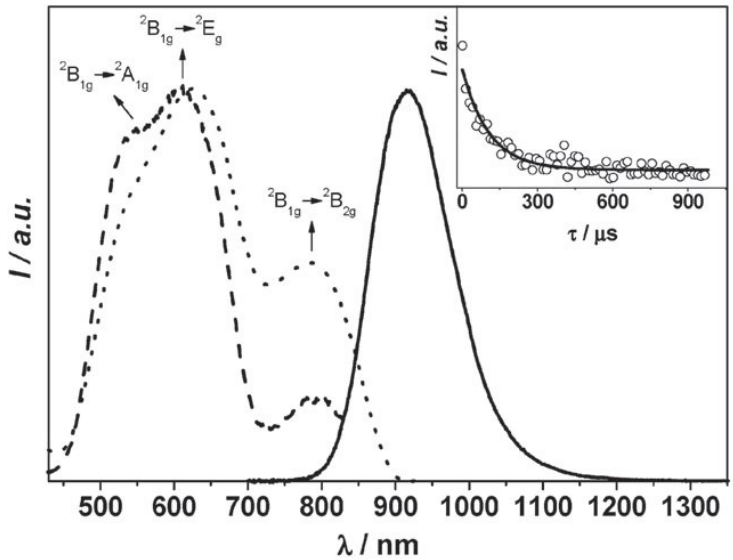

Figure 7 - Absorbance (dotted line), excitation (dashed line, λ_{em} = 916 nm) and emission (solid line, λ_{exc} = 637 nm, corrected for the detector response) spectra of powdered synthetic cuprorivaite. Inset: luminescence decay (107 µs, λ_{exc} = 637 nm). (ACCORSI G. ET AL. 2009)

1.10 OTHER PROPERTIES

EB is used as an optical chemosensor due to its photochemical stability and high luminescence, as well as a reference material for fluorescent indicators in radiometric and double-lived referenced (DLR) intensity measurements. Its temperature-independent luminescence has enabled the development of high-temperature EB-based thermographic emitters. In forensic chemistry, Egyptian blue can reveal latent prints due to its NIR luminescence, which differs from that of visible photoluminescent materials and does not interfere with materials at the crime scene. EB's chemical versatility allows it to be micronized while maintaining luminescence, and nanosheets of EB can be produced and used in security inks. EB is showing promise as an electrode

material for Li-ion batteries due to its potential to host lithium ions. Additionally, EB-nanosheets are highly promising in bioimaging applications due to their small size, photostability, and high brightness in the near-infrared (NIR) range. They have been successfully used for NIR imaging in plants and Drosophila embryos (SGAMELLOTTI AND ANSELMI 2022).

Evidences have shown that surfaces covered by EB prevent algal and fungal growth, this pigment as moreover an antibacterial effect on *Escherichia coli.* The antimicrobial effect is due to the slow solubilisation of Cu^{2+}. Maybe ancient Romans could have been aware of this properties since that they used EB mosaic tesserae in watery places (BOSCHETTI 2011; NICOLA ET AL. 2023).

Additionally, cuprorivaite releases Cu and Si ions that synergistically promote angiogenesis within safe concentration ranges, offering therapeutic benefits without cytotoxic effects for human tissue regeneration. This has garnered interest for its application in regenerative medicine, especially for wound healing dressings. Initially thought unsuitable for bone repair due to potential inhibition of osteogenesis, recent studies show that cuprorivaite nanosheets on 3D-printed scaffolds can combat osteosarcoma and enhance bone tissue regeneration. Additionally, cuprorivaite nanosheets are safe and biocompatible, making them useful in bioimaging and bio photonics (NICOLA ET AL. 2023).

1.11 EGYPTIAN GREEN

The so-called Egyptian green, green frit or turquoise frit was created since 2500 BCE in Egypt and later during Roman times. The initial components needed to synthetize it are the same ones of Egyptian blue, though the lime percentage must exceed the copper oxide. When the temperature of 1050-1100 °C is reached the decomposition of cuprorivaite occurs, with the formation of Cu-rich vitreous part containing wollastonite, tridymite and cristobalite, with an overall green colour that can vary from olive-green to blue-green. Contrary to the belief of some authors, Egyptian green was an intentionally produced compound and not a synthesis error (ULLRICH 1987; EASTAUGH ET AL. 2004; HATTON 2008; NICOLA ET AL. 2023).

1.12 HAN BLUE AND HAN PURPLE

Han blue and Han purple also known as Chinese blue (CB) and Chinese purple (CP) are too alkaline-earth copper silicates respectively with $BaCuSi_4O_{10}$ and $BaCuSi_2O_6$ chemical formulas. CB has a structure similar to EB, whereas CP differs both in his structure and chemical stability (Figure 8). The synthesis of these two pigments is even more articulated than the one necessary to create Egyptian blue, given that it requires higher temperatures (900-1000 °C) and barium containing raw

materials like barite ($BaSO_4$) or witherite ($BaCO_3$) which are less abundant than copper ones, moreover lead salts were used as catalyst and flux (BERKE 2007).

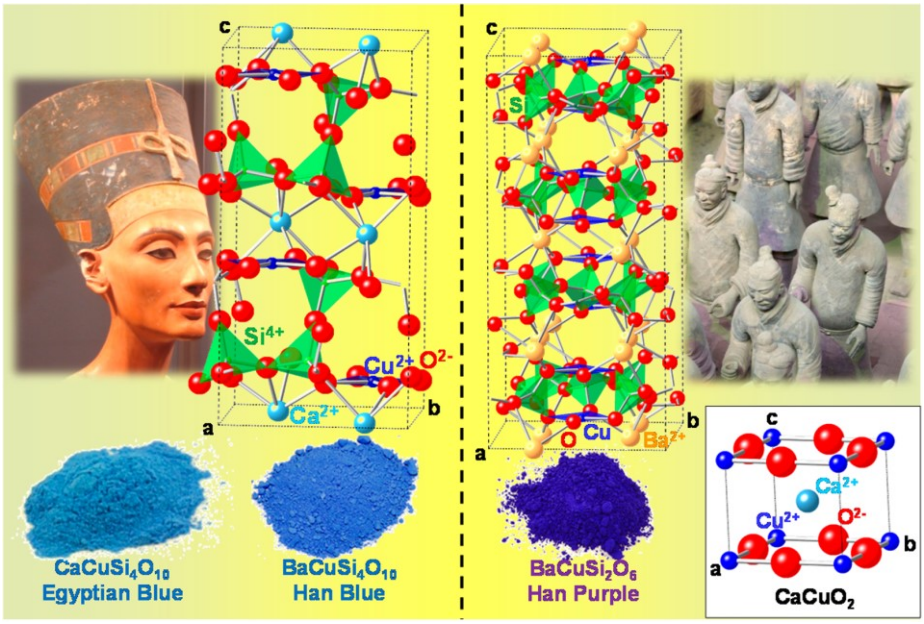

Figure 8 - Comparison between EB and HB chemical structure with HP one. (GARCÍA-FERNÁNDEZ ET AL. 2015)

Some authors suggest that both the compositional similarity of Chinese pigments to Egyptian blue and the greater complexity of synthesis of the former indicate that Han blue and Han purple derive from a technological improvement of EB probably known through the Silk Road although there is currently no evidence for this (BERKE ET AL. 2010). HB and HP have similar properties respect to EB showing also luminescence (Figure 9)(VERRI 2009).

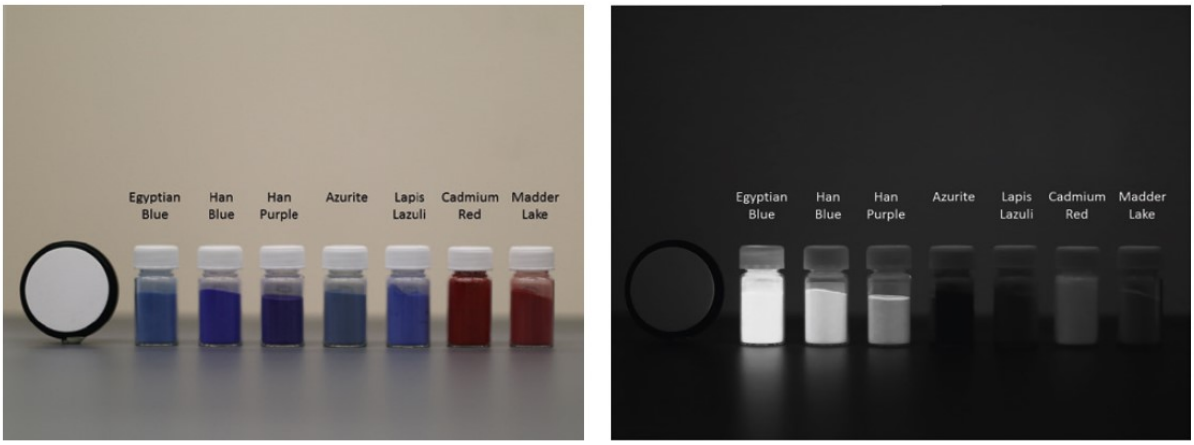

Figure 9 - Visible light image and VIL of some pigments (Modified after THAVAPALAN ET AL. 2016).

2. The history of Egyptian Blue Pigment

2.1 NOMENCLATURE

In antiquity not always there were enough terms to describe all the shades of colours and pigments existent, possibly because the perception of colours was different from today's and varied according to culture (BUSATTA 2014). The ancient terms to describe the colour of pigments are often not the same as those used to denote a specific colour, but their nomenclature derives for example from objects with that colour, toponyms or metonymy of other precious materials such as gold or lapis lazuli like today's emerald green indicating both a specific colour and the precious stone or from specific inventors names, production and extraction processes and trade networks (BECKER 2022).

In the ancient Near East, this new artificial pigment, as was the practice at the time, took its name from lapis lazuli (*ḫsbḏ* in Egyptian hieroglyphics) specifying its origin in fact was called *ḫsbḏ iryt* which meant 'furnace lapis lazuli' or 'artificial lapis lazuli'. Another Egyptian name used to define Egyptian blue was *mfkȝ.t* meaning turquoise. In Mesopotamia, the term used was *uknû merku* and meant 'moulded lapis lazuli' in Akkadian, in this language they used to distinguish also real lapis lazuli, 'lapis lazuli from the mountain' called *uqnû šadî,* from blue glass or "lapis lazuli from the kiln" *uqnŭ kūri* (BECKER 2022; EASTAUGH ET AL. 2004).

Ku-wa-no was the term used to name cobalt blue glass in Linear B, the language used by Mycenaeans and comes from *kuwanno* in Hittite language which derives from the Akkadian *uqnû* and the Ugaritic *iqnu.* Blue pigments were generally referred in ancient Greece with the term *κύανος* while the derived Latin term was caeruleum directly deriving from the already mention Linear B names. To distinguish among same colour different pigments usually the associated places like Aegyptium (EB), Cyprium (azurite), and Scythicum (lazurite) were specified (BECKER 2022).

The Greek author Theophrastus (c. 315 BC) mentions Egyptian blue with the name κύανος, specifyng that it is a colour of synthetic origin that can have various hues of blue depending on grain size, and also saying that the manufacturing technique was taken from Alexandria and brought to Puteoli in Italy (EASTAUGH ET AL. 2004; NICOLA 2023).

Pliny the Elder (77-79 AD) enumerates different typologies of Egyptian blue within the treatise Naturalis Historia reporting also the different prices of each one (NICOLA 2023).

The pigment exported throughout the Mediterranean over the centuries also took the name of *Alexandrian blue* given its commercialization in Alexandria (EASTAUGH ET AL. 2004). While in the De Architectura (20-30 BC) Vitruvius refers to Egyptian blue as *caeruleum* saying wrongly that was made firstly in Alexandria which was founded only in 331 BC although as we know the pigment was produced well before (BECKER 2022; EASTAUGH ET AL. 2004).

In the literature EB is sometimes erroneously referred also as *blue frit* even though these compounds are glassy in nature and not crystalline (ULLRICH 1987; EASTAUGH ET AL. 2004). Nowadays it was identified also with specific colour coordinates, but it should be taken into account that the colour of EB is not standardized and depends on a series of factors. (NICOLA ET AL. 2023).

The current common accepted name is Egyptian blue to indicate the artificial modern or ancient pigment and cuprorivaite to denote the natural or artificial mineral (NICOLA ET AL. 2023) and the known terminology used to indicate the pigment EB is summarized in Table 2.

Epoch and/or Author	**Name**
Ancient Egypt	*ḫsbḏ iryt (* lapis lazuli from the kiln)
	mfkȝ.t (turquoise)
Mesopotamia	*uknû merku* (molded lapis lazuli)
Aegean	kuwano (blue)
Theophrastus (315 BC) *De lapidibus*, XXXIII, VIII, 55	Κύανος (blue)
Pliny the Elder (77 AD) *Naturalis Historia* XXXIII, 57	Caeruleum Aegyptios
	Vestorianum (most refined part of Egyptian blue)
	Puteolanum or cyanon
	Lomentum (refined EB)
	Tritum (low quality EB)
Vitruvius (15 BC) *De architectura* VII.11.1	Caeruleum
Isidore of Sevilla (636 CE) *Etymologiae* Book XIX, Caput XVII	Venetum caeruleum
17th century	Cerulèe
Colour Index	PB31
Constitution Number	77437
Hex Code	#1034A6
RGB	16,52,166
CMYK	90% 69% 0% 35%
HSV/HSB	226°, 90%, 65%
Pantone	286 C
19th century	Blue de Pompéi
Current	Egyptian blue
Other common names	Alexandrian Blue, Italian Blue, Pozzuoli blue, Vestorian blue, Pompeian blue, Blue frit, Copper frit

Table 2 - Ancient and modern terminology used to identify the pigment Egyptian blue in different centuries (MERRIFIELD 1849; ULLRICH 1987;RIEDERER 1997;EASTAUGH ET AL. 2004; DAVIES AND JOKINIEMI 2008; BECKER 2022).

2.2 HISTORY

Egyptian blue is the blue material which was the most extensively used from early dynasties in Egypt till the end of Roman period in Europe. It was ground and used as a pigment on a variety of materials, or used as synthetised for the production of small objects or glazes. Probably the synthesis necessary to create it was discovered by chance during the production vitreous materials, such as glass coloured with copper, copper-containing glazes, faience with which it is sometimes mistakenly confused. The need for essential resources such as fuel, clay, copper, water and labour probably led to the co-location of various industries and, perhaps, a centralised supervisory system in which workshops shared or sourced raw materials from common suppliers. Moreover, easy access to trade routes would have facilitated both the procurement of these materials and the distribution of finished products. (RIEDERER 1997; HATTON 2008; NICOLA ET AL. 2023; KOVALEV ET AL. 2023).

2.2.1 ANCIENT EGYPT AND WEST ASIA

The first attested evidence of Egyptian blue is dated around 3100 BC in Egypt and expanded more in the 4th dynasty till the Ptolemaic-Roman period with also many evidences of artistic use also in Mesopotamian and in Persian sites like Persepolis, Pasargadae, Nineveh and it is the only blue pigment used in the 2nd millennium BCE in Egypt and Mesopotamia (RIEDERER 1997; EASTAUGH ET AL. 2004; HATTON 2008).

It was found by archaeologist on hieroglyphs, sarcophagi, funerary mask, sculptures, walls and tomb decorations, jars, objects of inorganic and organic nature, amulets and as ground pigment (RIEDERER 1997; EASTAUGH ET AL. 2004).

2.2.2 INDIA, CENTRAL AND EAST ASIA

In these geographical areas there seems to be no evidence of EB probably because for blue colour, natural ultramarine, azurite and indigo were used. Moreover, the two Chinese counterparts, Han blue and Han purple were found to be used as paint and on metal objects (RIEDERER 1997; EASTAUGH 2004).

2.2.3 GREECE

EB was imported by Egypt and spread in Aegean region by the 2nd millennium BC to adorn wall paintings, facades, temples and pottery (RIEDERER 1997; HATTON 2008).

Archaeological evidences of EB can be found in Minoan art at Keros, Knossos, Thera Mycenae, Pylos, Tiryns, Corinth and Cyprus where sometimes it was mixed with glaucophane and at Paestum, a city of Magna Grecia (EASTAUGH 2004; HATTON 2008; NICOLA 2023).

2.2.4 LATE BRONZE AGE

One of the most probable production centres during the New Kingdom in Egypt could be Amarna and Qantir where evidence of kilns, pottery, faience, glass production and ceramic, vessel, powder pigment residues and primary ingots are present even if there is no clear testimony of primary cakes production and secondary processing. The primary ingots can be classified into five shapes: large flat round, large flat rectangular, bowl-shaped, small sack-shaped and ball-shaped. Other sites in Egypt of probable secondary production were identified in Thebes and in Zawiyet Umm el-Rakham (HATTON 2008; KOVALEV ET AL. 2023).

Levant and Mesopotamia sites such as Tel Sera and Beth Shean (Israel), Assur (Iraq), Ugarit (Syria) and Tyryns in Greece suggests secondary workshops for processing EB into final objects rather than primary production centres (KOVALEV ET AL. 2023).

2.2.5 IRON AGE

The archaeological testimonies regarding this period are more limited but the continuous presence of EB finds suggest use and trade. In Ayanis (Turkey) there are evidencies of EB cakes like in palatial contexts in southern Anatolia (Karkemish), Nimrud, Nineveh, and Persepolis might indicate probable secondary processing while Naucratis (Egypt) could be a candidate of uncertain primary production since that the cakes found there, unlike the one from LBA, have flatten bottom and top, like the pellets of Hellenistic and Roman period (KOVALEV ET AL. 2023).

2.2.6 HELLENISTIC AND LATE ROMAN PERIOD

In Kos (Greece) there are evidences of late Hellenistic primary and secondary production dating to the 1st century BC. Here were found not only EB pellets successfully produced with blue hues and not successfully one with grey, green, and brown colour but also powdered pigment on pottery fragments. The presence of with evidences of earth pigments lumps, litharge rods metal contaminants, including gold and silver indicate broader specialization of the workshop and metallurgical activities (KOVALEV ET AL. 2023).

Memphis, Egypt, was a major centre of EB production dating from the 3rd century BC to the 2nd century CE, where pigment lumps were produced using a mixture of quartz sand, bronze flakes, and natron, as attested by Vitruvius. The mixture was placed in ceramic vessels lined with a layer of

lime-rich white slip to prevent adhesion and contamination of EB from the vessels (HATTON 2008; KOVALEV ET AL. 2023).

At Puteoli (Italy), despite literary evidence from Vitruvius and Pliny suggesting local Egyptian Blue (EB) production, direct archaeological evidence is limited. Some pottery pieces with green and blue incrustations were found, but no crucibles or production waste have been conclusively identified. Puteoli's role as a major port with extensive trade connections could have facilitated the transfer of EB production technology to Italy, though direct evidence of primary production is lacking. In Cumae (Italy), hundreds of crucible fragments with blue and green crusts, dating to the 1st century AD, were recovered. Two types of crucibles were identified: closed convex jars and open cylindrical forms. Closed-form crucibles were associated with Egyptian green synthesis, while open-form crucibles were linked to EB creation. Although no EB production sites have been traced, these findings indicate significant evidence of local production. At Liternum (Italy), large amounts of kiln waste, crucibles, and EB pellets dating to the 1st century AD were found, indicating substantial local production. While no kilns or workshops have been identified, the discovery of a complete crucible in a burial further suggests local EB production. Pottery fragments with EB incrustations reinforce the evidence of substantial local production, even if exact production sites remain undiscovered (KOVALEV ET AL. 2023).

Differences in composition between the Italian, English, and French samples and those from Memphis and Delos testify to different production centres although Egyptian blue is usually found in the form of small lumps throughout the Roman Empire, indicative of centralized production and large-scale trade testified also by EB traces in wrecked Roman ships found throughout the Mediterranean (HATTON 2008).

EB pellets dating from 1st to 3rd century AD were found in the Roman province of Noricum (Austria) both in Aguntum and Magdalensberg evidences of trade and secondary production with no traces of crucibles (KOVALEV ET AL. 2023).

2.2.7 ROMAN SITES AND ITALY

Egyptian blue was used by the Etruscans in the 6th century in paintings, tombs, objects, in Phoenician and Punic settlements in Sardinia and Spain. Romans used it for different purposes on a wide range of materials like wood, terracotta, marbles, underdrawings, mosaic tesserae not only in the capital but also in Pompeii, in Ostia Antica and in European sites of the Roman Empire in Europe regions like France, Switzerland, Belgium, Hungary, Austria, England, Norway and in West Asia and North Africa across the trade routes. The utilisation of Egyptian blue in Italy falls at the end of 1st century AD for unknown reasons (RIEDERER 1997; EASTAUGH 2004; NICOLA 2023).

Both Theophrastus in *De lapidibus* and Pliny the Elder in the *Naturalis Historia* mention the Egyptian blue but without specifically mentioning the recipe, while in Vitruvius' *De architectura* (1st century BC - 1st century AD) we can find the procedure needed to create caeruleum, which according to the author was invented in Alexandria and introduced to Italy, in Pozzuoli, by a certain Vestorio. The ingredients mentioned are sand, natron (sodium carbonate and bicarbonate) and copper; the calcium carbonate needed for the synthesis is not mentioned because pozzolan sand also contains calcium. The ingredients are grind and mixed forming a ball which is left to dry and then fired in an unearthed jar producing finally EB (RIEDERER 1997; SIDOTI 2018).

2.2.8 MIDDLE AGES

Until a few decades ago Egyptian blue was thought to have been used only till the fall of Western Roman Empire but actually its presence, albeit in a minor way, is also attested during the Middle Ages. Many different occurrences are present all over Europe on frescoes, wall paintings and illuminated manuscripts which are listed in the Table in the Appendix (NICOLA 2023).

Scholars had made various hypothesis and explanations regarding the reasons beyond the gradual decrease in pigment use and production like the glassmaking crisis, the lack of natron, the replacement of it with the other most used blue pigments, azurite and lapis lazuli (NICOLA 2023).

It is not clear if during the Middle Ages EB was still manufactured in some areas of the Eastern Roman Empire with low quality and reduced crystallinity with a synthesis involving zinc instead of natron, which was in short supply or recycled from ancient deposits or old works of art (NICOLA 2023).

The main medieval source refering to Egyptian blue are Vegetius in *De re militari* (IV – V century AD), Book IV, 37 in which he mentions a blue colour called *Venetum*, Isidore of Sevilla in his *Etymologiae* (636 AD) in Book XIX, Caput XVII who used the term *Venetum caeruleum* saying that it was invented in Alexandria and was produced in Italy with copper calcined in a kiln and not copper filings as reported by Vitruvius, this difference could testify to the independence of this source from the Latin sources. The toponym used by these two authors could suggest a medieval production centre in Veneto region in Italy. In the renowned handbook *Mappae Clavicula,* the term *Vestorianum* is cited in the recipe *XX Auri confectio* to fabricate brass but no formulas to made it are mentioned while in the Lucca manuscript is not quoted (ORNA 1980; SIDOTI 2018; NICOLA 2023).

2.2.9 RENAISSANCE

Recent discoveries have shown for the first time the presence of Egyptian blue after medieval period in the frame of Italian Renaissance famous master Raphael which raises several

questions as to the reason for the use of this pigment, i.e. whether the artist used pigment contemporary to him or taken from archaeological lumps, and whether he wanted to experiment with the use of Egyptian blue given his profound knowledge of the works of Vitruvius (ANSELMI ET AL. 2020; NICOLA 2023). In particular the presence of the blue pigment was attested in the Triumph of Galatea (ca.1512) and in some parts of the vault of Loggia of Cupid and Psyche in the Villa Farnesina by Raphael, in the Saint Margareth (1524) by Ortolano, in the Adoration of the Magi (1530s) and in the Holy Family (1520-1535) by Garofalo (BREDAL-JØRGENSEN ET AL. 2011; SIDOTI ET AL. 2018; SPRING ET AL. 2019; DE VIVO ET AL. 2019; SGAMELLOTTI 2022). The list of known historical occurrences of Egyptian blue in works of art and manuscripts from Middle Ages till renaissance can be found in Appendix B.

The next chapter contains an in-depth look at these painters and their works.

2.2.10 17TH – 18TH CENTURY

The English writer Mary Philadelphia Merrifield in her treatise on old manuscripts, art materials and techniques mentions EB under this definition: "FRIT. Blue pigment made by melting siliceous material with copper and other metallic salts, and grinding the mass to a very fine powder. Syn.: Cerulée, Smaltino, Turchino." (MERRIFIELD 1849). Merrifield cites the painter Pierre Le Brun who describes a kind of azure called Cerulée or "Turchino," is the azure of Pozzuoli, of Vitruvius, and the smaltino of the Italians (LE BRUN 1635).
As we can see in this case the nomenclature given to the pigment is different from the previous centuries and probably caused some misunderstandings with blue smalt, a cobalt-based pigment used by a lot of artists.

She cites also Canon Ramelli who was in possession of a manuscript containing old recipes for colours collected from 1659 to 1711 and entitled *"Raccolti di Secreti, Specifici, Remedj, &c.; ora adesso di Fra Fortunato da Rovigo, Laico Capucino, Infermiere nel Convento dei Capucini di Verona."* The friar talking about Egyptian blue states: *"The blue colour made at Pozzuoli" is the old vestorian azure; it was made of sand, "fior di nitro", and copper filings* (MERRIFIELD 1849).

Another author of 17th century, François, René, alias Etienne Binet describes EB saying: *"The cerulee called blue or turquin, is made by grinding sand with nitre, so diluted that it becomes like flour, we take brass filings from Cypre and sprinkle some on it in order to incorporate it, we mould some balls between our hands, we put them in a vessel and in a furnace, the brass and the sand by the force of the fire exchanging their sweat, mix in nature, and are reduced to a cerulea colour*." (BINET 1622).

The recipe of EB, under the name of "color ceruleo" is attested also in a chapter of a recipe book published in Venice in 1704 but it is just the re-proposition of Vitruvius pigment preparation (GALIPIDIO 1704).

2.2.11 19TH CENTURY – TODAY

After centuries of artigianal production, the commercial pigment was presented as "Bleu de Pompéi" by Lefranc & Cie© in the Universal Expositions of 1889 and 1900 (SIDOTI ET AL. 2018). The existence of the commercial French pigment is testified also in *An Atlas of Rare & Familiar Colour: The Harvard Art Museums' Forbes Pigment Collection* (TRINDER 2018) and in the chapter dealing with Egyptian blue in *Painting Materials. A Short Encyclopedia* (GETTENS AND STOUT 1966).

This pigment from the French brand already mentioned was found in two paintings: *Happy Dawn,* 1892-93 by Angelo Morbelli and in *Spring. Birch* by Robert Falk from 1907. Moreover EB was found among painting studio materials of Giuseppe Pelizza da Volpedo (1868-1907) but its quality was moderate (SIDOTI ET AL. 2018).

EB pigment was found during archaeological excavations in Pompeii and firstly qualitative analysed by Chaptal in 1809 and later by Sir Humphrey Davy in 1814 concluding that it was the same material named caeruleum in ancient sources (RIEDERER 1997; HATTON 2008).

Vauquelin in 1826 was the first to make quantitative analysis of EB and later in 1872 Rammelsberg obtained similar results (RIEDERER 1997).

Fouquè in 1889 identified the compound as $CaCuSi_4O_{18}$ confirmed through XRD analysis by Pabst (1959) and later by him with Mazzi (1962), attesting also that natural cuprorivaite is the same mineral. The first attempts to recreate EB were done by Laurie *et al.* (1914) and later by Chase (1971), Ulrich (1979 and 1987), Tite *et al*. (1984), Pagès-Camagna and Colinart (2003) and Hatton (2005) (HATTON 2008).

And recently synthetized to better understand structure and properties. Nowadays the pigments are available from commercial brands like *Kremer Pigmente* © (Figure 10) usually used as references for the analysis of the ancient samples of EB (NICOLA ET AL. 2019).

Figure 10 - *Kremer Pigmente* ©, in order from the left: EG, EB (particles < to 10 μm), EB (particles < 120 μm), CB and CP. Modified after (NICOLA ET AL. 2023)

2.3 EB PRODUCTION PHASES

As far as production processes are concerned, it is possible to distinguish three different archaeological contexts. The primary production site where Egyptian blue balls were produced from the raw materials, the secondary sites where pigment was ground or small objects were created, and the tertiary site where traces of pigment are found on objects or works of art. The production procedure is showed in Table 3 (KOVALEV ET AL. 2023).

Bulk raw material produced in primary workshops is referred to as 'bricks' or 'pellets' according to shape and size, while 'ingot' is used as a generic term for finished material. During the Late Bronze Age, primary workshops produced brick-shaped rectangular blocks of approximately 17 × 17 cm and larger, or round ingots with a diameter of 9-25 cm and a thickness of 2-3 cm. In the Iron Age, workshops produced smaller, roughly rectangular ingots measuring 6.5-8 × 3.5-4 cm and about 2 cm thick. Hellenistic and Roman workshops produced rounded pellets, typically 2-3 cm in diameter (KOVALEV ET AL. 2023).

	Procurement of raw materials	Raw materials processing / batch preparation	Firing	Processing	Application/Use
Resources Tools	Sand/Quartz pebbles Limestone/Shells Flux (natron/plant ash) Copper ore/scrap metal	Raw materials Grinding tools Know-how/recipe	Kilns Crucibles Fuel Labour	Grinding tools Carving tools Moulds	Pigment Beads/pendants/ small objects Tesserae
Activity	Collection Trade Recycling of bronze	Cleaning (?) Grinding Mixing Forming of cakes/pellets	Firing Temperature control	Grinding Carving Addition of more raw materials	
Archaeological evidence	Quartz pebbles (?) Scrap metal	Grinding tools	EB cakes/pellets Wastes Crucibles with traces of EB Kilns (?)	Powder residues of EB Grinding tools Palettes	

Table 3 – The different stages involved in EB production. (KOVALEV ET AL. 2023)

2.4 ANTIQUE PRODUCTION OF EGYPTIAN BLUE

In antiquity the raw materials used for the synthesis of Egyptian blue could have been derived from different sources giving the possibility of synthesising pigment in various locations depending on the availability of raw materials. The source of silica could have been directly crushed quartz pebbles or sand and in some cases, specific types of sand could also be sources of calcium already having the right proportion of $CaCO_3$ and SiO_2 which was used also for glass production. Calcium source can be added also as powdered limestone or shell. The needed copper was taken both directly from the metal, from alloys, from roasted sulphidic copper ores, from

malachite or azurite. The source of copper can be identified with the analysis of minor elements: arsenic from arsenical bronzes, tin from bronzes and lead from leaded bronzes (KOVALEV ET AL. 2023; NICOLA ET AL. 2023).

Like for the glass making, the necessary flux, to lower the melting point of silica and allow EB synthesis, was usually natron. Natron naturally forms as a crust around periodic lakes and desert rivers and is constituted by $Na_2CO_3 \cdot 10\ H_2O$ and other components like $NaHCO_3$, chlorides, sulphates, other carbonates and impurities. Another substance used as flux was soda-rich plant ash. Potassium found in some samples could be made from plant ash or sandy feldspars or earthenware crucibles (NICOLA 2023).

Despite the different productive centres present in antiquity, the ratio between raw materials remains constant. Any variability prevents the formation on cuprorivaite crystals and led to the formation of other products such as tenorite and cuprite caused by copper excess or wollastonite due to quartz excess. It seems that ancient manufacturers were aware that alkali right percentage is fundamental for a good synthesis and that NaCl presence, due to sand or plant ash would prevent the formation of EB, in fact it was removed with washing and sieving procedures (KOVALEV ET AL. 2023).

Respect to the stoichiometric EB archaeological cakes and pellets present a high excess of SiO_2 and mock sample have shown that a lack of silica produced a dark grey pigment. It is assumed that the firing process in the ancient synthesis of Egyptian blue took place in porous clay crucibles sometimes coated with a rich layer of lime with different designs. The process lasted between 10 and 100 hours and produced a dark blue, coarse-grained, friable conglomerate (KOVALEV ET AL. 2023).

The composition of Egyptian blue (EB) can reflect choices in raw material selection and production procedures. The type and amount of alkaline flux can act as a chronological and geographical discriminator by reflecting on the final sample in the glassy phase whose compositional analysis is complicated by the alterations it may undergo over time. A direct comparison of the elemental composition of the glassy phase in archaeological EB tablets and pellets shows a relatively high variation in K_2O content, apparently reflecting the use of plant ash as a flux. In addition, the grain size, which seems to have been around a few mm, and the quality of the mixing are other important factors influencing the growth of cuprorivaite crystals during firing (KOVALEV ET AL. 2023).

In Egyptian blue literature, archaeological finds are defined by various terms such as pellets, lumps, balls, small blocks, cakes, ingots, ‘loafs of bread’, disks or spheres. The shape of the raw synthesis product in Roman crucibles was spherical with a diameter of about 15-20 mm (NICOLA ET AL. 2023).

The archaeological samples vary in size depending on the era in which they were produced, with round or rectangular shapes and sizes of 15-20 cm in the Late Bronze Age, small rectangular blocks of 65-80 × 35-40 mm and a thickness of 18-22 mm in the Iron Age and much smaller pigment pellets of 1-4 cm in the Hellenistic and Roman periods. Trace elements such as tin and lead, as mentioned earlier, can help to understand to which epoch the samples belong, although when the source of copper was bronze, understanding its origin is difficult. Egyptian blue could either be ground into powder and used as a pigment or undergo a second firing to obtain a lighter EB with a finer texture. The presence of an excess of silica in historical samples may indicate the addition of quartz to change the colour of the pigment. The resulting powder could be mixed with other pigments and binders and used for the decoration of various objects and buildings. For the production of items such as inlays, beads, scarabs, and amulets, the pigment powder was placed in a special mold and refired to create the desired shape. The use of EB for the production of mosaics is attested in Roman times, where Egyptian blue spheres were directly cut into tesserae (HATTON 2008; BOSCHETTI 2011; KOVALEV ET AL. 2023).

2.5 HISTORICAL PRODUCTION CENTRES OF EB

Characteristics of Egyptian Blue (EB) production sites (Figure 11) typically featured closed-form crucibles with flat bottoms, which became larger during the Hellenistic and Roman periods. Roman sites lack direct archaeological evidence of workshops, relying instead on literary evidence and crucible fragments for identification. Proximity to trade routes played a significant role in raw material procurement and distribution. Secondary workshops, often found in palatial contexts, stored and processed EB on-site for local use rather than for primary production. Criteria for identifying EB workshops include the presence of crucible fragments, unsuccessfully produced EB, and secondary workshops indicated by shallow ceramic vessels, grinding stones, and traces of multiple pigments (Table 4). Analytical approaches such as chemical composition and raw material origin are crucial for identifying and tracing EB production sites, with the shape and typology of EB cakes and pellets providing additional clues. Archaeological evidence remains essential for understanding the context and scale of EB production (KOVALEV ET AL. 2023).

Figure 11 - Map with the production centres and the processing workshops involved in the creation and manufacture of EB (KOVALEV ET AL. 2023).

		Primary					Secondary				
Period	Site	Crucibles (fragments)	Unsuccessfully produced EB	HT workshop setting (kilns)	HT tools/waste, industrial debris	Other HT products (glass, metal)	Processing (EB objects, moulds)	Distinct chemical composition *	Distinct shape of EB products	EB on-site consumption	EB in storage/trade context
Late Bronze Age	Amarna (Egypt)	✓		✓	✓	✓			✓		
	Qantir (Egypt)	✓		✓	✓	✓					
	Zawyet Umm El Rakham (Egypt)						✓			✓	✓
	Kheruef tomb, Thebes (Egypt)										✓
	Tel Sera (Israel)								✓		✓
	Beth Shean (Israel)								✓		✓
	Assur (Iraq)								✓		
	Ugarit (Syria)						✓		✓		
	Tiryns (Greece)				✓	✓			✓	✓	
Iron Age	Ayanis (Turkey)				✓	✓		✓	✓	✓	
	Bastam, Çavuştepe, Van (Turkey)							✓	✓	✓	
	Naucratis (Egypt)			✓	✓	✓	✓		✓		
	Karkemish (Turkey)							✓		✓	
	Nimrud (Iraq)									✓	✓
	Niniveh (Iraq)									✓	
	Persepolis (Iran)									✓	
Hellenistic/Roman**	Kos (Greece)		✓	✓	✓	✓		✓		✓	
	Memphis (Egypt)	✓		✓	✓	✓					
	Puteoli (Italy)										
	Cumae (Italy)	✓									
	Liternum (Italy)	✓			✓						✓
	Aguntum (Austria)					✓					✓
	Magdalensberg (Austria)			✓	✓	✓			✓	✓	✓

Table 4 - Criteria used to classify primary and secondary workshops. HT: high temperature, *chemical composition not always analysed, **not all Roman sites are mentioned. Modified after (KOVALEV ET AL. 2023).

2.6 HAN BLUE AND HAN PURPLE

It is uncertain whether the invention of blue and violet pigments of Egyptian and Chinese origin is related or not. From one point of view, it is very likely that the independent development of the production of vitreous materials, faience and glazes in both the Egyptian region, Mesopotamia and ancient China led to the invention of Egyptian blue, Han blue and Han purple pigments in an unrelated way, as there is no evidence of a geographical overlap in the production or transmission of the synthesis technique of these pigments (Figure 12).

On the other hand, it is also true that pigments of Chinese origin are of later date (ca. 800 BC) and are based on a more advanced knowledge of synthesis techniques due to the need to achieve higher temperatures and better control of the initial components and the knowledge could be spread along the Silk Road (Table 5) (BERKE H. ET AL. 2010).

What is sure is that, analogously to Egyptian blue invention, the technology involved in the creation of HB and HP pigments falls within the production framework of highly refractive index glasses and they were first used to create small objects linked with faience and glaze production. Contrary to EB, the two Han pigments can be found just in China and in a minor extend in Japan moreover their existence is limited to the duration of the Han dynasty, with the total disappearance of these pigments after the fall of the Empire in 220 AD and their rediscovery only in recent times (1980s) (NICOLA ET AL. 2023).

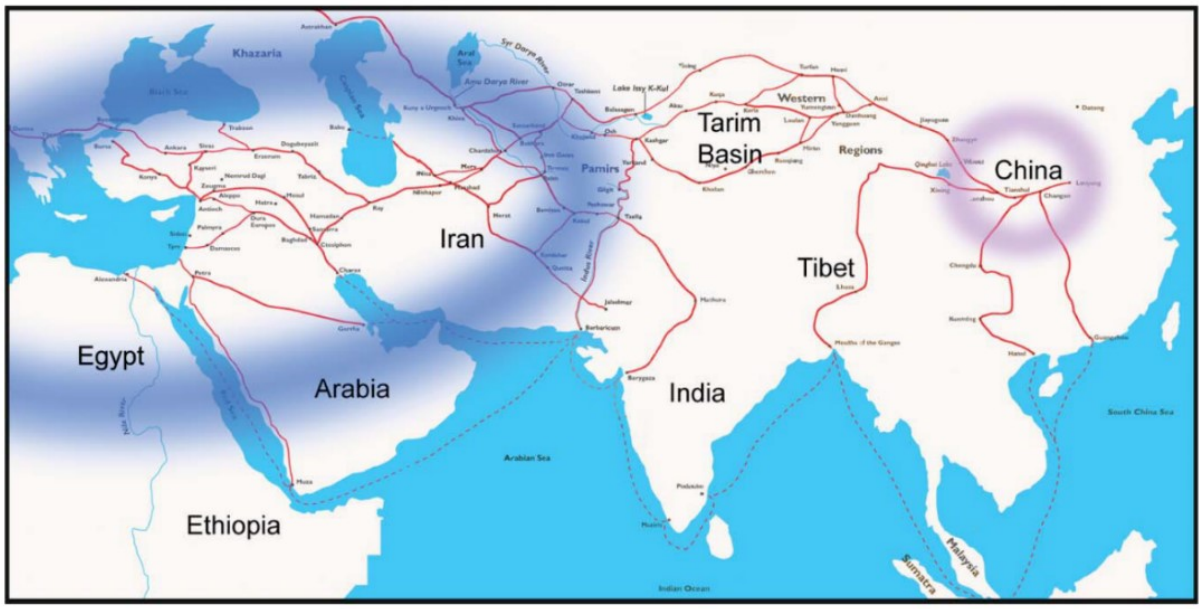

Figure 12 - Geographical map with the comparisons of ancient distribution of EB in blue and HB and HP in violet and the paths of Silk Road in red (Modified after BERKE 2007).

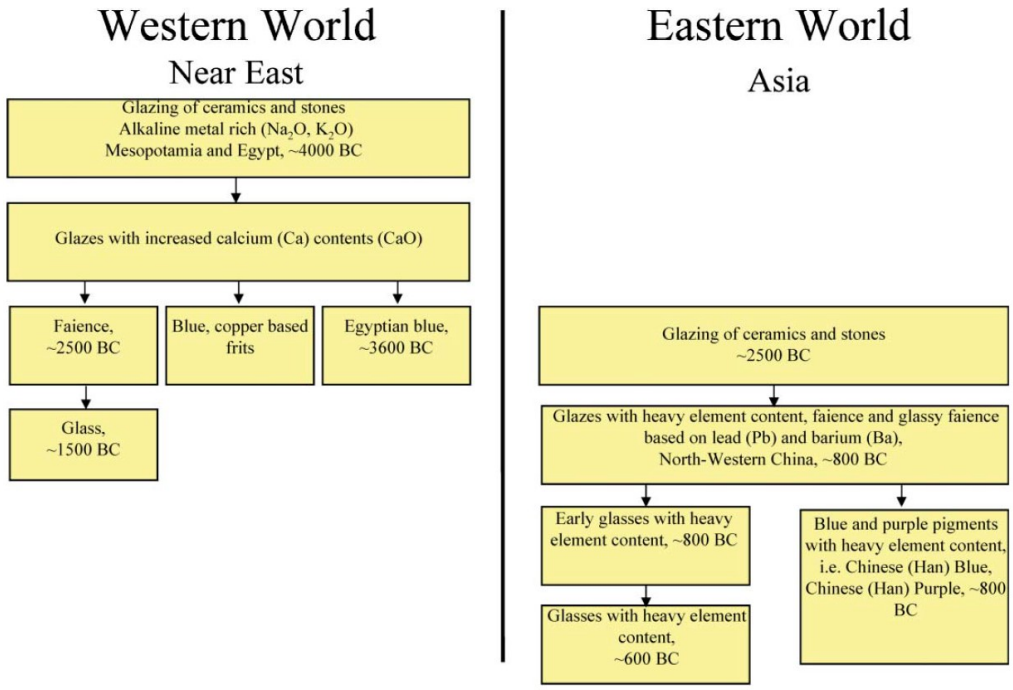

Table 5 - Scheme illustrating the evolution of the alkaline earth copper silicate pigments: EB, HB, HP. Modified after (BERKE 2007).

3. Insight into modern paintings

Recent discoveries regarding the use of Egyptian blue during Renaissance after a long medieval period of sporadic use has raised new questions regarding both the knowledge of the pigment by the great painter Raphael and two exponents of the Ferrarese school, Garofalo and Ortolano, and their artistic relationships.

The initial investigation, conducted exclusively with the VIL technique, enabled the blue pigment to be reliably and preliminarily identified due to its intense luminescence. Although this characteristic is common to other pigments already mentioned, such as HB, HP, cadmium red or yellow, EB can be distinctly recognised by its unique colour, particle size and historical context. (Spring, Billinge, and Verri 2019)

Brief biographies of the artists with a focus on the works in which the pigment was detected are illustrated below and the picture of the paintings named in this chapter can be found in Appendix B.

3.1 RAPHAEL

Raphael Sanzio, born on the 6th of April 1483, in Urbino, was the son of Magìa di Battista di Nicola Ciarla and Giovanni di Sante di Pietro, a renowned painter, from who derives the patronymic Santi latinised as Santius, hence Sanzio. His father's influence led Raphael to study under Perugino, with whom he initially collaborated before branching out to create his own independent and innovative works. Raphael's artistic career flourished with numerous religious paintings and altarpieces, particularly in Perugia. He collaborated with his friend Pinturicchio in Siena, while receiving commissions from notable patrons such as Scipione Borghese and the Duke of Montefeltro. The artistic environment of cities like Florence, Siena, and possibly Venice, where Raphael travelled, brought new influences back to Urbino. Vasari, in his biography, praised Raphael for his rare talent and perfection, seeing him as the embodiment of the artistic ideals of the 15th century's humanistic tradition. Raphael reached the heights of Renaissance art alongside Michelangelo and Leonardo da Vinci, with his work representing a culmination of this artistic era. Raphael's contributions extended beyond painting beeing also a talented architect. Inspired by figures like Leon Battista Alberti, Piero della Francesca, Ghirlandaio and Bramante, and having followed masters such as Perugino, Pinturicchio, and Signorelli, Raphael later worked with artists like Sodoma and Lorenzo Lotti. He also served Pope Julius II della Rovere and Pope Leo X de Medici in the decoration of Vatican rooms and undertook private commissions for the Nasi, Taddei, Doni, and Canigiani families. His innovations included not only perfect volumetric representation and character expressiveness but also a narrative approach that portrayed scenes as stories rather than traditional triumphal depictions. As a leading figure in the revival of classical antiquity, Raphael left a lasting legacy, with his pupil Giulio Romano continuing his artistic influence. Raphael died in Rome in 1520, but his work remains a pinnacle of Renaissance achievement (SGARZINI 2006).

His profound knowledge of Pliny and Vitruvius suggests that the Egyptian blue found in two of his works may have been re-synthesized by the artist himself, rather than being ancient or recycled (ANSELMI ET AL. 2020).

3.1.1 THE TRIUMPH OF GALATEA

Villa Farnesina (Figure 13), which currently bears the name of Cardinal Alessandro Farnese, who acquired the villa in 1579, was commissioned in the early 1500s by the wealthy and powerful Sienese banker and patron of the arts Agostino Chigi, who entrusted the construction and decoration the painter and architect Baldassare Peruzzi. (GERLINI 2007)

Figure 13 - Villa Farnesina in Rome (MALAFARINA 2003).

The fresco depicting the nereid goddess Galatea is located on the longest wall of the villa's namesake room. The ceilings painted by Baldassarre Peruzzi (1512) and the lunettes by Sebastiano del Piombo address mythological, astronomical, and astrological themes (1511-1512). To the left of Raphael's work is fresco, depicting the cyclops Polyphemus (Figure 14) admiring his beloved (GERLINI 2007).

Figure 14 - The cyclops Polyphemus by Sebastiano del Piombo. (MALAFARINA 2003)

The dating of Raphael's work is based on a letter from the Urbinate to Baldassare Castiglione in which he informs his friend that he has completed the model for St. Peter's Basilica, which serves as a terminus ante quem for chronological attribution given that Castiglione had visited Rome in 1513 and would thus have seen the Villa of Chigi and its frescoes (GERLINI 2007).

For the composition, the artist seems to have been inspired by a poem by Poliziano, Mantegna's drawing "Battle of the Sea Gods," and the reliefs of Sienese marine sarcophagi. The figure of Galatea stands dynamically at the centre of the composition in a triumphant pose with her head and gaze directed upwards towards the fresco of Polyphemus. The nereid sails the sea aboard a shell pulled by two fierce dolphins, and the iconography immediately recalls Botticelli's Birth of Venus. The sea goddess is surrounded by other marine deities, summoned by a Triton blowing a conch on the right and another, mirroring it, riding a hippocamp on the left. In the foreground, a nereid struggles to free herself from a bearded Triton, while another in the background rides a centaur. Putti complete the scene: one amorino holds the reins of the marine chariot, another is hidden behind a cloud holding arrows, and three flying putti with bows are about to shoot darts at Galatea. The presence of the wind is evident from the fluttering hair and drapery of the protagonist (BECK 1994; GERLINI 2007).

This fresco represents the first attestation of the presence of Egyptian blue in the Renaissance period. VIL analysis have revealed the presence of Egyptian blue on Galatea's fresco to depict sky, water and to highlight some detail of the fresco such as the eyes of nereid. This choice of Raphael seems not to be an accident: the great Sanzio seems to have wanted to pay homage to the mythological subject by using the Egyptian blue pigment already employed by the ancient Romans in their paintings (Figure 15) (ANSELMI ET AL. 2020; NICOLA ET AL. 2024).

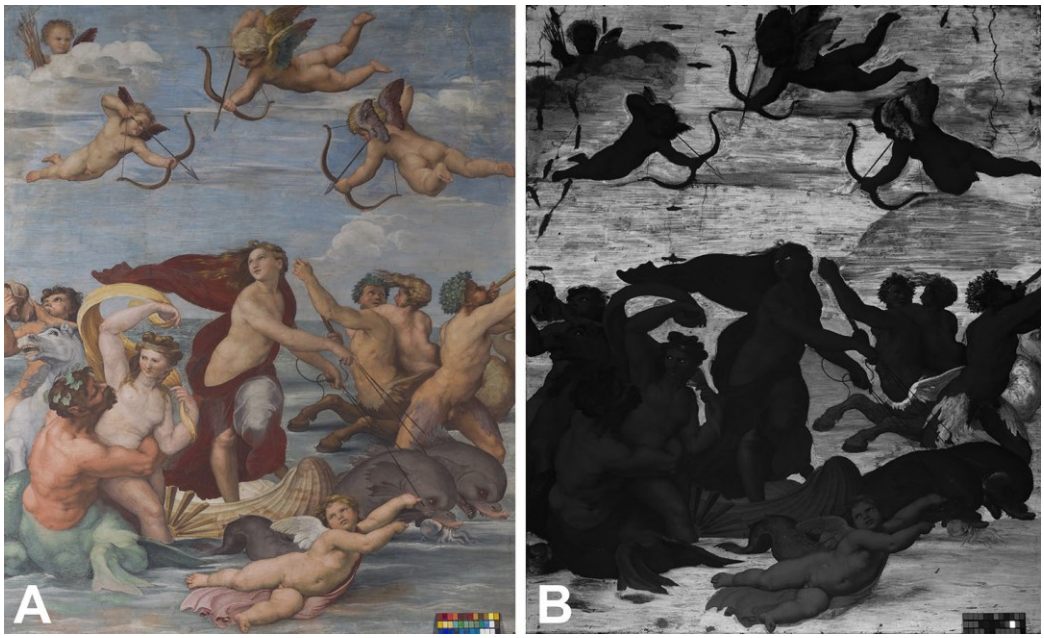

Figure 15 - *The triumph of Galatea* visible image (A) and VIL image (B) (NICOLA ET AL. 2024).

3.1.2 Loggia of Cupid and Psyche

Agostino Chigi in 1517 commissioned Raphael to decorate of the gallery adjacent to the Loggia of Galatea, which was named *Loggia of Cupid and Psyche* (Figure 16) as it took up the myth of the same name narrated in the Metamorphoses of Apuleius. The theme chosen for the pictorial cycle by Sanzio, being themed nuptial theme, is fitting, as the patron was about to celebrate his wedding with Francesca Ordeaschi and wanted to impress the guests with a majestic setting (Malafarina 2003).

Figure 16 - Prospective view of Loggia of Cupid and Psyche (Malafarina 2003).

The preparatory drawings were executed by Raphael who designed the series of scenes alluding to symbols and biographical episodes of Chigi and his consort, also citing the Latin author's concept that divine love makes humans immortal. The loggia is conceived as a continuation of the *viridarium* and the pavilion vault is entirely decorated with botanical-themed festoons that frame the characters painted on the spandrels, sails and vaults. The story centres on the falling in love of the God Love with the beautiful Psyche, which provokes the wrath and envy of Venus, who had already tried in vain to make her fall in love with a despicable man, she subjects the unfortunate woman to endless trials until Jupiter made her desist and Love was able to marry his beloved. The adventures of Psyche are painted in the pendentives while in the centre of the ceiling two frescoes simulating two tapestries depict *The Council of the Gods*, which sanctions the gods' acquired benevolence towards Psyche and the *Convito* with the wedding banquet that constitutes the happy ending of the narrative. The execution material execution of the frescoed scenes was entrusted to Sanzio's pupils, Giovan Francesco Penni, Raffaellin del Colle and Giulio Romano while that of the festoons of flowers and fruit to Giovanni da Udine (Malafarina 2003; Gerlini 2007).

Recent investigations, and new analyses, strengthened by historical evidence from previous micro-sampling and related chemical-physical studies (Giancarlo Sidoti, Claudio Seccaroni, and Paola Santopadre 2018) have shown the extensive presence of EB also in this room of the Villa Farnesina through immediate visualization given by modified night vision goggles (MNVG) in a total not-invasive way (Figure 17) (NICOLA ET AL. 2024).

Figure 17 - VIL image of the ceiling of *Loggia of Cupid and Psyche* with green areas showing the presence of EB and red ones denoting its absence. (NICOLA ET AL. 2024)

3.2 ORTOLANO

Giovanni Battista Benvenuti is an Italian Renaissance painter born in or near Ferrara, better called Ortolano, a name acquired because his father was a kitchen gardener, famous in his time and whose many paintings were transferred from Ferrara to Bologna as said by Agostino Superbi (SUPERBI 1620).

Information about his life, dates of birth (about 1487) and death (after 1527) are uncertain, as both signed works and documents about him are few and not always reliable, (BALDASSINI 2021), his figure has long been confused with that of another contemporary artist, Benvenuto Tisi called Garofalo since their names, the other possible birthplace (Garofalo, a municipality near Ferrara), their similar style and their belonging to the "Ferrarese school". (BARUFFALDI 1844) Because of these factors even its existence throughout the centuries has been questioned (LADERCHI 1856) and many of the paintings now recognized as on him had been attributed to Garofalo (MORELLI 1897).

Although Vasari does not mention him among the Ferrara painters, today's critics instead recognise Ortolano as an important Renaissance painter having a distinguishable style (MANCINI AND PENNY 2016).

Even some scholars Given Raphael's stylistic influences on some of Ortolano's paintings, he may have met the great Urbino artist in Bologna during the latter's journey to Florence in the early years of the 1500s (J.D. Passavan 1882; J.A. Crowe and G.B. Cavalcaselle 1871) or he could just have seen some works of the Urbinate in the Estense collection or through the prints of Marcantonio Raimondi. Reconstruction through historical documents of any contacts between Ortolano, Raphael and Garofalo turns out to be problematic but it seems that a possible journey to Rome maybe in company of Garofalo could be placed around 1515-1516 in which occasion both artist could have had the possibility to study the works of Sanzio. Both Ortolano and Garofalo took inspiration from the works of Gian Francesco Maineri, Boccaccino and Lorenzo Costa active in Lombardy and Emilia and also from Perugino, Correggio, Giorgione and Dosso Dossi (BALDASSINI 2021).

3.2.1 SAINT MARGARETH

The painting *Saint Margareth* is one of the few works from Ortolano which are dated, the year 1524 is reported in a cartouche on the lower right (BALDASSINI 2021) and at that time Ortolano was in Ferrara as attested in a document (FRABETTI 1966).

This painting was previously attributed to Garofalo or Luca Penni but in 1865 the authorship was given to Ortolano by Cavalcaselle (FRANZ 2018).

The panel was originally preserved in the Chiesa di Santa Maria della Consolazione in Ferrara (GUARINI 1621) and later moved to Rome where its presence is testified in the collection of Cardinal Silvio Valenti Gonzaga thanks to its depiction in a 1749 painting by Giovanni Paolo Pannini. After the death of Cardinal Gonzaga his collection was auctioned off in Amsterdam in 1763 and the Saint Margareth was purchased for the King of Denmark. (BREDAL-JØRGENSEN ET AL. 2011) Nowadays the work of art is now in the storage of the National Gallery of Denmark in Copenhagen (SMK) after been moved from the galleries of Christiansborg Royal Palace where it was attested in 1824 (FRABETTI 1966). In the centre of the painted wood curved panel, we find the figure of the Saint cloaked in red and blue, in adoration toward heaven, standing monumentally, with her right foot crushing the Devil, also depicted on the right in the form of a monster. Behind the Saint, on the right are ruined columns symbolic of antiquity while in the background is depicted the scene of her martyrdom, a typical iconography of “scenes with saints,” the depiction of a village completes the composition. The representation of Saint Margareth looking at heavenward in adoration, is inspired by *Saint Cecilia* of Raphael present in Bologna around 1514 (BALDASSINI 2021). *Saint Margareth* represent one of the few examples of Renaissance paintings in which there is the presence of Egyptian blue pigment as attested by VIL analysis (Figure 18).

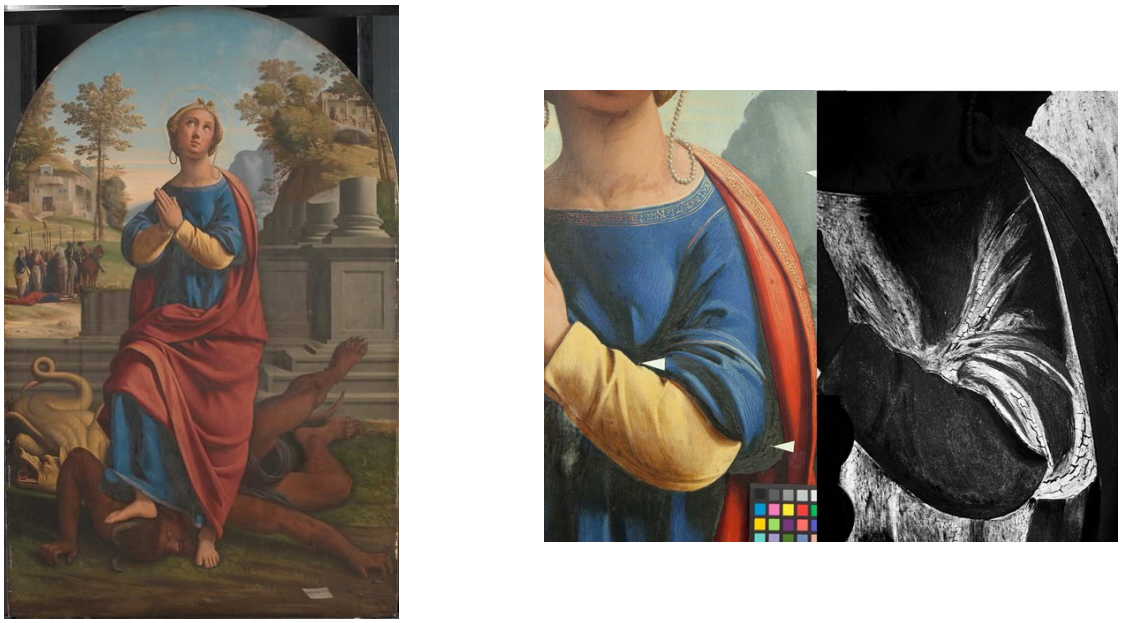

Figure 18 – On the left the painting of *Saint Margareth* (courtesy of Troels Filtenborg) and on the right detail of the left arm of *Saint Margareth* in visible light (left) and in its VIL image (right) (BREDAL-JØRGENSEN ET AL. 2011)

3.3 GAROFALO

The painter Benvenuto Tisi is known as Garofalo because his family hometown was Garofalo, today near Rovigo and he used to sign some of his paintings with a pink (garofano or garofalo in Italian). He was born around 1481 in Ferrara and he learned to paint from Boccaccio Boccaccino, painter of the Estense court at the time, working alongside Lorenzo Costa, Lazzaro Grimaldi and Niccolò Pisano on some religious works and he was closely related with Titian, Giulio Romano, Ludovico Ariosto. Garofalo acquired the style of this group of artists and became one of the leading artists in Ferrara, receiving commissions also from the Dukes of Este for whom he was an important painter of religious themes. He visited Venice towards the end of the first decade of the 16th century and was influenced stylistically by his friend Giorgione. Garofalo visited Rome together with Girolamo Sacrati probably in 1512 having the opportunity to view the works of Raphael with whom he may have collaborated. He was much influenced by the great Sanzio even though he never achieved his skill in the rendering of movements, expressive and gestural, moreover many admirers found his work monotonous and even if he was a good colourist his colour palette was the same all over his career. His two greatest rivals were Ortolano as already seen and Dosso Dossi, in fact the latter also worked for the Este family. Garofalo painted many pictures with religious and secular themes, rarely portraits, most of the early works of art depicting Madonnas in a vertical format but he created also small paintings for domestic devotion like with adoring Virgin and Adoration of Magi. It seems that many of his drawings were lost, usually he preferred wood panels for his oil paintings even if for mythologies and allegories he used canvas.

He was also active as a designer for wood carvers and tapestry. In the last years of his career, he led a workshop where his pupils produced many works with a religious character. His fame as a painter grew in the 18th century whereas during the 16th century was not so great outside Ferrara. Towards the end of his life, he became blind and died in 1559 (MANCINI AND PENNY 2016; DE VIVO ET AL. 2019).

3.3.1 THE HOLY FAMILY WITH SAINTS ELIZABETH, ZACHARIAS, JOHN THE BAPTIST (AND FRANCIS?)

This painting was acquired by the National Gallery in 1839, after several changes of hands of private collectors. It probably came to Britain via France and was first exported from Rome in the late 18th century. According to Waagen the panel was among the paintings belonging to the Aldobrandini collection in Rome in 1603 and probably originally was part of the Este collection (KUSTODIEVA AND LUCCO 2008; MANCINI AND PENNY 2016).

The date of the work of art is not certainly attributed and it was collocated by Neppi during the 1540s while according Pattanaro a more reliable date is around 1520s giving its similarities with *Madonna of Francis I* of Raphael from which Garofalo have taken the poses of Saint Joseph, Elizabeth and the standing little Jesus and the stylistic similarities with a painting of 1517 representing an adoration of the Child preserved today in Dresden. Other elements to be considered for the date of the Holy Family of London are the paintings *Slaughter of the innocents* of 1519 and *Holy Family* of 1523ca preserved at Padova which must predate the painting at the National Gallery; these paintings present Raphaelesque elements and it seems that from the Padova painting Garofalo repropose the figures of all the characters (KUSTODIEVA AND LUCCO 2008).

The theme of the painting shows the first meeting between baby Christ and baby Saint John the Baptist. Jesus, risen from a golden cradle is greeting his older cousin after John gave him a goldfinch, symbol of future Christ's Passion. The Infant Jesus is supported by the Virgin Mary behind whom is Saint Joseph, while the Baptist is held by Saint Elizabeth, his mother, who is seated next to her elderly husband Zachariah with her hand raised. The last figure, on the left should be Saint Francis even if his robe is lighter than the traditional Franciscan one. Behind the group of characters there is a classical wall with an open window from where it is possible to see a landscape with a city and a mountain. Above the scene on a group of clouds there is a host of musician angels and God the Father with a triangular halo pointing to heaven (MANCINI AND PENNY 2016).

VIL investigation revealed an extensive use of Egyptian blue in the painting (Figure 19) (SPRING ET AL. 2019).

Figure 19 - *The Holy Family*, visible image on the left and VIL image on the right (SPRING ET AL. 2019).

3.3.2 ADORATION OF THE MAGI

The other painting of Garofalo in which the presence of EB was attested is an oil painting on panel date 1530s (Figure 20) (DE VIVO ET AL. 2019).

The year of execution is not uniquely defined, according to Baraldi is close to the date of other two paintings with a similar diagonal composition, *Resurrection of Lazarus* of 1532 and *Invention of the Cross* of 1536 and probably with which the painting was originally placed. While Pattanaro thinks that it should be closer to the first years of the third decade of 1500 since that it is close to *Resurrection of Christ* of 1520. Another important date is 1522, when the cartoon of the Adoration of the Magi by Baldassarre Peruzzi, which inspired Garofalo is at Palazzo Bentivoglio in Bologna. Another version of the *Adoration of the Magi* is preserved in Museo di Capodimonte in Naples which is not clear if is a prior version or a copy. With *The Holy Family with Saints Elizabeth, Zacharias, John the Baptist (and Francis?)* and the *Madonna of the Veil* it shares the detail of the daily fog giving a possible clue for the date while a similar child is present also in *The Pagan Sacrifice* (KUSTODIEVA AND LUCCO 2008).

Regarding the historical information about ownership, we know that the painting was acquired by King William I of the Netherlands in Paris in 1823, together with other works from the collection of the widow of Count Edmond de Bourke, Napoleon's Danish ambassador in Naples and Madrid. He had probably acquired the Garofalo painting from the confiscated property of Don Manuel Godoy, former Prince of Peace and de facto Prime Minister of Spain under King Charles

IV, with whom he had fled after Napoleon conquest of the Spanish capital. Godoy, in turn, had received paintings as gifts from the kings of Spain, including possibly the Garofalo, a plausible hypothesis given the Farnese copy in the Capodimonte Museum, which would suggest that the original painting was brought to Spain as an inheritance from his mother, Elisabetta Farnese, by King Charles III, leaving a copy of it in Naples (DE VIVO ET AL. 2019).

The possible function of the painting, given its small format and subject, can be interpret as an altarpiece for private devotion and the composition adopted by the artist is similar to other paintings of his repertoire (DE VIVO ET AL. 2019).

In the background, in the distance, is a fortress on a mountain at the foot of which is a city. On the left of the composition are two groups of soldiers on horseback and people on foot, one in the background in front of the city and one behind a low wall. The youngest of the Magi, standing on the left of the painting, holds a golden vase and looks towards Jesus. Joseph is crouched and half-hidden between them and the Madonna, dressed in red and blue, holding the baby Jesus, covered by a white cloth, on her lap. On the right are the other two Magi, one with a long white beard, kneeling with a white ceramic vase decorated with blue motifs and with his turban on the ground in the foreground; the other standing in the background with his head turned upwards to the left, holding a golden casket wrapped in a piece of cloth. Next to the latter is a man holding a book, pointing to another man at the star of the comet. Behind this last group of characters is a ruined building with a vaulted door (KAISER 1881).

The investigation with VIL have highlighted the presence of EB in some blue parts of the robes of the characters (Fig. 18) (DE VIVO ET AL. 2019).

Figure 20 – Visible light photograph (a) of The Adoration of the Magi and VIL image (b) (DE VIVO ET AL. 2019).

4. Instruments and techniques

In order to have a complete overview of the characteristics of the samples a multi-analytical approach (Fig.) was chosen starting from the observation of the specimens at first with the stereomicroscope and then with the polarizing microscope and the confocal microscope to acquire high resolution images. Thanks to the optical observation it was possible to identify the peculiarities of the samples, mapping the various areas to know the exact location in which the following spectroscopical and SEM analysis would be performed.

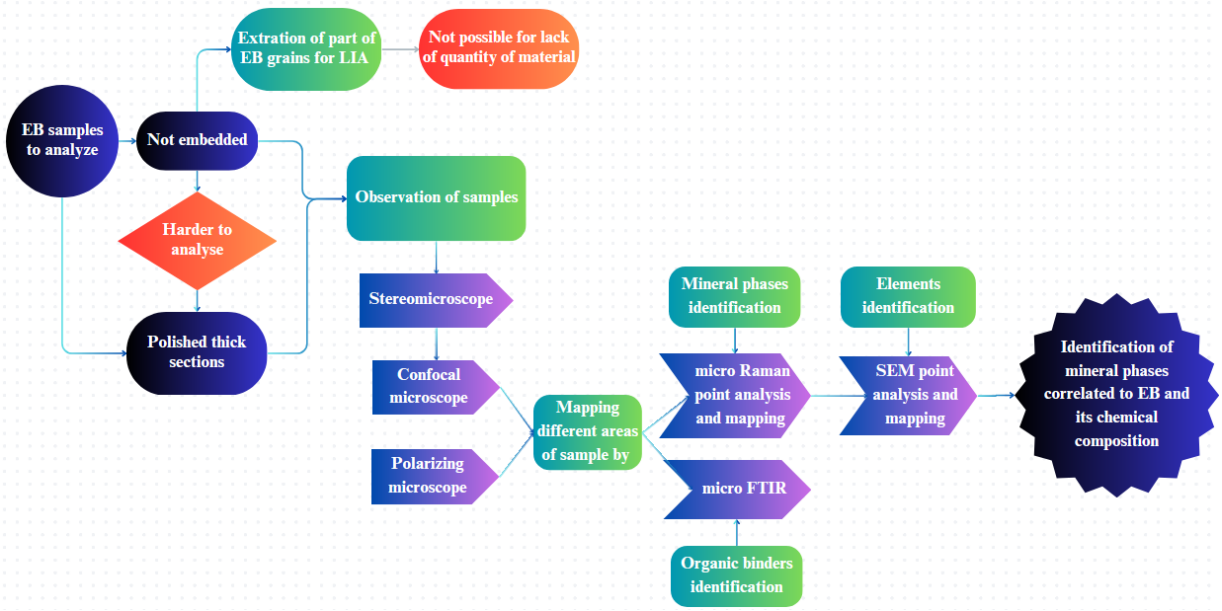

Figure 21 - Workflow of the performed analysis

The following paragraphs provide a synthetic and basic overview of the instruments and techniques chosen to analysed the Egyptian blue samples.

4.1 Optical Microscopy

Optical microscopy is the most used and basic technique to observe and magnify objects in many scientific fields. Despite its simplicity, it is a powerful tool for investigating the main optical characteristics of samples, giving a preliminary idea of, for example, their size, shape, colour and texture.

4.1.1 STEREOMICROSCOPY

A stereo microscope or dissecting microscope is a type of optical microscope that allows to observe samples at low magnifications, usually till 50x and directs light to each eye from two independent light paths through two separate lens system producing a three-dimensional appearance of the specimen observed. The advantage of the stereomicroscope is that permits to look also at thick and opaque samples since that it works in reflection mode even if in some case also the transmitted light mode is possible moreover using this type of microscope allows to have a great working distance and depth of field. Another substantial benefit is that the image remains upright instead of being laterally reversed like in most other compound microscopes, making it easier to understand the spatial relationships within the specimen (HAMMOND AND EVENNETT 2005).

For our purposes, stereomicroscope (Figure 22) was used as a preliminary tool to observe the main characteristics of the samples under analysis and to select parts of them for subsequent analysis. Even during the processing of the embedded samples, the stereomicroscope was useful to understand the degree of polishing of the samples.

Figure 22 - Stereo Microscope *Nikon SMZ645* with zoom range of 0.8x - 5x magnification present at Geoscience department of Padua University.

4.1.2 POLARIZING MICROSCOPE

Unlike the simple microscope, which has only one magnifying lens, a compound microscope is equipped with both a condenser lens and a variable objective lens that allows magnifications of usually up to 2000x. The image can be viewed either directly through the eyepiece or on the PC screen. Generally it can be used in transmission mode in which light pass through the sample to create the image or in reflection mode with the image formed by the reflected light from the object surface (HOLIK 2001).

A polarizing microscope (Figure 23) is a type of compound microscope equipped with a polariser and an analyser that linearly polarise the light. If, in the transmission mode, the two filters are crossed, i.e. positioned with the polarisation directions perpendicular to each other, the optical properties of anisotropic materials can be revealed (HOLIK 2001).

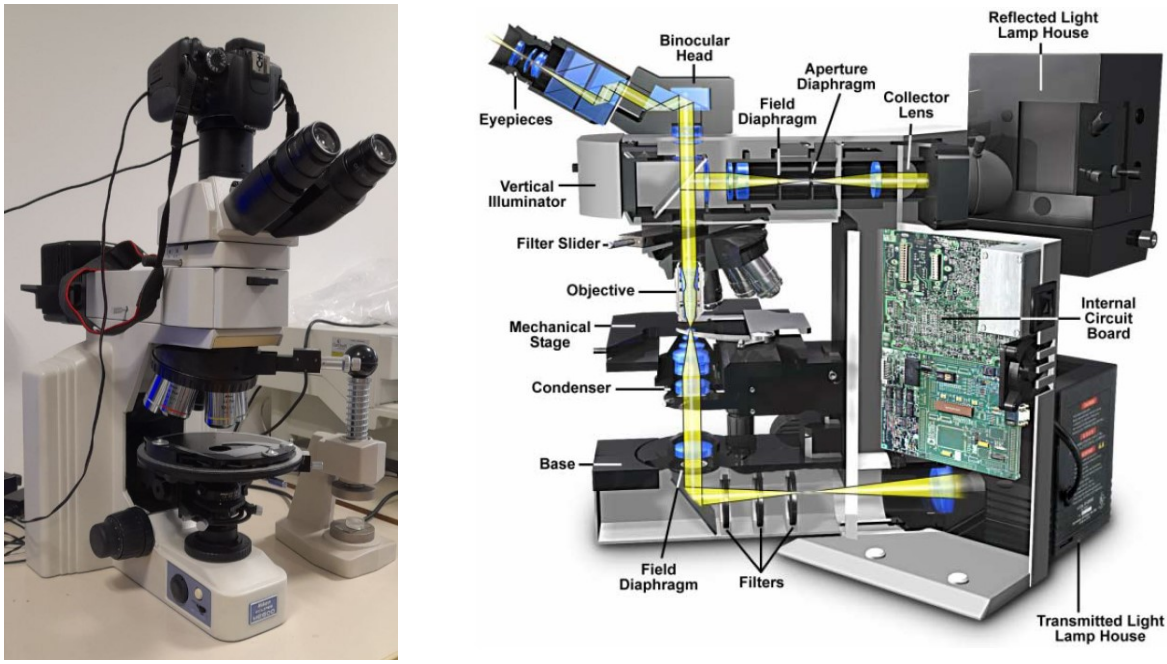

Figure 23 - The polarizing microscope *Nikon Eclipse ME600* with five objectives (5x, 10x, 20x, 50x and 100x) equipped with a *EOS 600D camera* and the small press at Geoscience department of University of Padua (left) and the scheme of the light paths of reflected and transmitted light mode (right) (DAVIDSON M.W. AND ABRAMOWITZ M. 2002).

Before the observation of the specimens the polished sections were attached to a watch slide with some plasticine and squeezed under a small press so that they were orthogonal to the observation axis. Only the embedded samples under examination were observed just in reflection mode since the samples are polished thick sections at different magnifications with parallel, staggered and crossed polarisers, photographed and elaborated through the software associated with the camera.

4.1.3 LASER SCANNING CONFOCAL MICROSCOPY (LSCM)

In contrast to the conventional microscope, which is limited by geometric optics and aberration over large fields of view, confocal microscopy allows even unpolished and rough specimens to be viewed fully in focus. The term "confocal" refers to an optical configuration in which both the illumination and detection systems are focused on the same point in space, allowing the confocal microscope to detect only light from the focal plane, thus improving image resolution and contrast and reducing interference from out-of-focus light (ELLIOTT 2020).

In the laser scanning confocal microscope (LSCM) (Figure 24), a laser, usually argon or krypton-argon, scans the surface of the sample on the Cartesian axes at different focal depths (z-axis), reconstructing a fully focused three-dimensional image using photo-stacking techniques and visualizing the roughness details of samples (ENCYCLOPÆDIA BRITANNICA, INC. 2024).

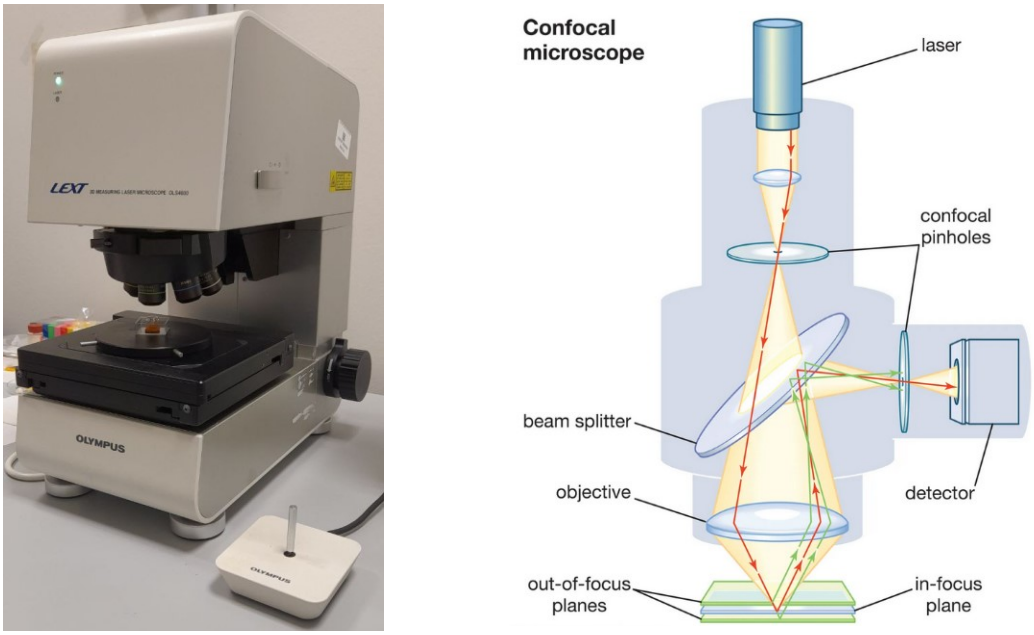

Figure 24 - *Olympus LEXT OLS 4000 3D Laser Measuring Microscope* in the Geoscience department of Padua University (left) and schematic representation of a confocal microscope. (ENCYCLOPÆDIA BRITANNICA, INC. 2024)

The *Olympus* confocal microscope is supplied with 5x 10x 20x 50x and 100x lenses and with the stitching mode the associated software allows to create a mosaic image composed of high magnification single frames. Laser scanning can also measure dimensions, roughness, areas and volumes. This kind of microscope was used to acquire high resolution all focused images of the not-embedded samples to visualize single grains of minerals and appreciate their 3D surfaces.

4.2 VIBRATIONAL SPECTROSCOPIES

Vibrational spectroscopies are non-destructive techniques based on the fact that each molecule has different vibrational properties that depend not only on the types of atoms and chemical bonds that characterise it but also on its geometry in space and its chemical surroundings. Therefore, each spectrum obtained is a fingerprint for the identification of the unknown compound (CAMPANELLA ET AL. 2021).

Raman and infrared spectroscopy allow the identification of both organic molecules and inorganic minerals present in the compound under analysis. They are complementary techniques that can be used in parallel since some vibrational modes are silent in one technique and active in the other following different selection rules. Their coupling with optical microscopes makes it possible to investigate micro areas of heterogeneous samples even with small concentrations of molecules (ARTIOLI 2010).

4.2.1 RAMAN SPECTROSCOPY (RS)

RS is based on the capability of a sample to scatter incident light. Most of the scattered light has the same frequency as the incident light (elastic or Rayleigh scattering), but a small fraction is scattered at different frequencies, lower or higher than the initial frequency (inelastic Stokes and anti-Stokes scattering). (Figure 25). This frequency variation is called Raman shift. When molecules interact with incident radiation, they experience changes in their polarizability, forming an instantaneous dipole. If this distortion of the electron cloud aligns with a possible vibrational state of the molecule, the mode is Raman active (CAMPANELLA ET AL. 2021; ARTIOLI 2010).

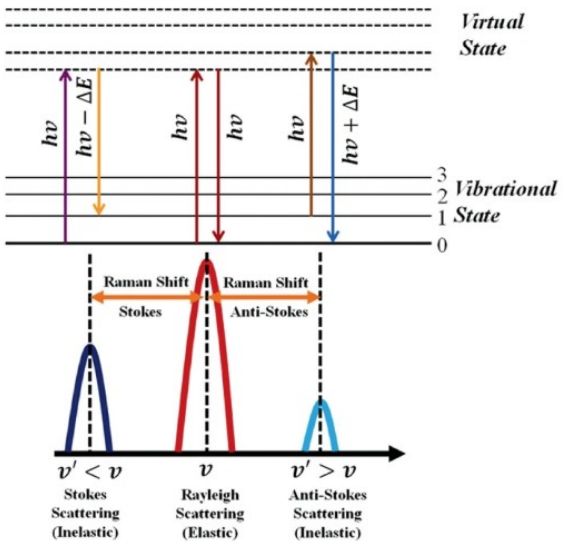

Figure 25 - Diagram representing vibration levels of a molecule involved in an elastic (Rayleigh) and anelastic (Stokes and Anti-Stokes) scattering (PANDEY ET AL. 2021).

The light source of a Raman spectrometer is usually a He/Ne laser which beam is converged into an optical system with different possible magnifications and send to the sample. The scattered signal is detected by a spectrophotometer with a grating device to record the intensity of Rayleigh scattering. To have better spectra modern instruments are equipped with a Michelson interferometer and the signal to noise ratio is improved thanks to Fourier transformed signal Fig. (ARTIOLI 2010).

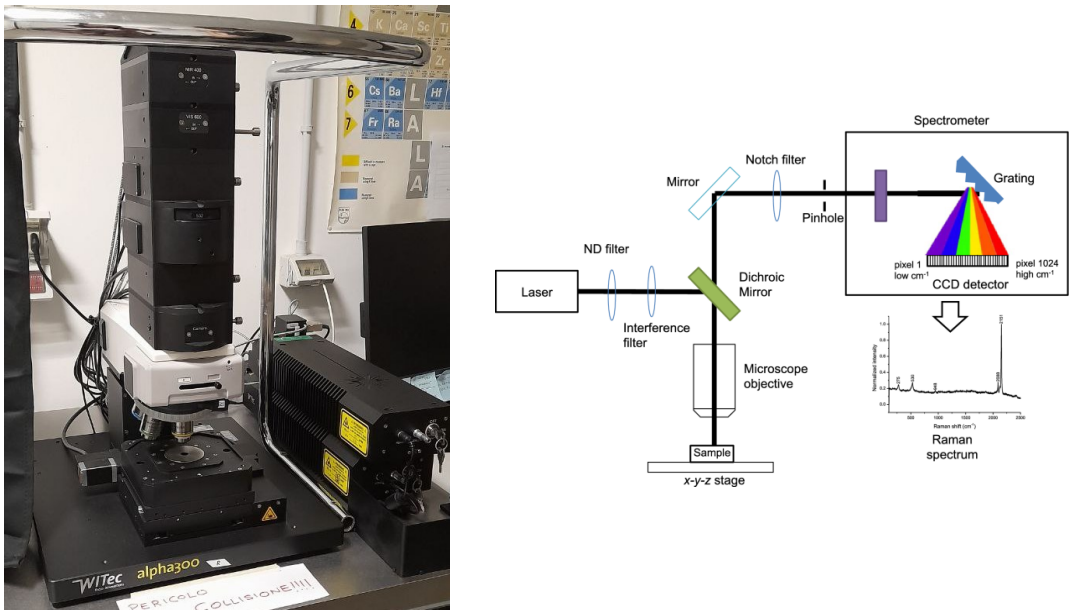

Figure 26 - Raman spectrometer WITec alpha300 R at the Geoscience department equipped with 532 nm and 785 nm lasers (left) and schematic diagram of Raman instrument (right) (CAMPANELLA et al. 2021).

Raman spectroscopy is better in the identification of pigments which have signals at low wavelengths, often not easily reachable by FTIR and the laser Nd/YAG at 1064 nm makes it possible to overcome the problem of fluorescence often present in aged organic materials constituting cultural heritage (ARTIOLI 2010).

During this research micro-Raman single grain technique was of paramount importance to identify the mineralogical phases constituted by really tiny mineral grains in the samples.

To have appreciable spectra, 50x and 100x objectives were adopted, accumulation and integration time were optimized to obtained the best signal to noise ratio and the power of laser was set in order not to alter or burn the grains.

To obtain an image in false colours useful to look visually at the phases and the reaction borders present in some samples the function mapping was used.

4.2.2 FOURIER TRANSFORMED INFRARED SPECTROSCOPY (FTIR)

IR absorption spectroscopy exploits infrared radiation that has wavelengths (in the range 4000 cm^{-1} - 400 cm^{-1} usually) equal to those required to induce vibrational transitions in molecular chemical bonds. For a mode to be IR active, there must be a change in the dipole moment of the electric charge and the energy absorbed must be equal to the difference between one vibrational mode and another (Figure 27) (BERTHOMIEU, HIENERWADEL 2009).

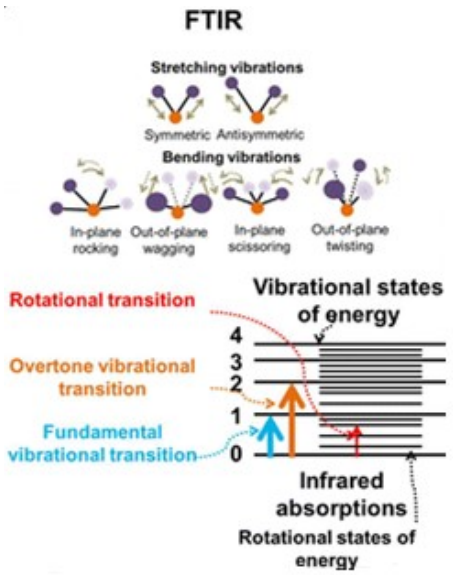

Figure 27 – Types of vibrations and vibrational energy levels involved in FTIR (DOMÉNECH-CARBÓ AND OC 2016).

The dispersive mode is no longer widely used, and as with Raman, modern IR spectrometers (Fig.) are equipped with a Michelson interferometer, and the absorption spectrum is reconstructed using the Fourier transform (FT), resulting in a marked improvement in spectral resolution and sensitivity (ARTIOLI 2010).

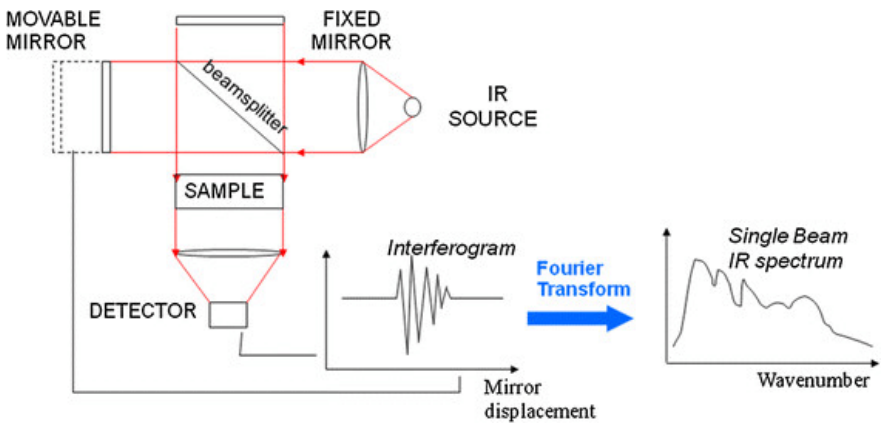

Figure 28 - Diagram representing a FTIR spectrometer with the resulting spectrum (MEZZETTI AND LEIBL 2017).

FTIR spectra can be obtained through various measurement geometries. The absorption mode measures the attenuation of the incident beam as a function of frequency expressed in wave numbers (cm^{-1}). When the mode in transmission is impossible as for thick sections, absorption spectra can be measured in reflectance geometry. In the presence of minute amounts of untouchable sample, data can be collected through reflection or diffuse reflectance Fourier transform spectroscopy (DRIFT) in a totally non-invasive manner. While the attenuated total reflectance technique (ATR) involves pressing the liquid or solid sample against the surface of a crystal, usually germanium, zinc selenide or diamond. In this mode the infrared light encounters the interface between the crystal and the sample being totally internally reflected. This reflection creates an evanescent wave that penetrates a few micrometres into the sample (Figure 29) (ARTIOLI 2010).

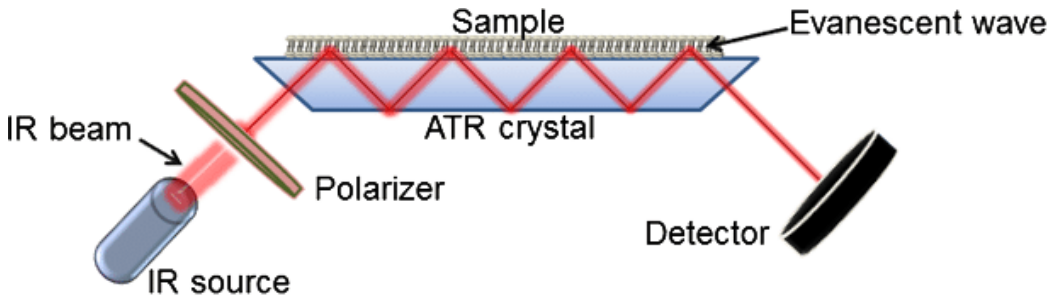

Figure 29 – Representation of ATR-FTIR system. (AUSILI A. ET AL. 2015)

FTIR spectroscopy is sometimes more effective than Raman spectroscopy in analysing fluorescent materials such as aged organic materials found in cultural heritage. (ARTIOLI 2010) Therefore, on the sample of the Ortolano painting that had low Raman spectra, we tried to perform some FTIR measurements in both reflection and ATR mode (Figure 30) where possible to understand the composition of some organic parts, such as varnishes.

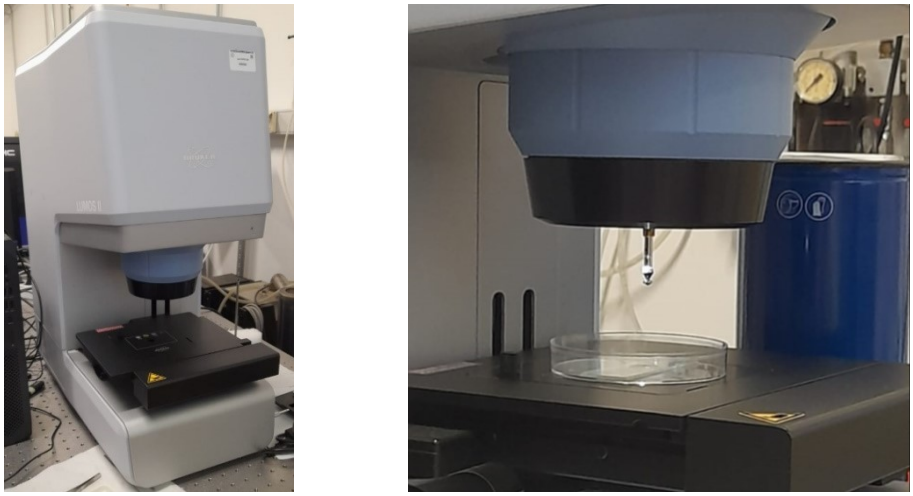

Figure 30 – *Bruker LUMOS II* FTIR spectrometer with the retractable crystal for ATR analysis.

4.3 SCANNING ELECTRON MICROSCOPY (SEM)

The SEM (Figure 31), unlike the OM, which uses visible light channelled through optical lenses to magnify the sample up to a maximum of 1000x, exploits an accelerated electron beam at 102-104 eV, with a wavelength of 0.123-0.012 nm, which allows for a magnification of up to 100 000 times. The incident beam is synchronised with the detector, which collects at each point the signal resulting from the interaction of the electron beam with the sample (ARTIOLI 2010).

The interaction of the incident electron beam generates a teardrop-shaped reaction vessel wherein different phenomena take place (Figure 31) that require specialised detectors to be used. The main ones are high-energy backscattered electrons from the sample originating from the beam, low-energy secondary electrons emitted by the atoms in the sample and characteristic X-rays (ARTIOLI 2010).

The number of secondary electrons emitted by the sample surface depends on the inclination and orientation with respect to the incident beam, having more electrons emitted if the surface is facing the detector and less if its inclined away from it which results respectively on the image in lighter areas, where more electrons were emitted and darker areas with less ones. Moreover, as the angle increases, the escape distance for secondary electrons decreases on one side, leading to more electrons being emitted and detected making steep surfaces and edges appear brighter than flat surfaces. These differences produce a well-defined three-dimensional effect in SEM images, highlighting topographical details of the sample. (ARTIOLI 2010; JIANG et al. 2019)

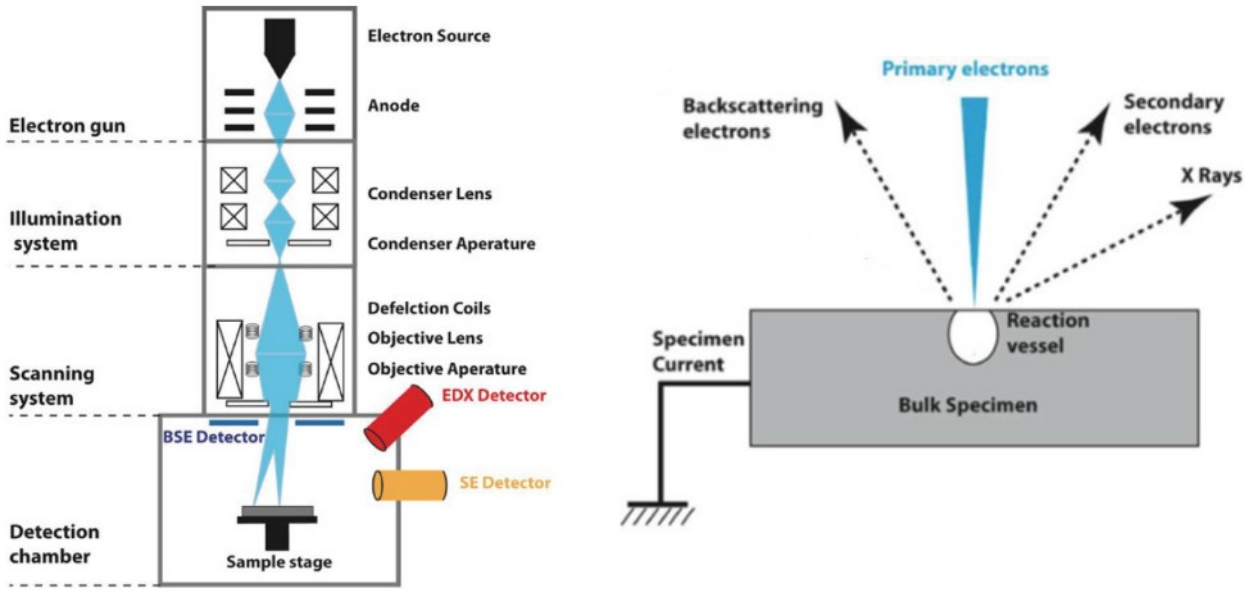

Figure 31 - Schematic representation of the principal components of a SEM (left) and the different types of main interactions between the incident electron beam and the specimen (right) (Modified after JIANG ET AL. 2019).

Backscattered electrons also create images that highlight the 3D surface of the specimen with contrast determined not only by the angle between the surface, the incident beam and the detector but also by the presence of heavy elements which appear brighter because they backscatter electrons more strongly than light elements. The energy dispersive spectrometer (EDS) permits to detect characteristic X-rays of elements with the possibility of map elemental distribution of materials (ARTIOLI 2010).

Samples must be analysed in vacuum to avoid scattering and absorption from air particles; they require also to be coated with metal for imaging and graphite for chemical analysis to avoid charging accumulation. If the samples cannot be coated or are hydrated, measurements can be performed at low pressure (up to 2.5 kPa) with environmental scanning electron microscopes (ESEM) (ARTIOLI 2010).

Having wanted not to coat the samples in order to have the possibility of carrying out other spectroscopic analyses, the polished sections containing Egyptian blue were analysed with ESEM (Figure 32) by extrapolating both secondary electron images and EDS false-colour maps showing the elements present.

Figure 32 - ESEM *FEI Quanta 200* at the CEASC of University of Padua.

5. Samples description and preparation

5.1 RENAISSANCE SAMPLES

5.1.1 ORTOLANO SAMPLE

The sample "**KMSsp7 Ortolano"** in two fragments (Figure 33) kindly provided by Dr. Troels Filtenborg was extracted from the painting *Saint Margaret* (Fig.) preserved at the deposit of Staten Museum for Kunst (SMK) of Copenhagen in Denmark.

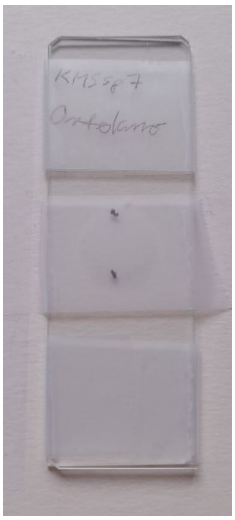

Figure 33 - The two fragments of KMSsp7 Ortolano sample enclosed between two concave microscope slides.

This sample was taken from the left sleeve of the Saint (Figure 34) were previous visible-induced luminescence (VIL) analysis have shown strong signal (Figure 35) (BREDAL-JØRGENSEN ET AL. 2011).

Figure 34 - Yellow arrow indicates the location of the sampling (courtesy of Troels Filtenborg).

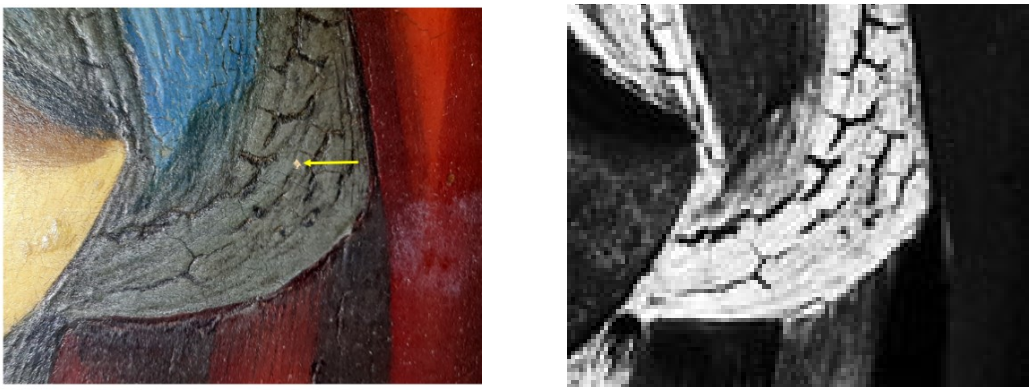

Figure 35 - Detail of the sleeve showing the sampling location (courtesy of Troels Filtenborg) and Corresponding VIL image of the sampling area (modified after (Bredal-Jørgensen et al. 2011)).

The analysis of the cross section from a similar sample, with a comparable appearance revealed the following stratigraphy: gesso ground stratum, very thin unpigmented layer, imprimitura containing lead white and tin yellow, a layer of azurite mixed with an organic red and at the top a degraded layer with brownish and transparent areas of ultramarine mixed with cuprorivaite and a little black. (Information provided by Troels Filtenborg).

The preliminary Raman measurements performed in Belgium with micro-Raman (Figure 37) on one (Figure 36) of the two fragments thanks to the help of Gert Nuyts in Prof. Koen Janssens' laboratories in Antwerp gave poor results since the Raman signal was covered by fluorescence due to the deteriorated organic part of the pictorial sample.

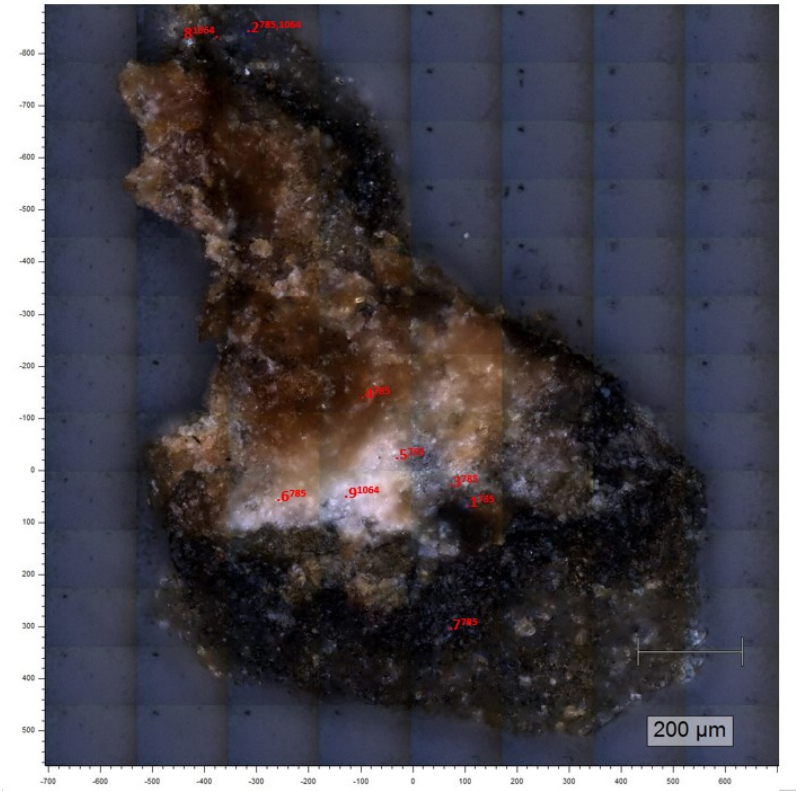

Figure 36 - Stitching image of the fragment analysed done with the micro-Raman with indication of points analysed.

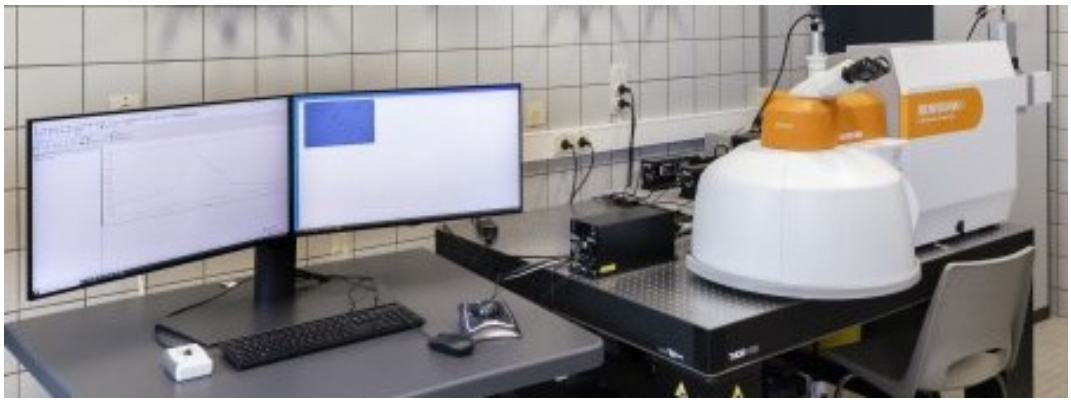

Figure 37 - Renishaw® InVia™ Qontor Raman microscope at University of Antwerp.

The Raman spectrometer was equipped with four different laser sources at 405 nm, 532 nm, 785 nm and 1064 nm. The first two lasers gave too much fluorescence while the other two permitted the acquisition of the spectra but of low quality with fluorescence bands due to the organic parts of the sample and not clearly distinguishable peaks.

The spectra of 1064 nm laser source gave really noisy spectra with just a few peaks visible at 544,2 cm^{-1} and 1008 cm^{-1} which as visible from the (Figure 38) can be reconveyed to gypsum and natural ultramarine pigment. The only really small peaks that can be seen in the spectra acquired with 785 nm are at 549 cm^{-1} and 1009 cm^{-1} which can be again to the presence of lazurite mineral, the principal component of lapis lazuli pigment a to gypsum. (Figure 39).

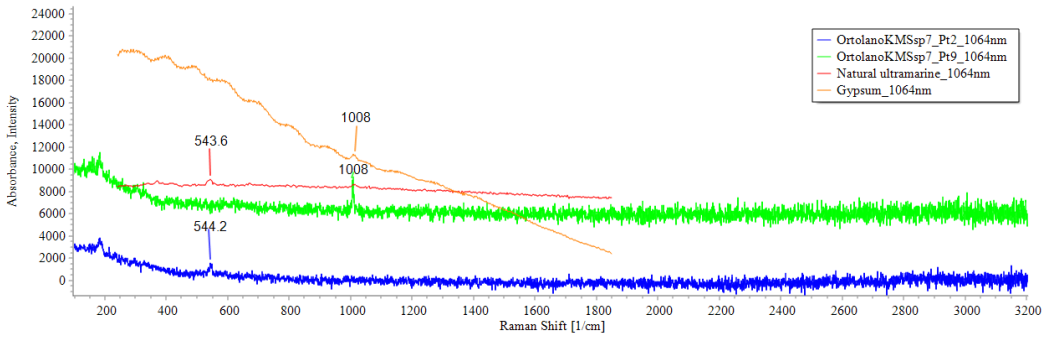

Figure 38 - Spectra acquired with 1064 nm laser source compared to the ones of natural ultramarine and gypsum.

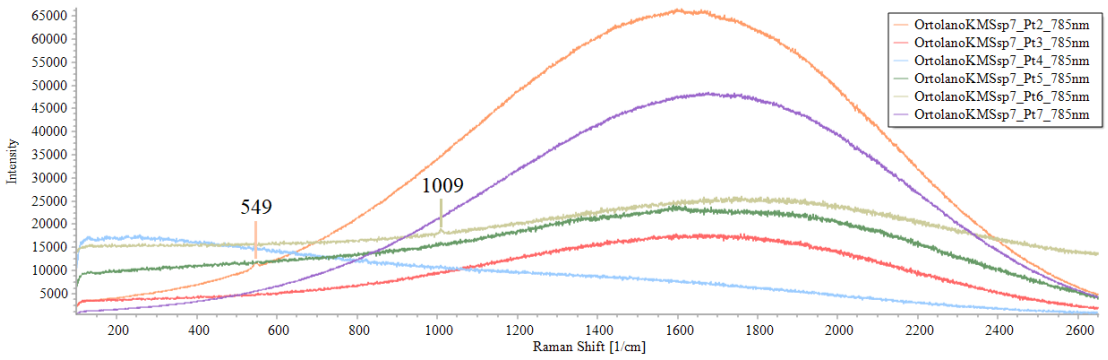

Figure 39 - Spectra acquired with 785 nm laser source.

Given the difficulties encountered in Antwerp on the intact fragment in Padova it was decided to use the other piece that had broken off to test whether the Raman signal would give better results.

The small particles were spread by Prof. Artioli on 3 small aluminium stubs (Figure 40) using a small platinum rod under stereomicroscope. All the stubs were fixed with play dough inside three square plastic boxes to protect them, the three cases were put into a small cardboard box to facilitate transportation.

The three stubs were prepared differently but, in each case, allowing for eventual later handling of the fragments. On the first stub (sample No. 1) a piece of carbon conductive tape was applied with a small piece of glass on top of it on which the fragments were placed. On the second stub (sample No. 2) also covered with a piece of carbon conductive tape a piece of aluminium foil was attached and finally placed the sample pieces. The remaining part of sample was placed directly on the third stub (sample No. 3).

Figure 40 - From the left: sample No.1 on glass, sample No.2 on aluminium foil, sample No.3 directly on stub.

The three sample were observed under the confocal microscope to map the distribution of the particles. For each sample, a stitching map was made (Figure 41) to visualize the groups of fragments facilitating the subsequent Raman and SEM analyses.

Subsequently almost each group of particles was photographed at higher magnifications and mapped onto the stitching done earlier by serving coloured and numbered squares with the same numbering as the zoomed images (Figure 41).

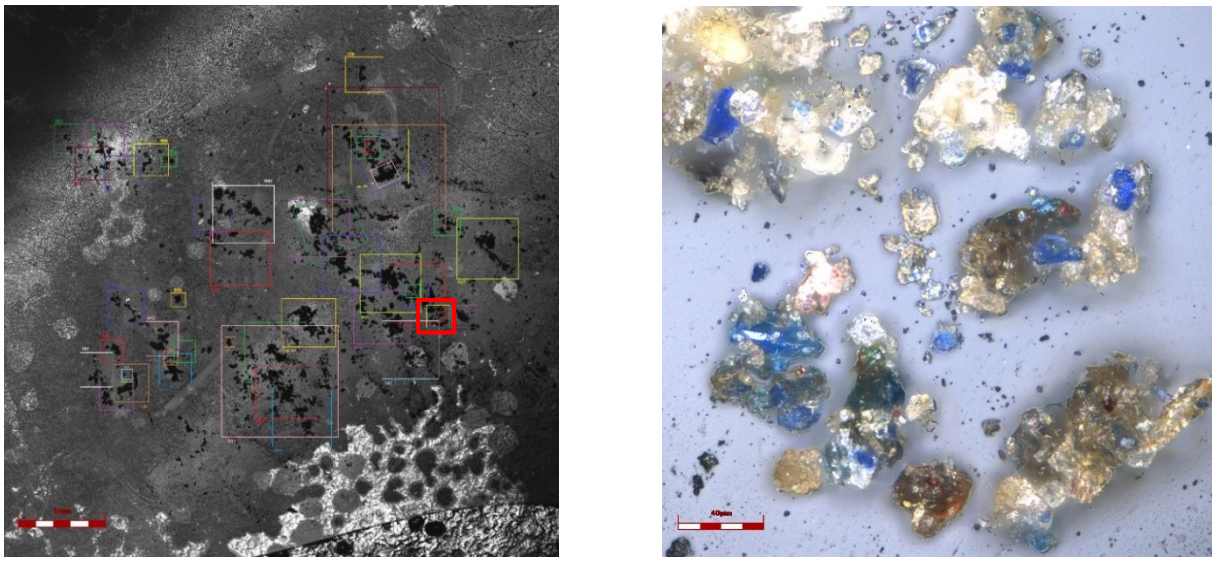

Figure 41 - Confocal microscope stitching image (scale 1 mm) of sample No. 1 with numbered squares referring to related magnifications and an example of a magnified area (red square on left image).

The initial idea was to identify the Egyptian blue particles, collect them to perform lead isotopic analysis (LIA) in order to understand the provenance of the pigment comparing the isotopic ratios of lead associated with copper present in the cuprorivaite of our samples with data tabulated in the literature.

The other fragment remained intact was photographed entirely with confocal microscope (Figure 42) in order to have a general idea of the stratigraphy and some specific areas were also imaged at high magnifications (Figure 42).

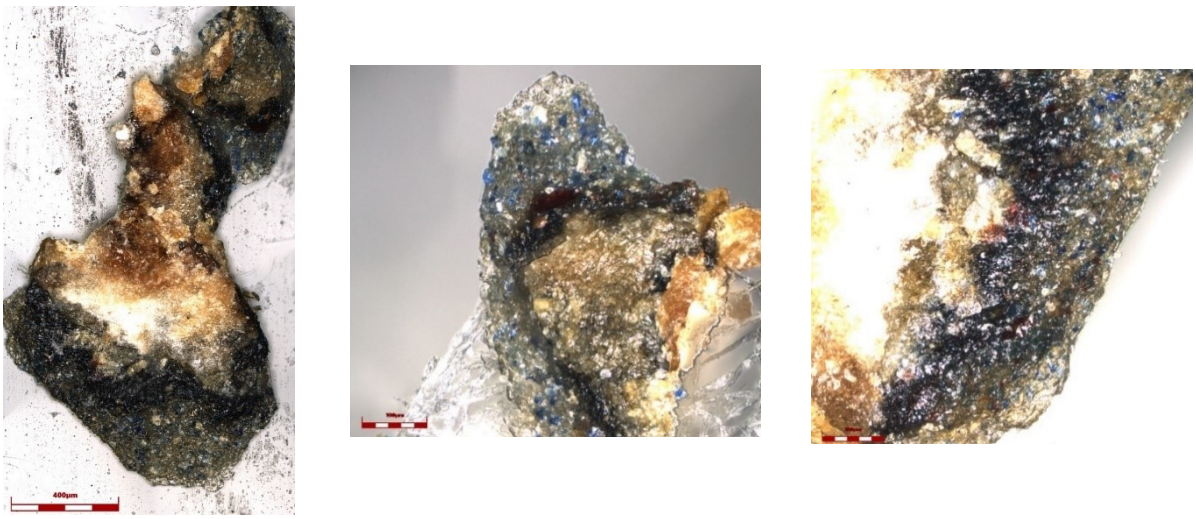

Figure 42 - Confocal microscope image of the fragment “entire” of Ortolano (left) with 2 magnified areas (centre and right).

Given the difficulties encountered in the manipulation of the sample and especially with Raman analysis (see next chapter) due to the rugosity of the sample and the tiny dimension of the mineral grains, a small fragment with the same stratigraphy of "Ortolano entire sample" was embedded in resin.

The tiny fragment, selected under the stereomicroscope was embedded in a two-component clear epoxy adhesive Araldite ® 2020 mixing 10 parts of component A and 3 parts of component B, in particular 10g of A and 3g of B and then let dry in the oven at 40°C for 10 hours. Then it was put on a vacuum pump to remove eventual bubbles.

Finally, the sample was removed from the cylinder used to embed it in the resin, it was smoothed on the back through a 1200 grit silicon carbide abrasive disc, polished for 3 minutes on a cloth using a 1 micron diamond suspension (Figure 43), and then polished further for 2 minutes with the same suspension (Figure 43).

Figure 43 - From the left bi-component Araldite ® resin, diamond suspension and polisher.

The sample was later photographed with confocal microscope and polarizing microscope with parallel, staggered and crossed Nicols (Figure 44).

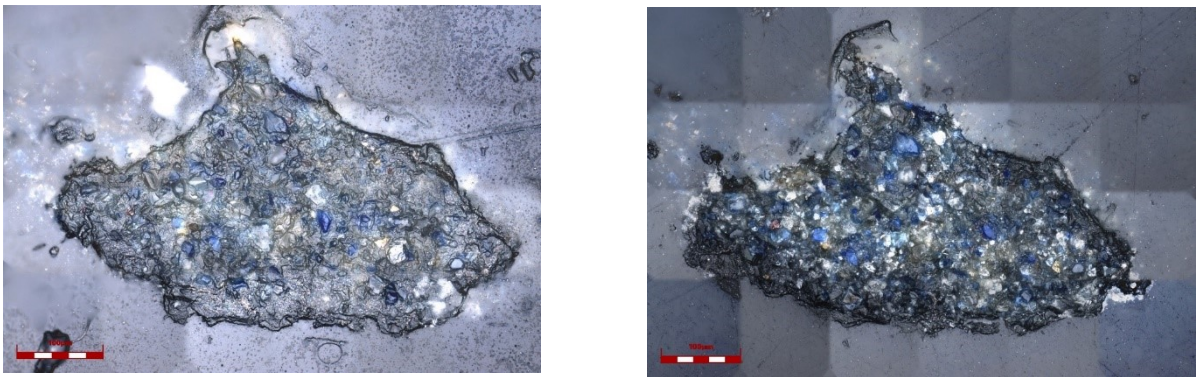

Figure 44 - Confocal microscope pictures of the tiny fragment of Ortolano embedded in resin after the first polishing and after the second one.

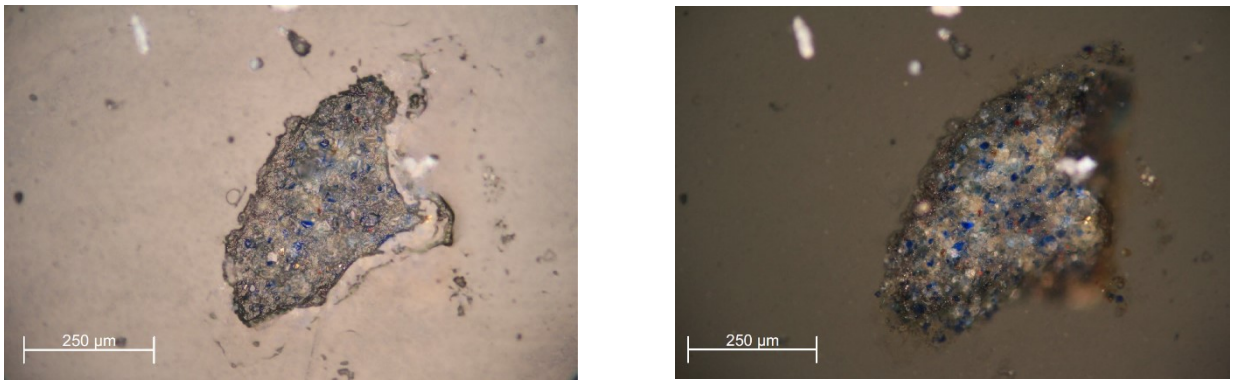

Figure 45 - Polarizing microscope image of Ortolano embedded samples with staggered (left) and crossed Nicols (right).

5.1.2 RAPHAEL SAMPLE

The other unique and precious Renaissance sample (Figure 46) was graciously supplied by Prof. Giancarlo Sidoti and is preserved at the archive of Istituto Centrale del Restauro in Rome. It was extracted from a scene in "Loggia of Cupid and Psiche" (Ill.) painted by Raphael in Villa Farnesina in Rome.

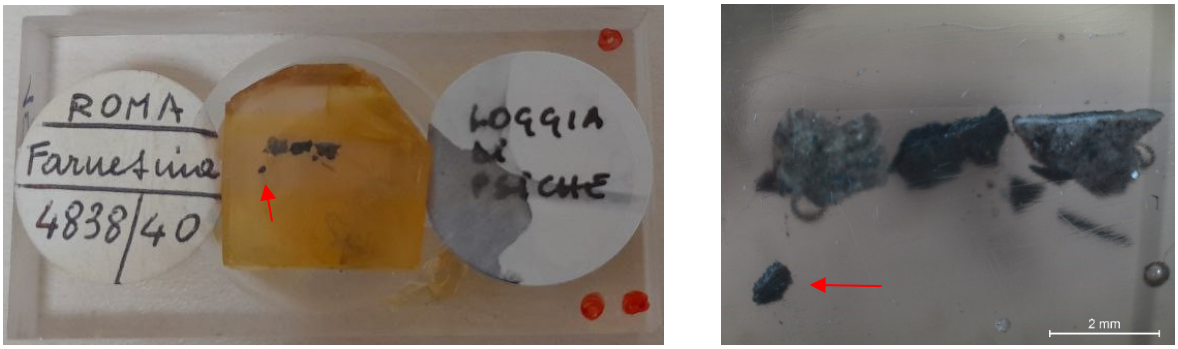

Figure 46 - Section 4838/40 from The Loggia di Psiche of Villa Farnesina in Rome (left) and its magnification acquired with stereomicroscope (right) (courtesy of Dr. Giancarlo Sidoti).

The exact location of the collecting of the sample No. 4838/40 from 'Psyche's Lodge' is not certainly identified although in the ICR archive the sampling point is recorded as the upper corner nail in the sail with Cupid pricking his finger (Figure 47) (SIDOTI ET AL. 2018).

Figure 47 - Detail of the spandrel with Cupid pricking his finger.

The specimens embedded in the section of polyester resin No. 4838/40 were previously analysed with VIL technique that revealed the presence of EB in three of the four fragments.

Two of the fragments embedded in the resin block have already been analysed. The leftmost large one positioned flat (Figure 48) has a light blue layer, while in the central fragment (Figure 49) there are two different light blue strata, 100 microns thick. In both cases, VIL investigation revealed the presence of EB whose crystals are 80-100 microns in size. As for the other blue pigment present in the central fragment from SEM-EDS analysis (Figure 49) it turns out to be azurite with grains 10-20 microns in size (SIDOTI ET AL. 2018).

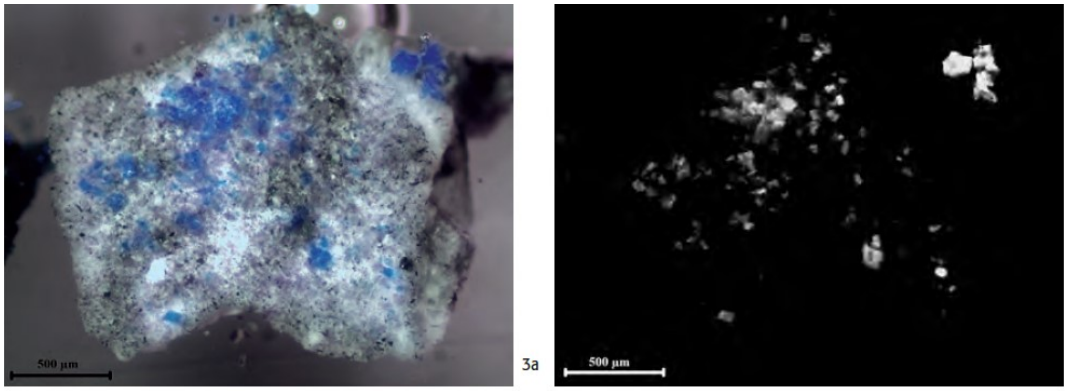

Figure 48 - Fragment flat positioned observed with OM (left) and its VIL image (right) (SIDOTI ET AL. 2018).

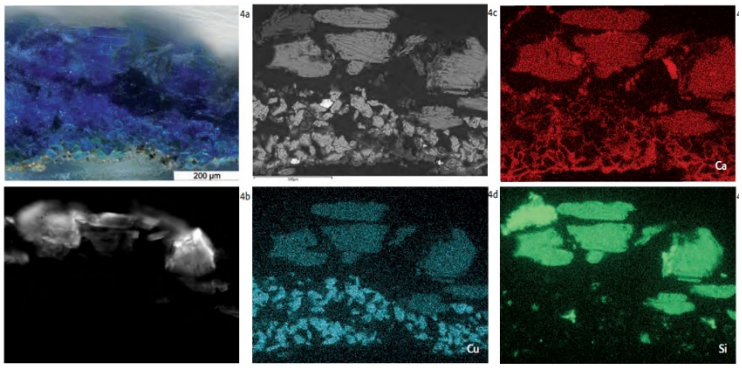

Figure 49 - Optical image of vertically positioned fragment (up-left), VIL image (down-left), SEM image (up-central), EDS maps of calcium (up-right), copper (down-central) and silicon (down-right) (SIDOTI ET AL. 2018).

Since these two fragments have already been analysed and the results published, they need to be carefully preserved in the ICR archive. The usable sample was the tiny oblique fragment on the lower left of Figure 46 (marked by an arrow), which has revealed from previous VIL investigation to have the presence of EB grains Figure 50.

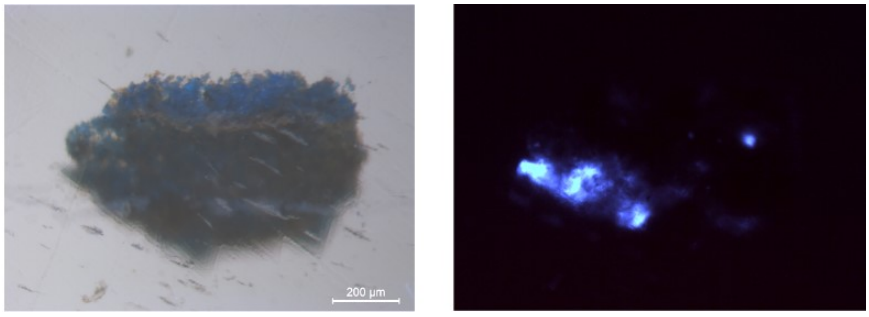

Figure 50 - Magnification of the tiny fragment (left) and the correspondent VIL (courtesy of Dr. Giancarlo Sidoti).

The small fragment was later photographed with confocal microscope which can visualize just the exposed part of the fragment mainly composed of azurite particles with EB particles probably under the resin's surface.

Figure 51 - Detail of the polished section after the removal of the small fragment.

In order to expose the area with the presence of EB and preserve the other untouchable samples it was decided to take off from the polished section the tiny fragment.

To do this delicate operation a mini core drilling was performed using a Dremel with a small core drill bit of about 1 mm of diameter (Figure 52). The tiny fragment was embedded in resin like Ortolano sample and then photographed with polarizing (Figure 53) and confocal microscope (Figure 54).

Figure 52 - The small core drill bit used to extract the tiny fragment.

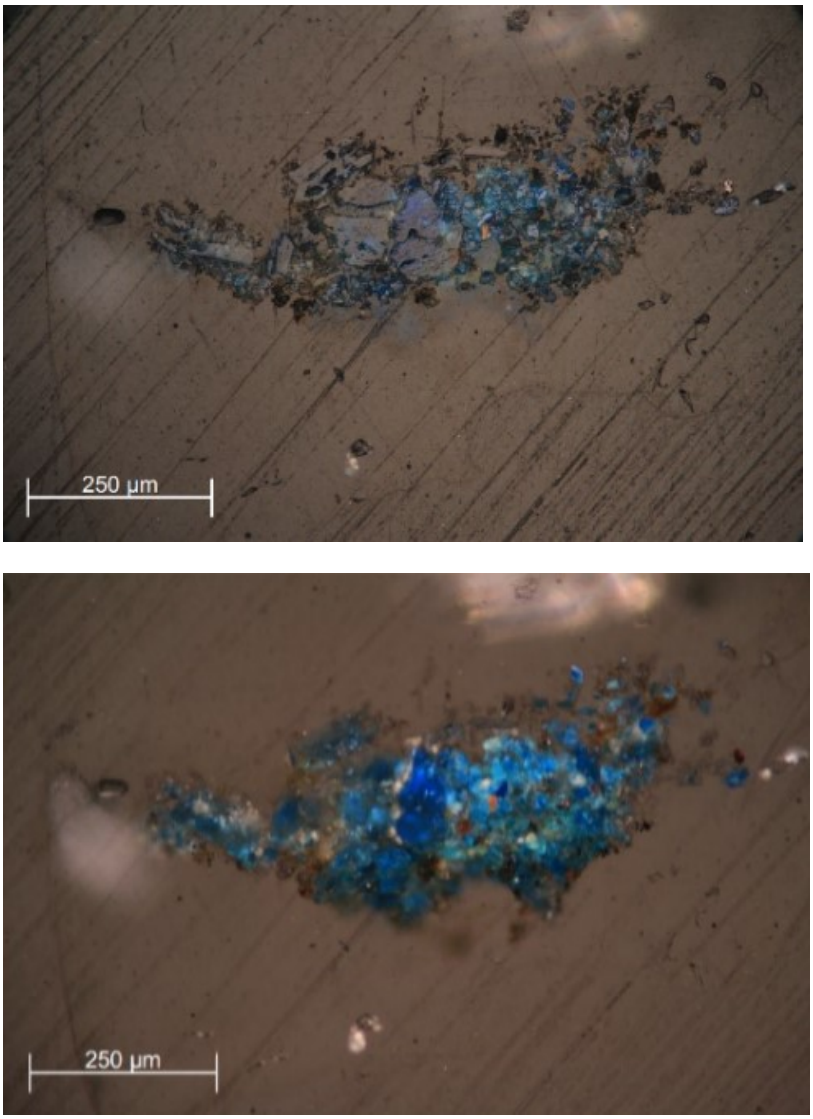

Figure 53 - Polarizing microscope images with staggered (up) and crossed (down) polars.

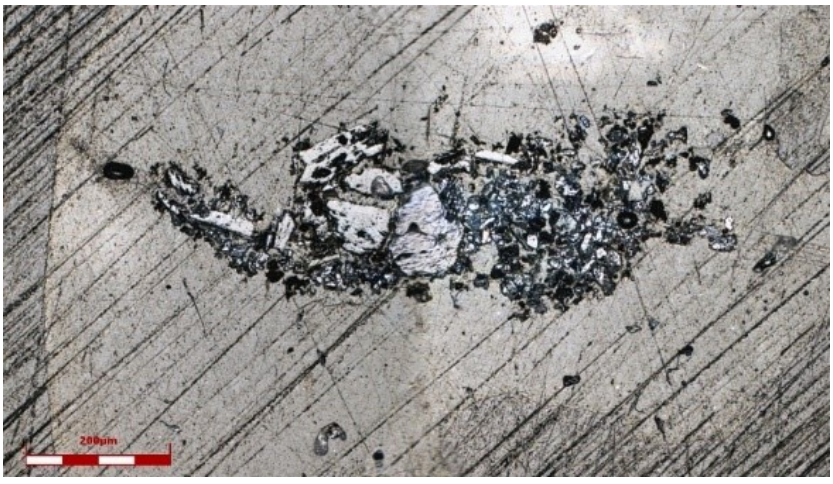

Figure 54 - Confocal microscope photograph of Raphael sample.

5.2 ROMAN SAMPLES

Two ancient Roman samples from Ostia (Rome) and Liternum (Naples) present at Geoscience department of Padua university were also analysed for reference and comparison purposes. Both samples have been embedded in the same polished section.

To understand the composition, the degree of purity and the reaction front in the two reference samples, both point analyses and Raman mapping were carried out and later SEM.

5.2.1 OSTIA SAMPLE

Ostia sample is a small fragment of raw Egyptian blue (Figure 55).

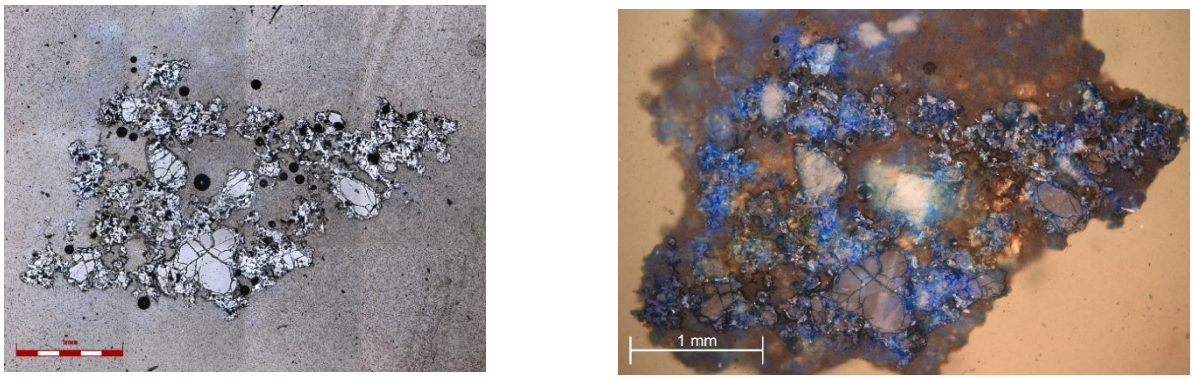

Figure 55 - From the left confocal image and polarizing microscope image in crossed polars of Ostia sample.

5.2.2 LITERNUM SAMPLE

Liternum sample is constituted by a fragment of EB raw pigment still attached to a fragment of terracotta crucible visible on confocal image (Figure 56).

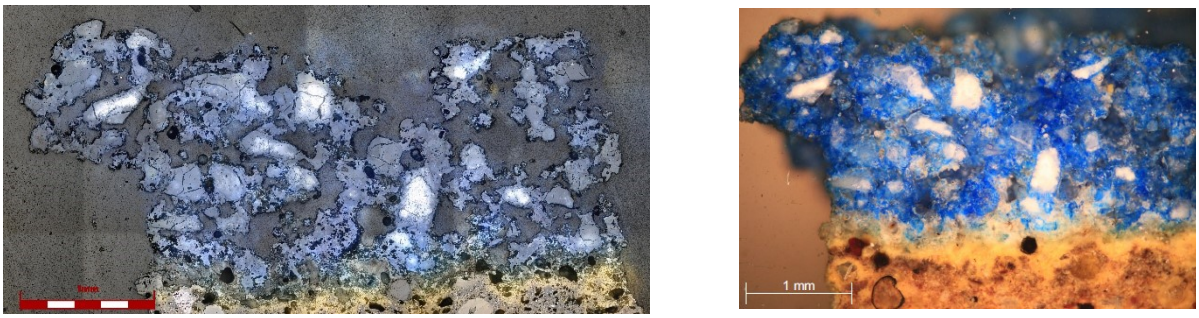

Figure 56 - Confocal and polarizing microscope image in crossed polars of Liternum sample.

5.3 LeFranc samples

LeFranc samples from 1929 and from 1937 were kindly provided by Doctor Giovanni Verri.

Commercial Egyptian blue LeFranc sample grains from 1929 were observed with confocal microscope and a stitching map was created giving the possibility to localize easily the single fragments for future analysis.

Figure 57 - Egyptian blue pigment by LeFranc© from 1929 (on the left) and 1937 (on the right).

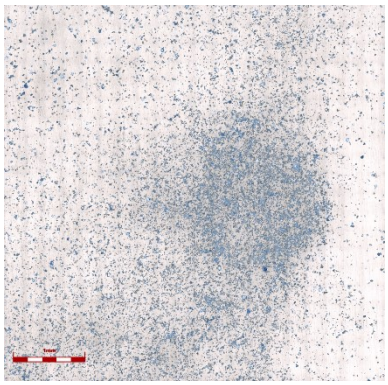

Figure 58 - Stitching map of LeFranc sample from 1929 made with confocal microscope software.

For now, only some spot Raman analysis has been done to have a reference standard for cuprorivaite. Below is a summary table of the samples analysed (Table 6).

Type	Name	Description	Performed analysis
Renaissance samples	**KMSsp7 - Ortolano**	Entire fragment	Raman
		1 – fragmented sample on glass	Raman
		2 – fragmented sample on Al foil	-
		3 – fragmented sample on stub	Raman, SEM
		Part of "entire fragment" embedded in resin	Raman, ESEM
	4838/40 - Raphael	Fresco fragment embedded in resin	Raman, ESEM
Commercial pigment	**B127 - Lefranc & Cie©1929**	EB powder	Raman
	B128 - Lefranc & Cie©1937	EB powder	Raman
Roman samples	**EB - Ostia**	Fragment in epoxy resin	Raman, ESEM
	EB - Liternum	Fragment in epoxy resin	Raman, ESEM

Table 6 - Summary table of the analysis performed on the samples.

6. Analysis

6.1 RAMAN ANALYSIS

For Raman analysis a 532 nm laser source was used, with variable number of accumulations, integration time and power of the source according to the mineral involved in the analysis. Because some minerals are more resistant than others to degradation and have stronger Raman signals with less source power.

On each sample many point analysis were performed in order to detect and identify cuprorivaite crystals and the associated mineral components constituting the samples. For each sample the images taken with the microscope incorporated on the Raman instrument are reported, together with the point analysis and relative spectra compared with reference mineral spectra.

6.1.1 ORTOLANO SAMPLE

The Ortolano sample was the most difficult to analyse because it is a tiny fragment of an oil painting, with a complex organic matrix: a number of different minerals and substances are present. The optical detection of cuprorivaite crystals is visually complex since two other blue pigments, azurite and lapis lazuli, are also present. Not only they can be optically confused with cuprorivaite because of the colour, but also the EB crystals are aften very thin, so that the laser beam penetrates them completely, revealing the underlying minerals that often have a stronger Raman signal.

Initially, a few analysis points were made on the "Ortolano glass" sample with a view to possibly extracting the cuprorivaite grains for the isotopic analysis This proved impossible due to the small quantity of the sample and the consequent scarcity of cuprorivaite grains.

An attempt of analysis was done also on "Ortolano entire sample" but the analysis was difficult due to the scarcity of pigment signal over the noise produced by fluorescence of the sample matrix.

For these reasons a fragment near "Ortolano entire sample" with the same stratigraphy was embedded in resin.

Some of the Raman results are represented with first the point analysis and then the correspondent spectra.

6.1.1.1 ORTOLANO GLASS SAMPLE

In this sample it was possible to identify lead tin yellow pigment as already attested by previous published studies (BREDAL-JØRGENSEN ET AL. 2011).

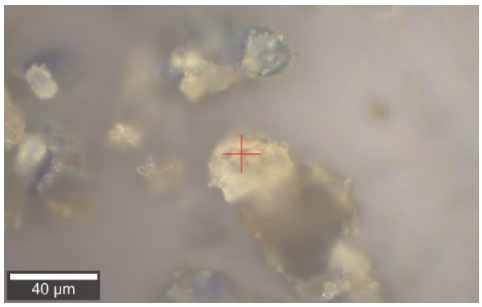

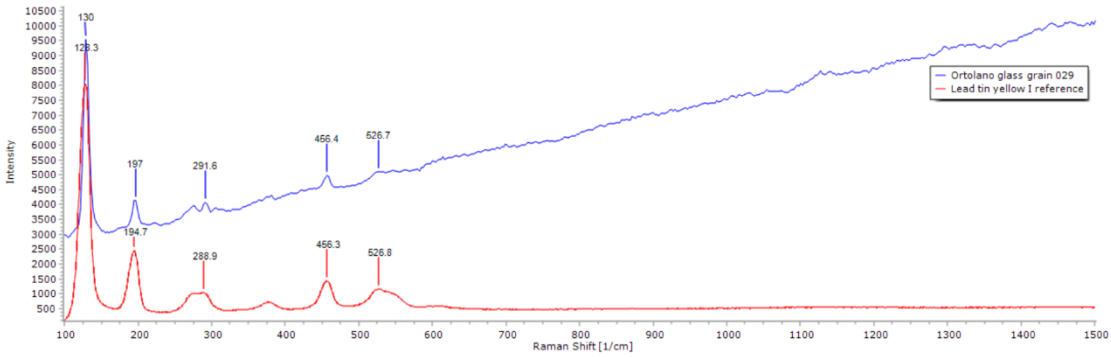

It was found also a grain of red colour which can correspond to a red organic dye like carmine lake even if Raman is not resolutive. The presence of it in the painting was already cited in the paper regarding Ortolano's Saint Margareth analysis (BREDAL-JØRGENSEN ET AL. 2011).

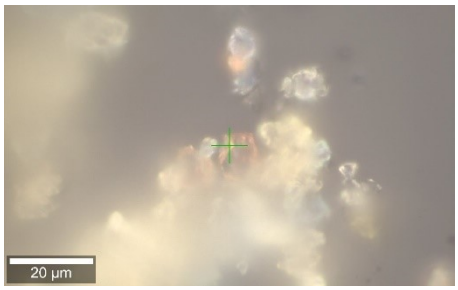

The presence of azurite and lapislazuli in Ortolano sample was confirmed by Raman point analysis. Here are reported two examples of point analysis acquired.

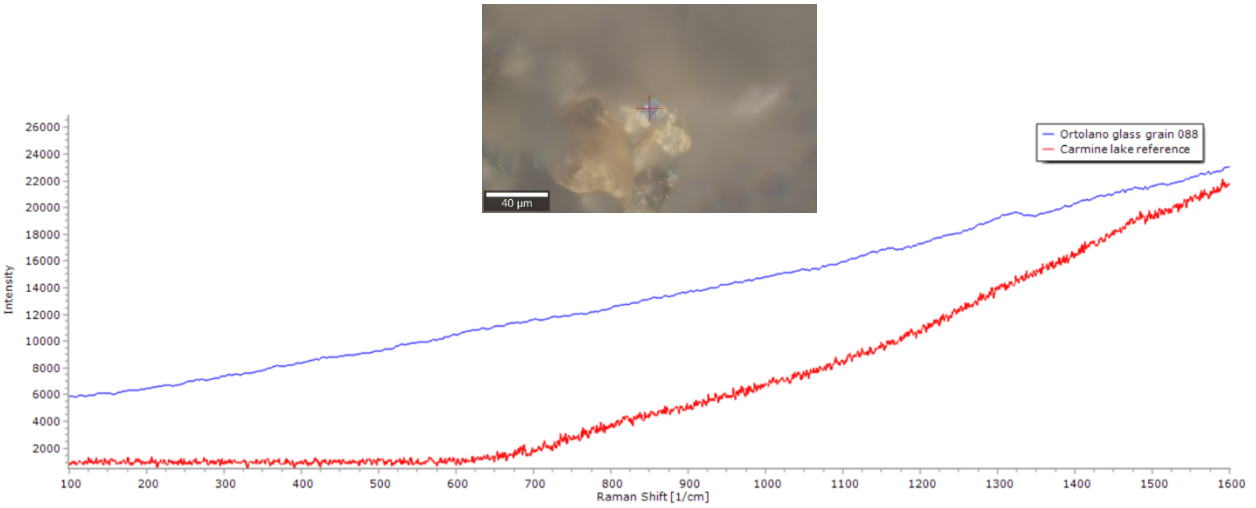

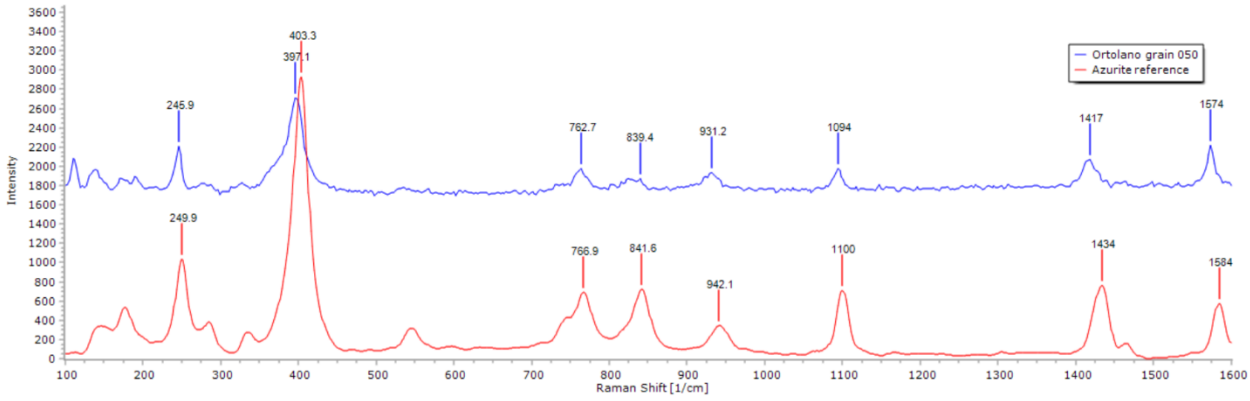

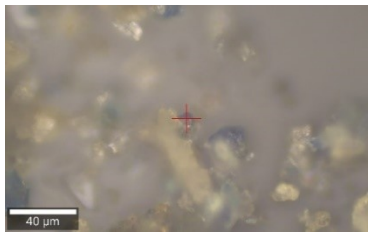

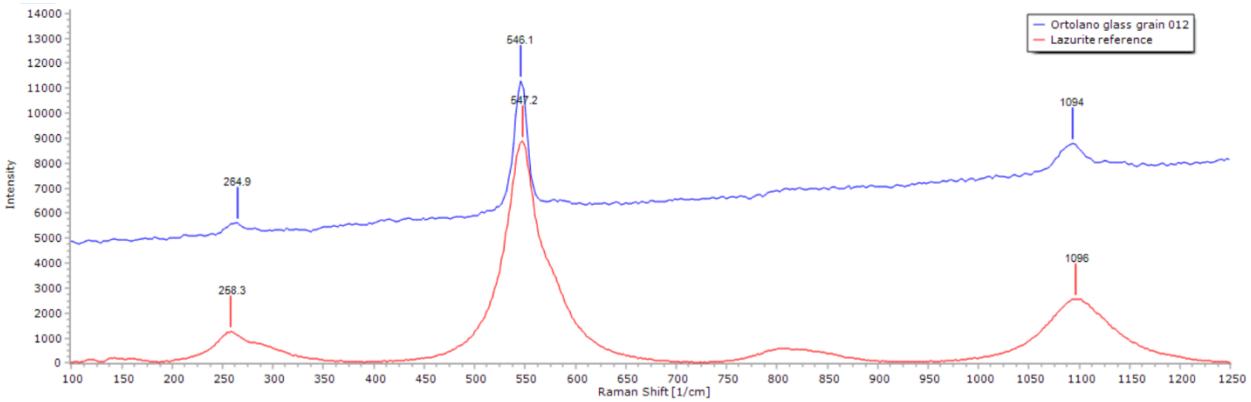

6.1.1.2 ORTOLANO RESIN SAMPLE

Thanks to the embedding in the resin of the Ortolano sample it was possible to identify cuprorivaite grains to perform subsequent SEM analysis.

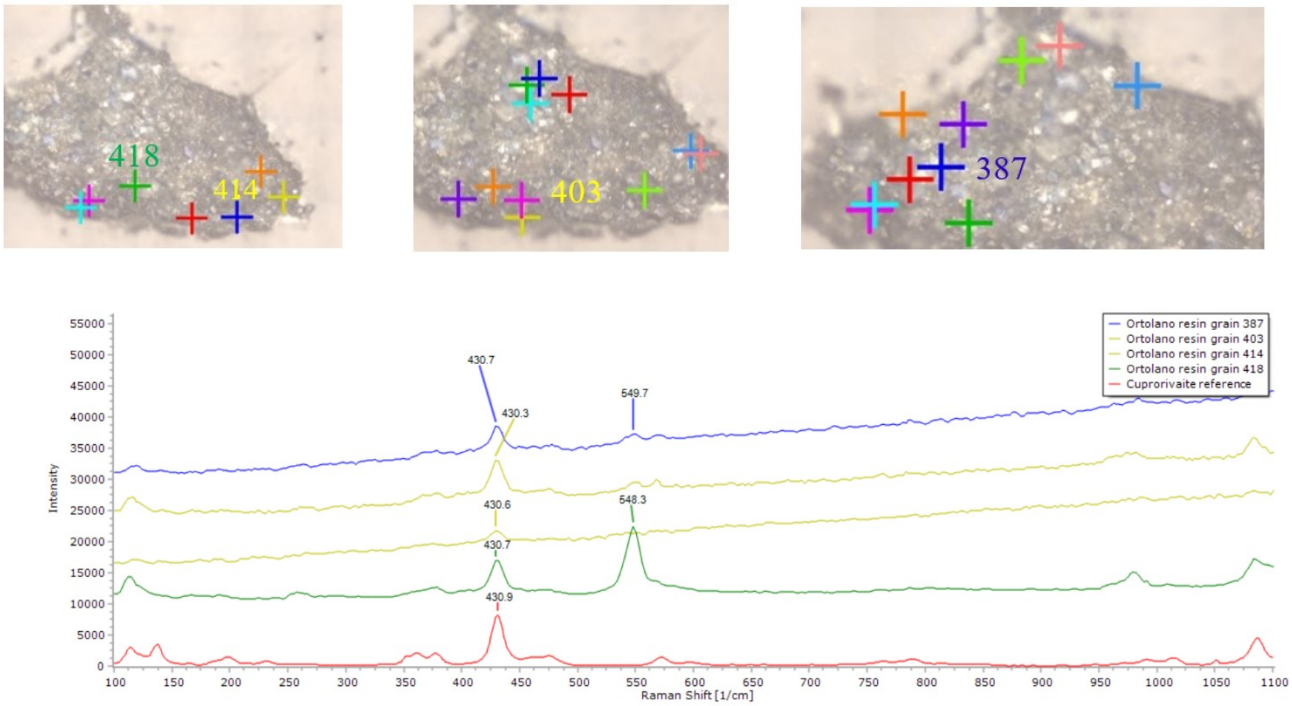

6.1.2 RAPHAEL SAMPLE

To know where the crystal of cuprorivaite were concentrated, before the drilling operation from the resin, many Raman point analysis were done. In Figure 59 cuprorivaite crystals are circled in red while azurite is circled in yellow, calcite in green, quartz in pale azure and anatase in dark yellow. The spectra identified before coring are shown below with azurite spectra in Figure 60 and cuprorivaite spectra in Figure 61.

Once denoted the area with EB grains with Raman analysis, the drilling was done and then the small fragment embedded in the resin in a proper position in order to have the cuprorivaite crystals exposed.

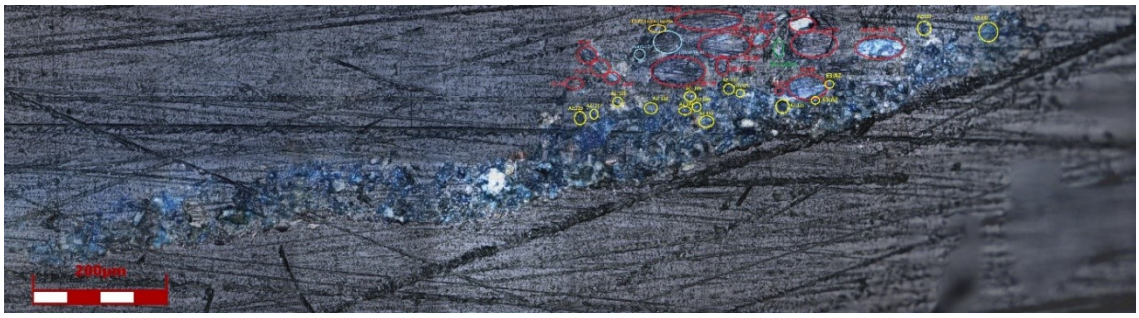

Figure 59 – Confocal microscope image of Raphael grain embedded in the old resin of ICR.

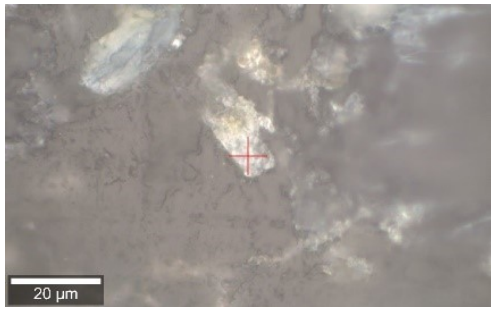
20 µm

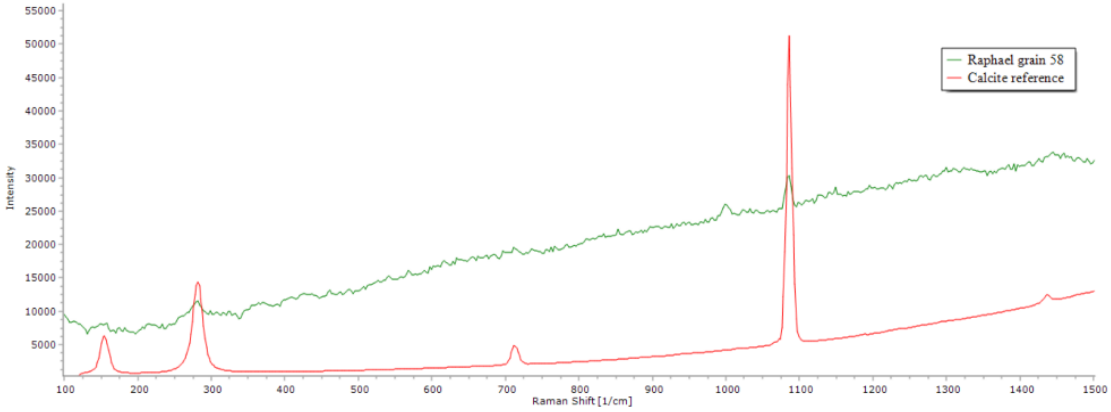
Raphael grain 58
Calcite reference
Intensity
Raman Shift [1/cm]

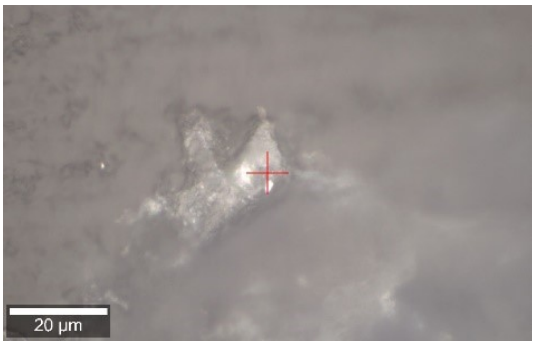
20 µm

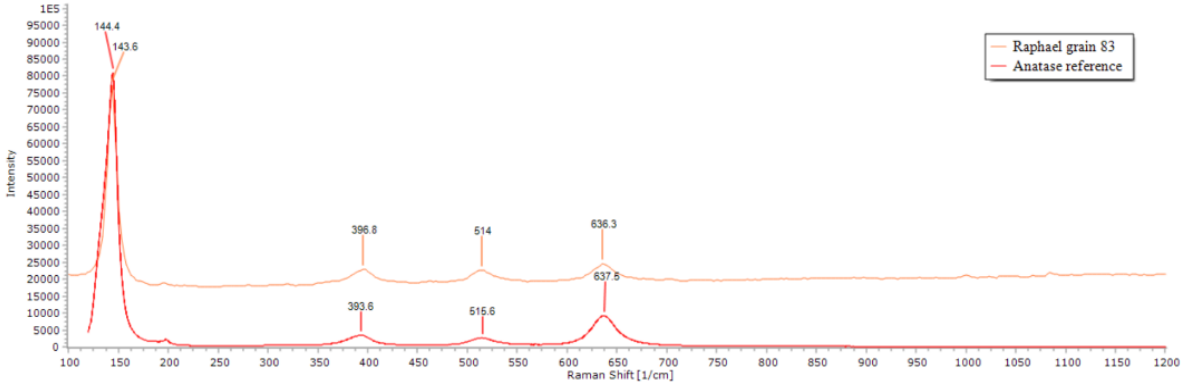
Raphael grain 83
Anatase reference
144.4
143.6
396.8
514
636.3
637.5
393.6
515.6
Intensity
Raman Shift [1/cm]

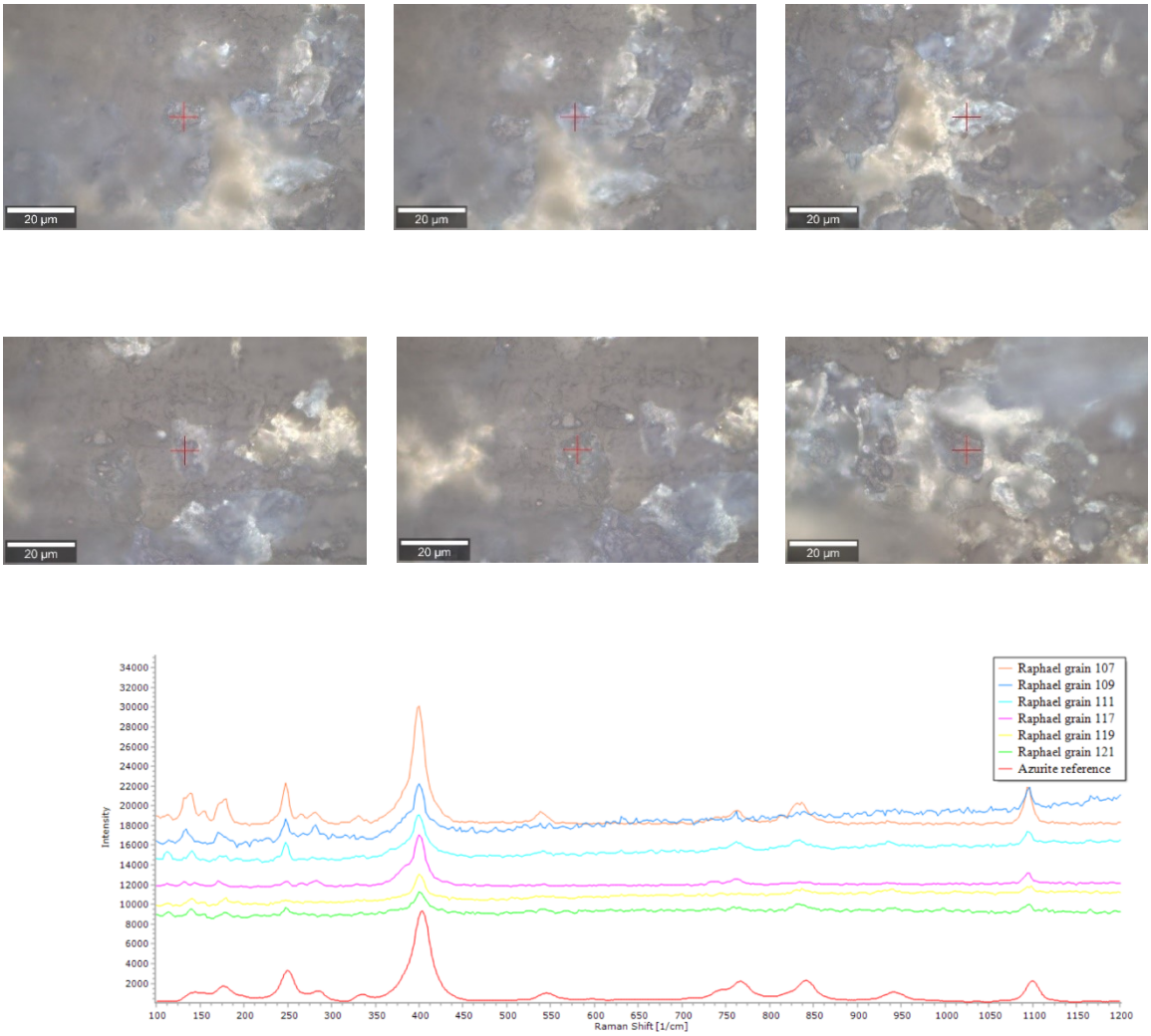

Figure 60 - Above points analysis from the up left corner to the up-right grain 107, grain 109, grain 111 and from the down left corner to the down left grain 117, grain 119, grain 121.

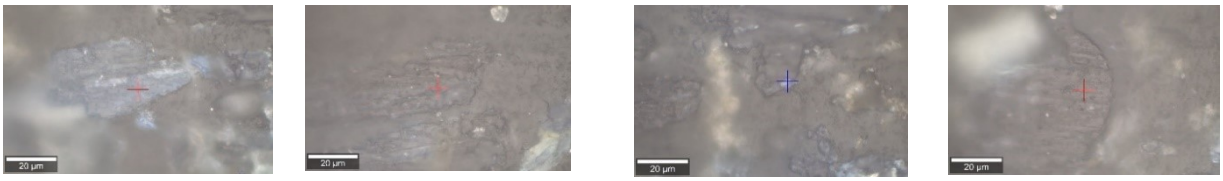

Figure 61 - From the left grain 61, grain 67, grain 74, grain 129.

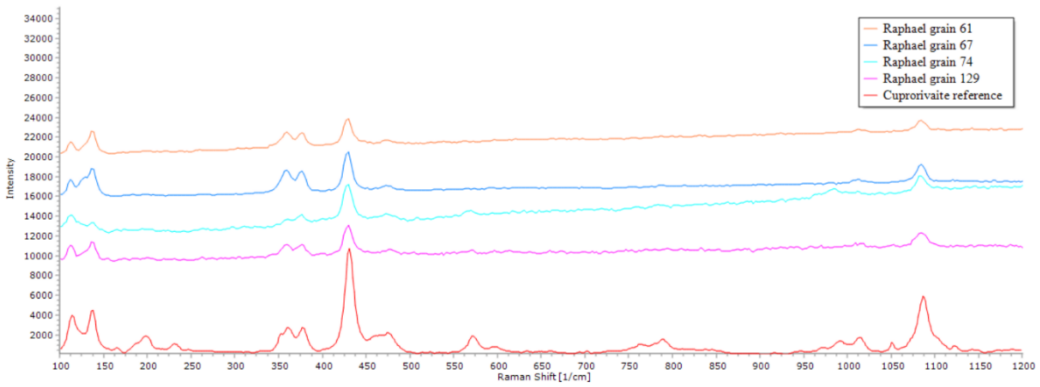

Once the samples were re-embedded in the resin, many point analysis were done to identify the cuprorivaite grains. In addition to cuprorivaite grains, other minerals have been identified, whose spectra are shown below. The colours of the crosses indicating point analysis correspond to the colours used for the spectra.

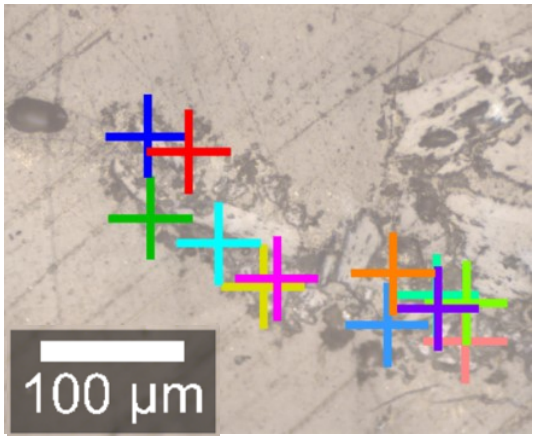

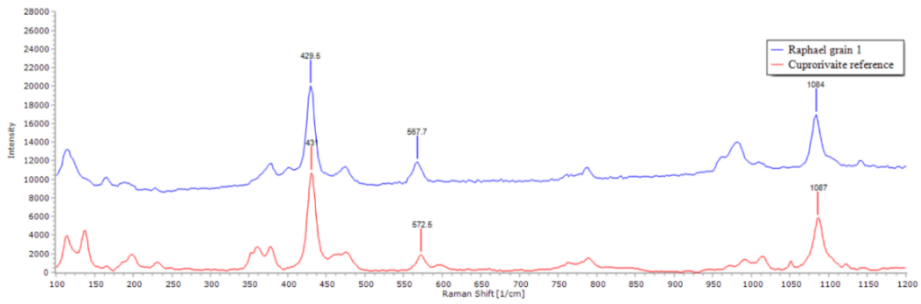

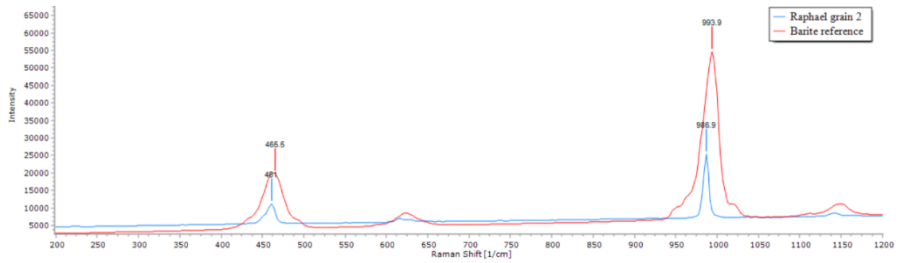

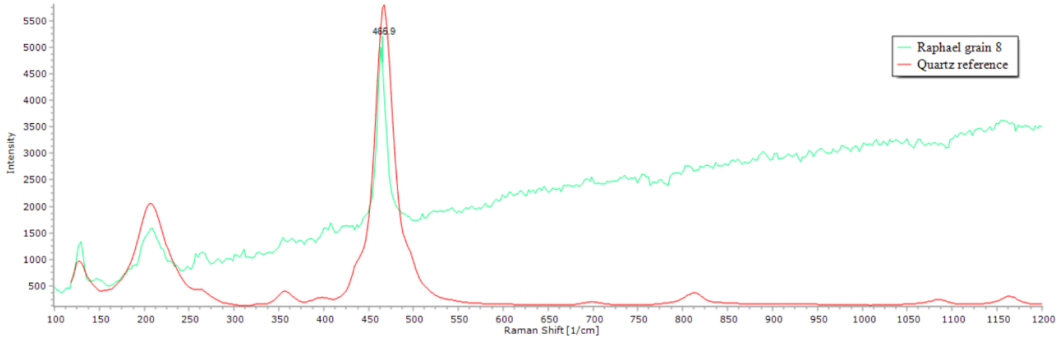

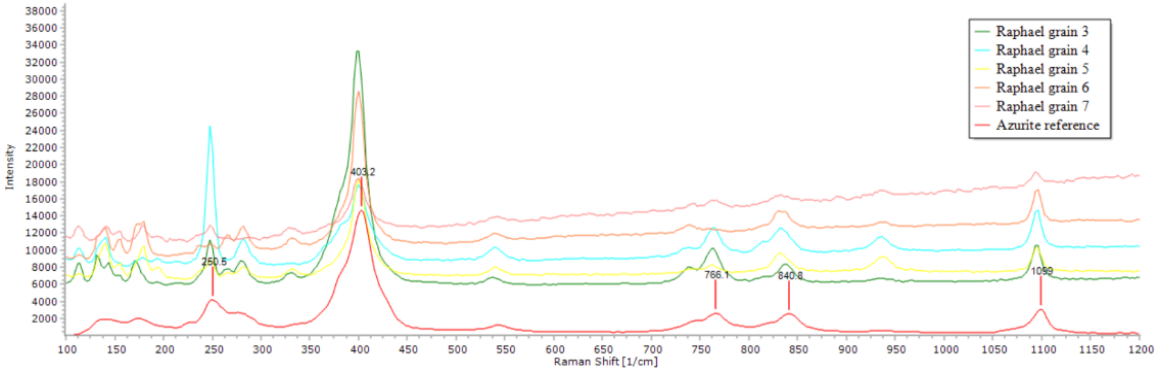

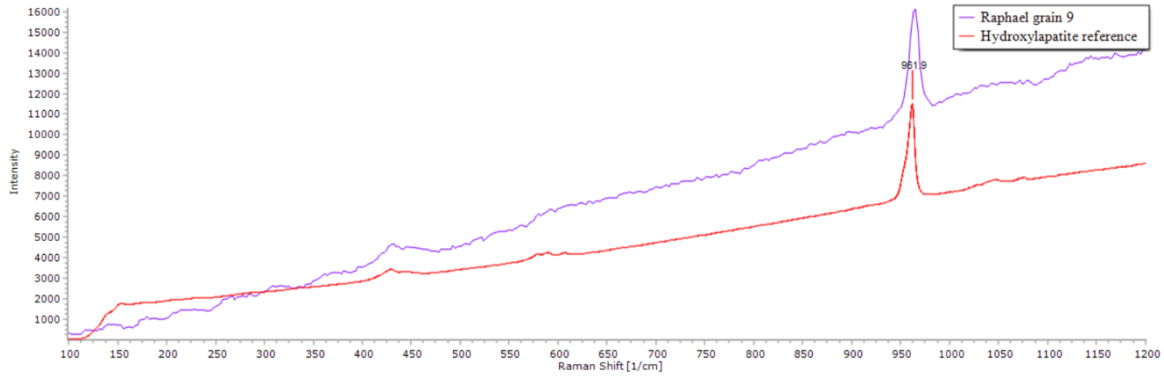

The colours of spectra correspond to the colours of the point analysis, the spectra missing were of pour quality.

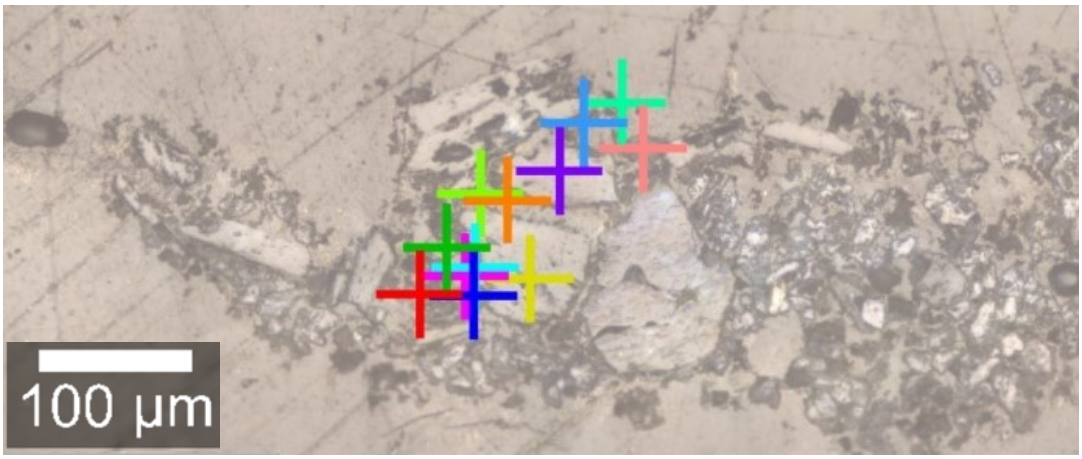

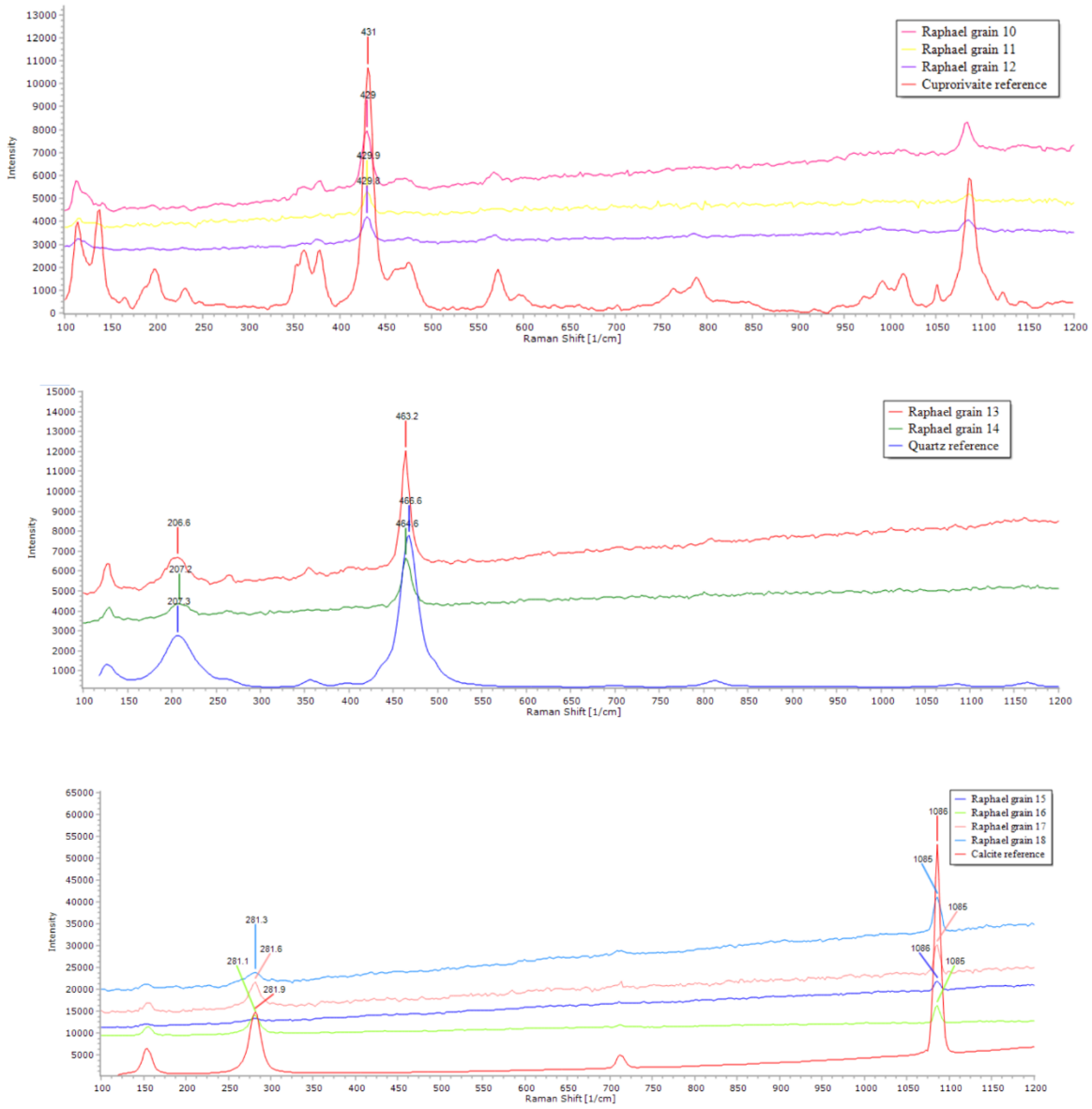

In conclusion, through point analysis all cuprorivaite grains of the sample were identified and are circled in the following image to better visualize them (Figure 62).

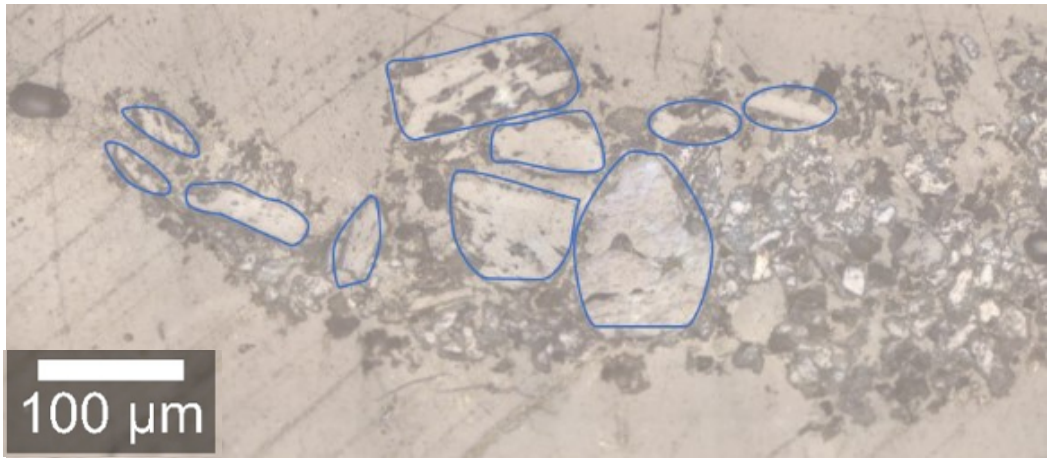

Figure 62 – Detail of cuprorivaite grains in Raphael sample.

6.1.3 LEFRANC SAMPLES

These two Egyptian blue commercial samples analysed with micro-Raman spectrometer have confirmed the main presence of cuprorivaite. As it is possible to see from the photographs of cuprorivaite grains the colour can be variable according to the orientation of the grains like also the shape which can be more or less angular.

6.1.3.1 LEFRANC 1929

In the LeFranc 1929 not only cuprorivaite (Figure 63) was detected but also the high-temperature polymorphs of SiO_2, trydimite (Figure 64) which forms at 870°C and cristobalite (Figure 65) at 1470°C, revealing a variation of temperature towards high values during the synthesis of the pigment. (DARIZ, SCHMID 2021)

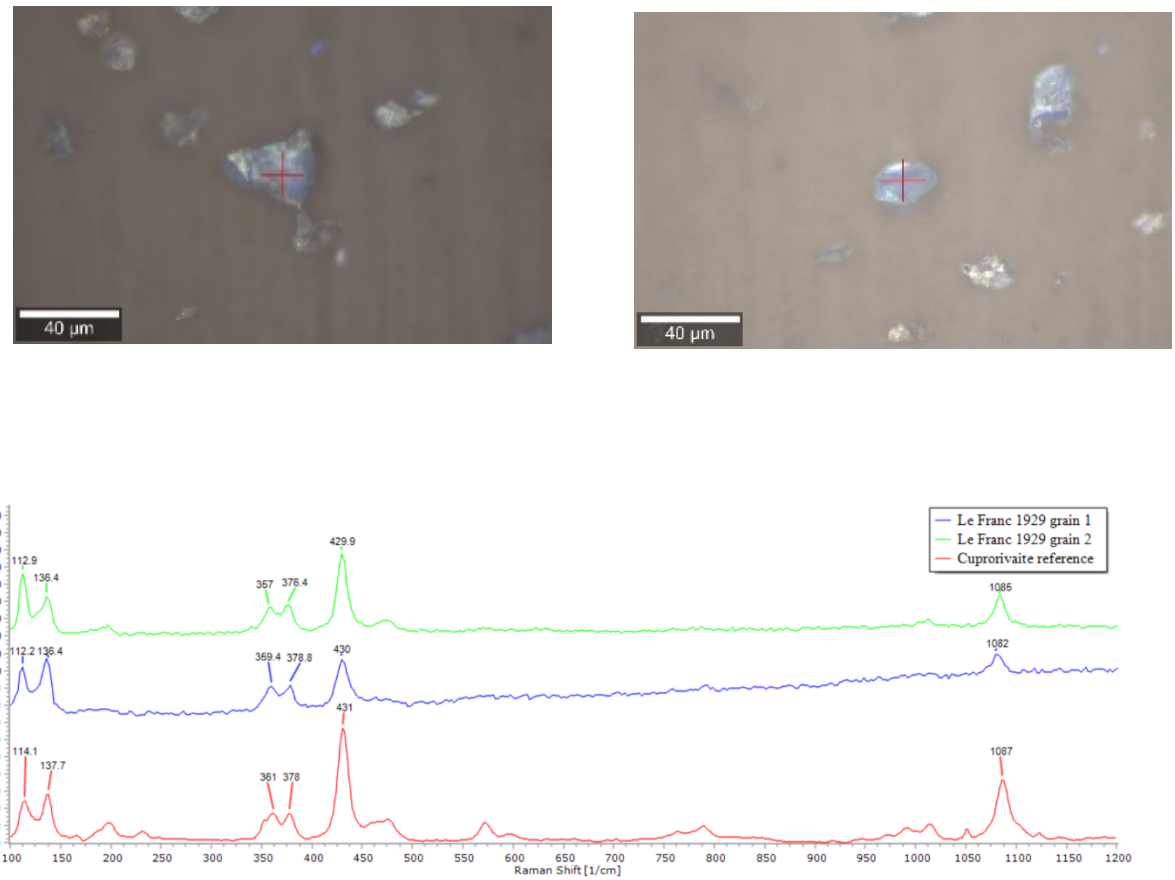

Figure 63 - Above, point analysis made on two various grains (grain 1 left and grain 2 right) of LeFranc 1929, below comparison between Raman spectrum of that grains and relative reference spectrum.

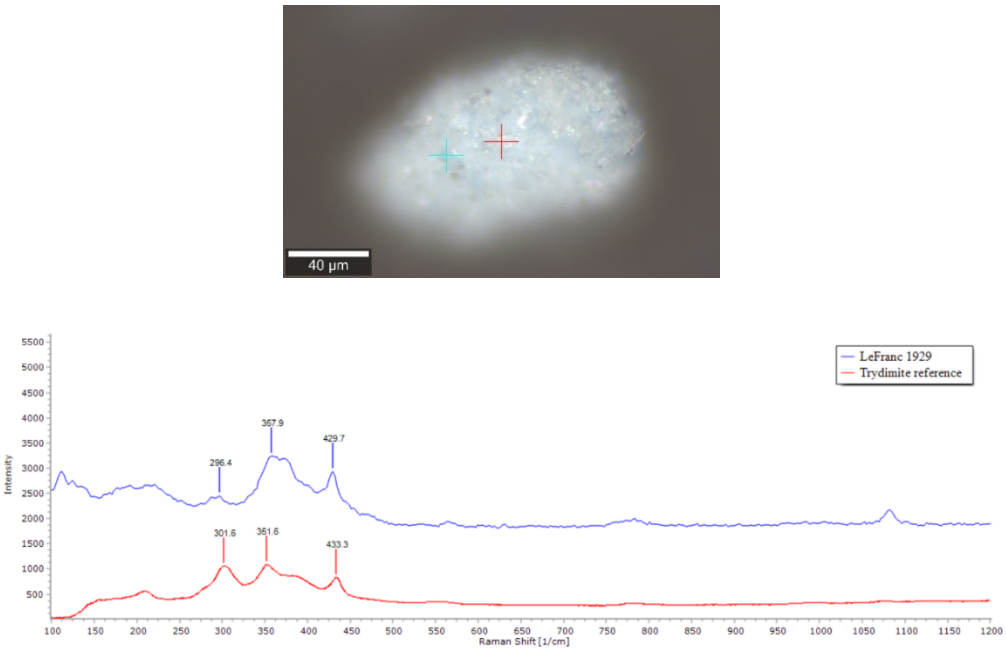

Figure 64 - Above, point analysis made on a conglomerate grain of LeFranc 1929, below comparison between Raman spectrum of that grain and relative reference spectrum.

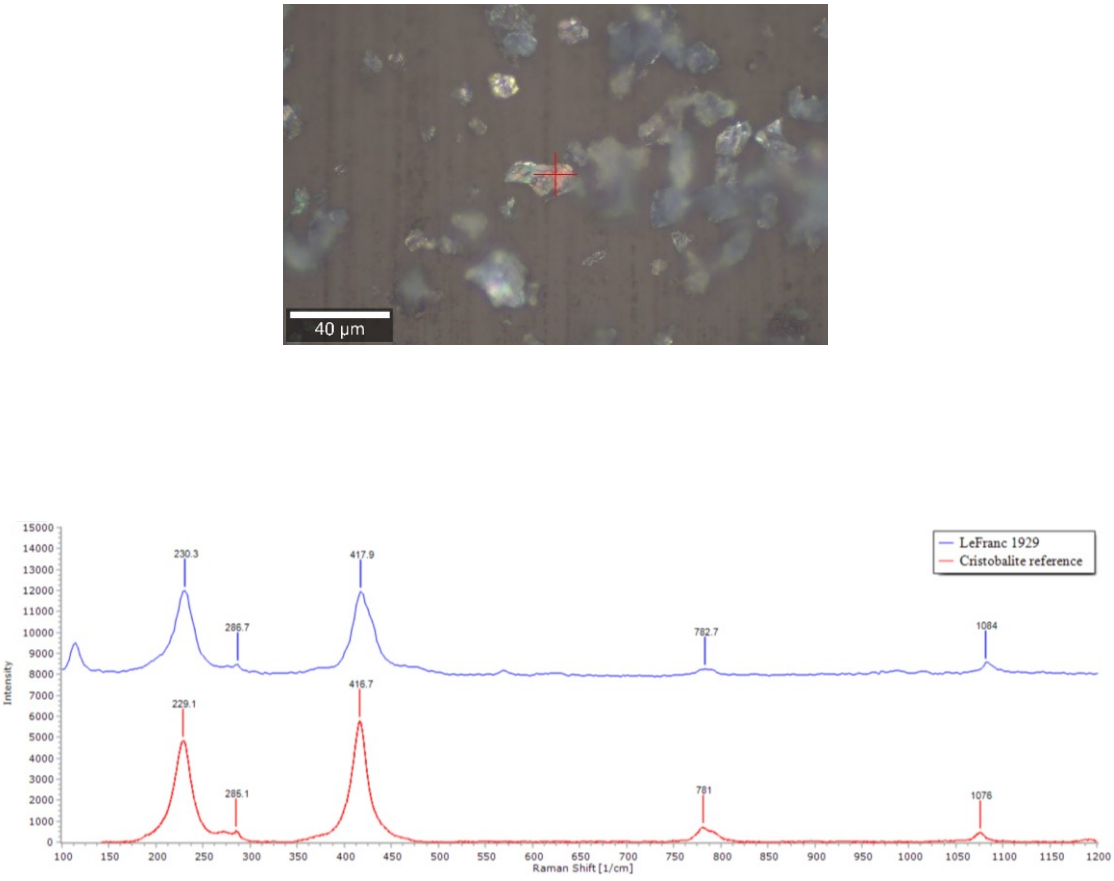

Figure 65 - Above, point analysis made on a grain of LeFranc 1929, below comparison between Raman spectrum of that grain and relative reference spectrum.

6.1.3.2 LeFranc 1937

In this sample we found out cuprorivaite mineral as expected but also the presence of calcite, probably deriving from the unreacted reagent (Dariz, Schmid 2021).

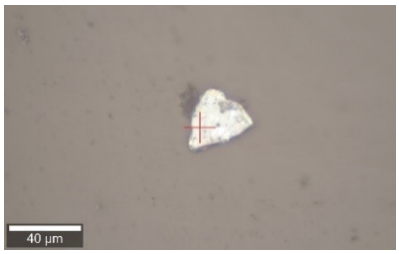

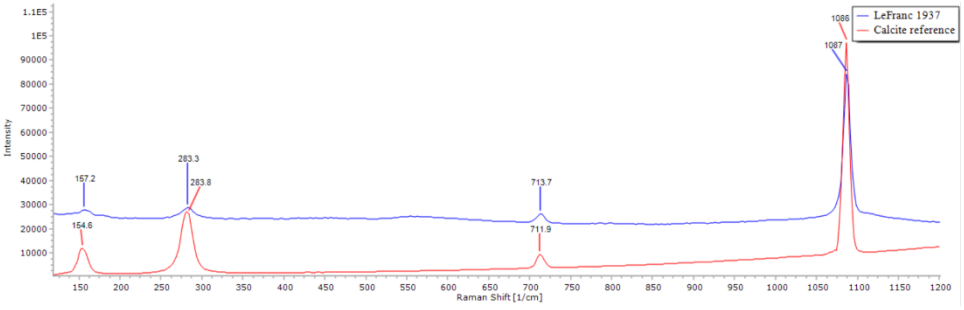

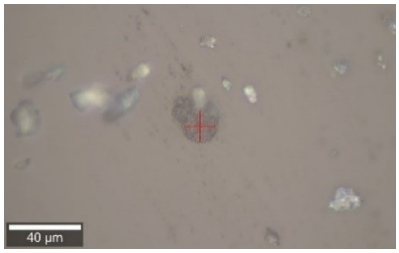

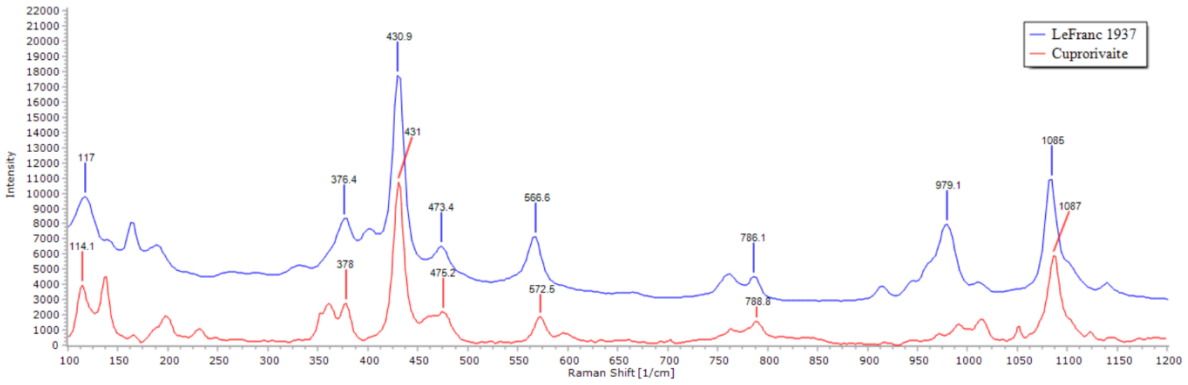

6.1.4 OSTIA SAMPLE

The same procedure was done on Ostia sample founding not only cuprorivaite but also other minerals due to the raw materials used for the synthesis of the pigment found also in other EB studies (DARIZ, SCHMID 2021).

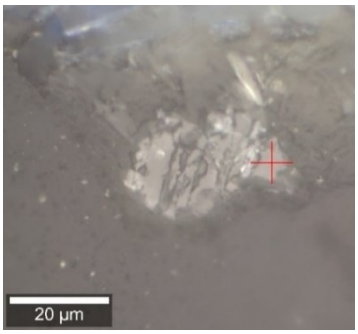

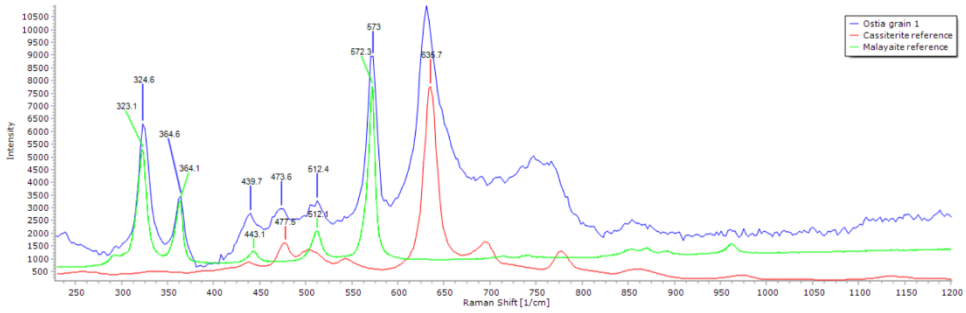

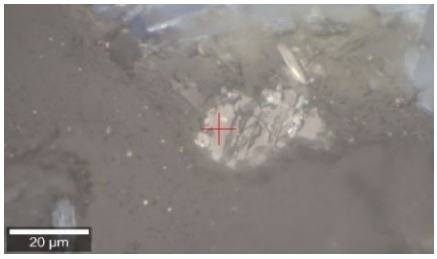

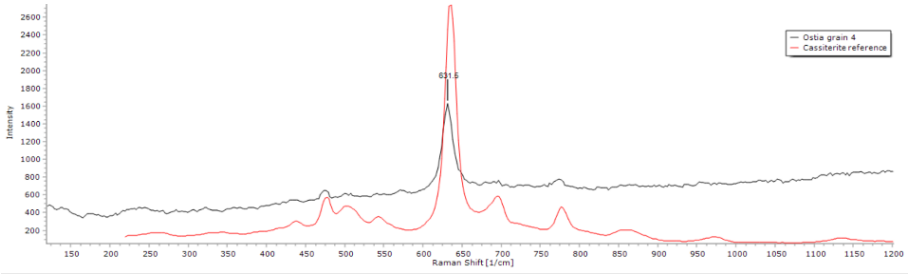

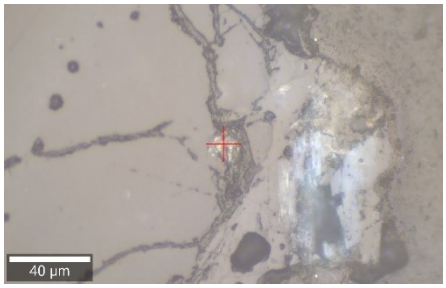
40 µm

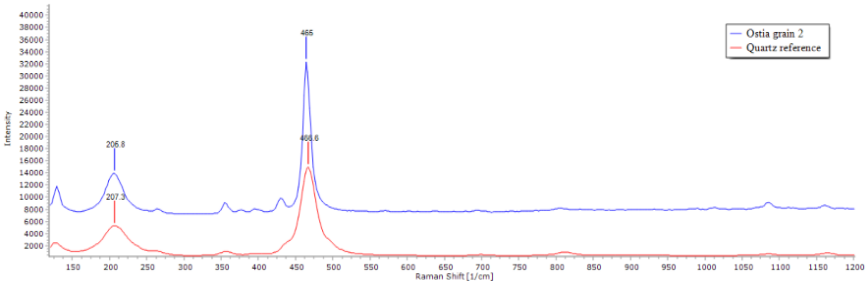
Ostia grain 2
Quartz reference
Intensity
Raman Shift [1/cm]
206.8
207.3
465
466.6


20 µm

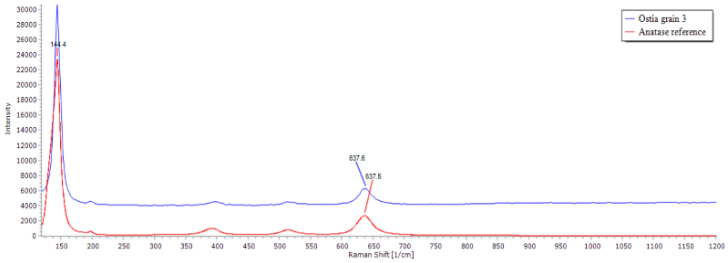
Ostia grain 3
Anatase reference
Intensity
Raman Shift [1/cm]
144.4
637.6
637.6

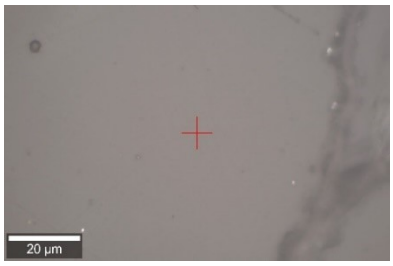
20 µm

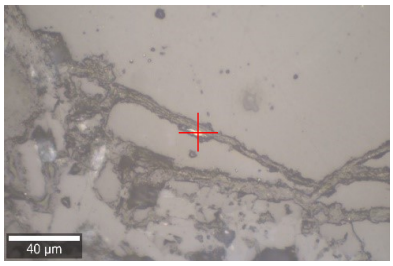
40 µm

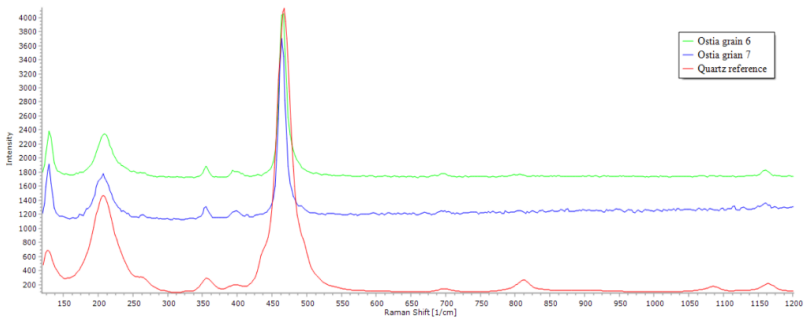
Ostia grain 6
Ostia grian 7
Quartz reference
Intensity
Raman Shift [1/cm]

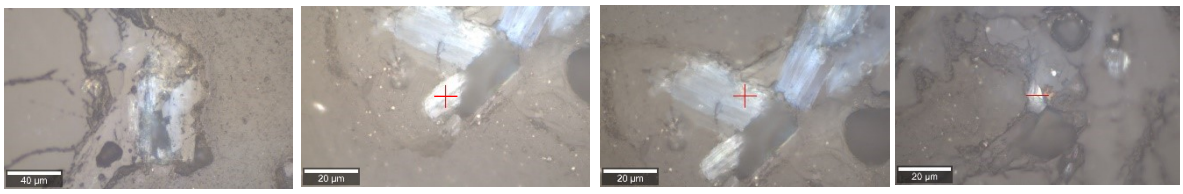
40 µm
20 µm
20 µm
20 µm

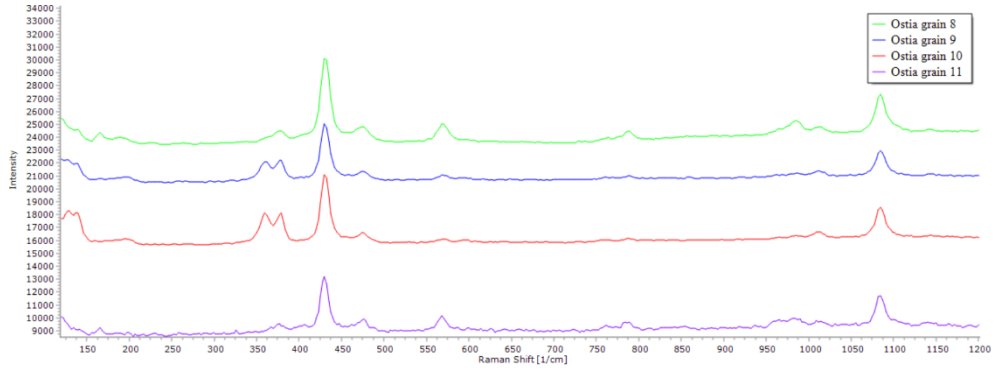
Ostia grain 8
Ostia grain 9
Ostia grain 10
Ostia grain 11
Intensity
Raman Shift [1/cm]


20 µm

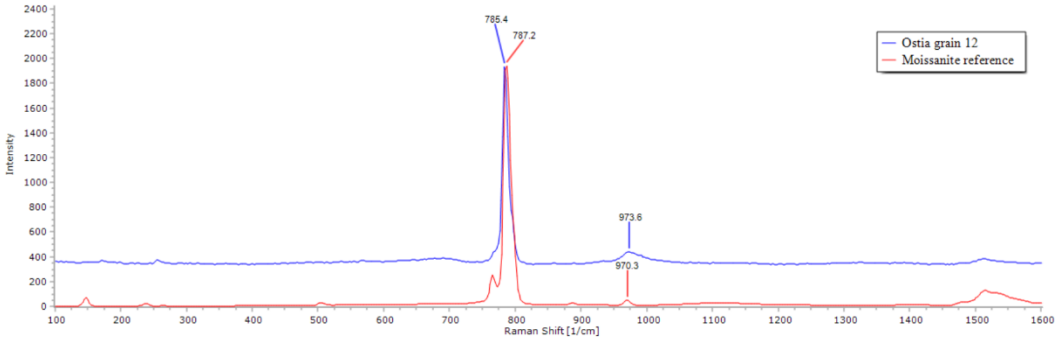
Ostia grain 12
Moissanite reference
785.4
787.2
973.6
970.3
Intensity
Raman Shift [1/cm]

6.1.4.1 OSTIA SAMPLE RAMAN MAP

Once a significant area (Figure 66) of the sample was identified, a Raman map (Figure 67) was performed to better understand the interface of cuprorivaite crystal formation and the presence of other minerals.

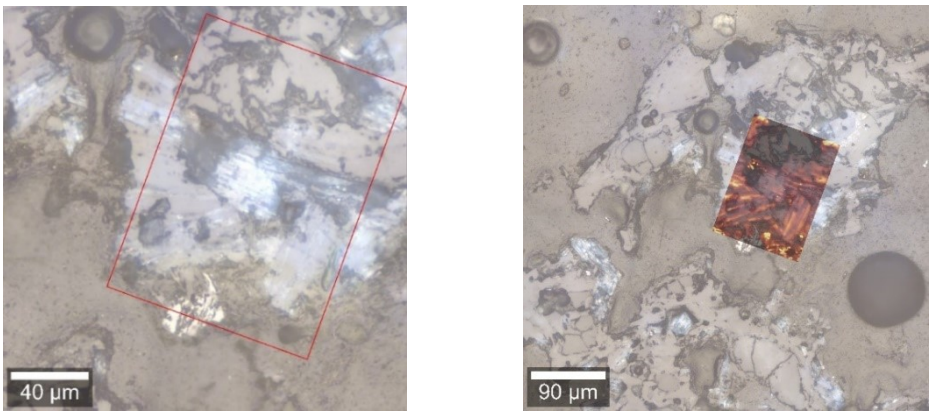

Figure 66 - The area on the samples chosen to perform Raman map (left) and the location of Raman map in false colours on the sample (right).

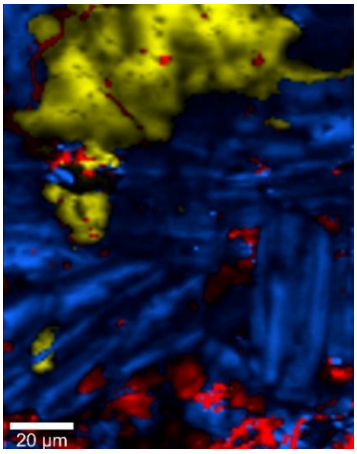

Figure 67 - Detail of the Raman map in false colours of the same area with cuprorivaite in blue, quartz in yellow and malayaite in red.

To better visualize the different mineral components of the area individual mineral zones are shown (Figure 68).

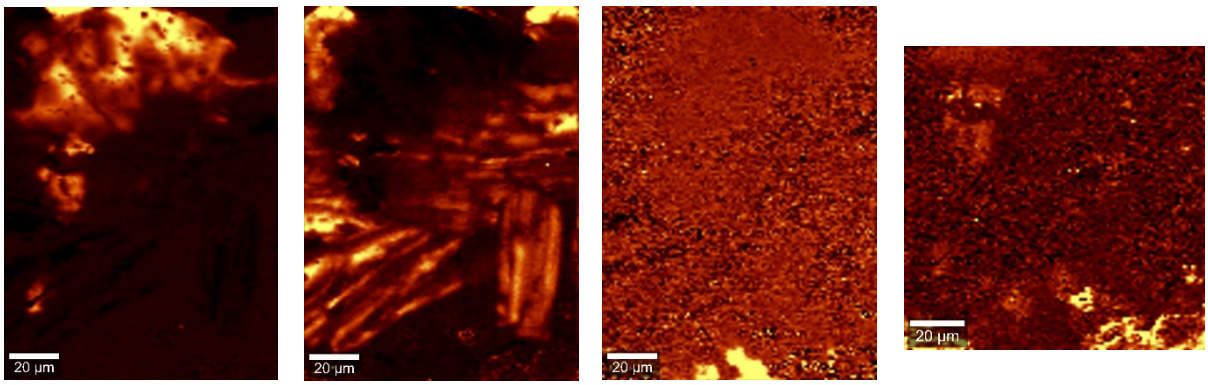

Figure 68 - Detail of the different phases found with Raman map, from the left quartz, cuprorivaite, malayaite and cassiterite.

6.1.5 LITERNUM SAMPLE

Many points analyses were performed to have a general mineral characterization of the sample and various points were named with a sequential numeration (es. grain 1).

The Raman analysis on Literum sample have confirmed the presence of cuprorivaite and revealed the presence of diopside ($CaMgSi_2O_6$) (Figure 69) and calcite which derives from the sand used to synthetize the pigment. (DARIZ, SCHMID 2021)

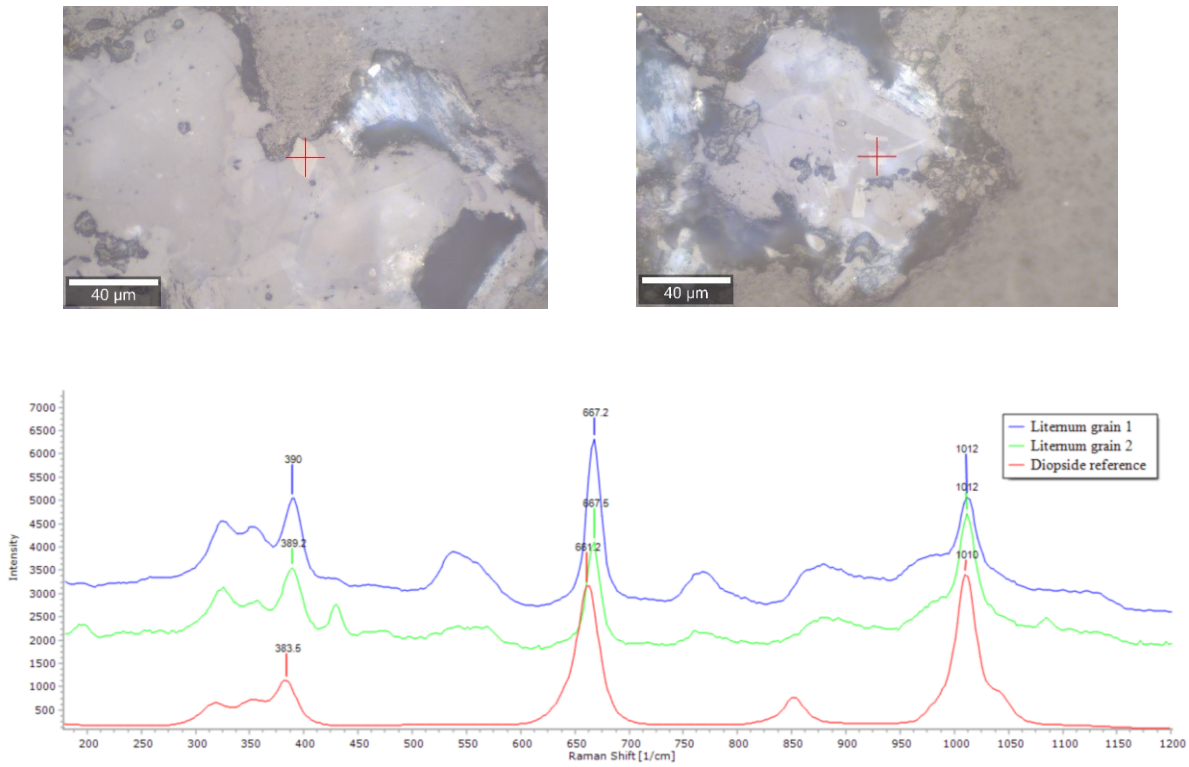

Figure 69 - Above, point analysis made on Literum samples, below comparison between Raman spectrum of that grains and relative diopside reference spectrum.

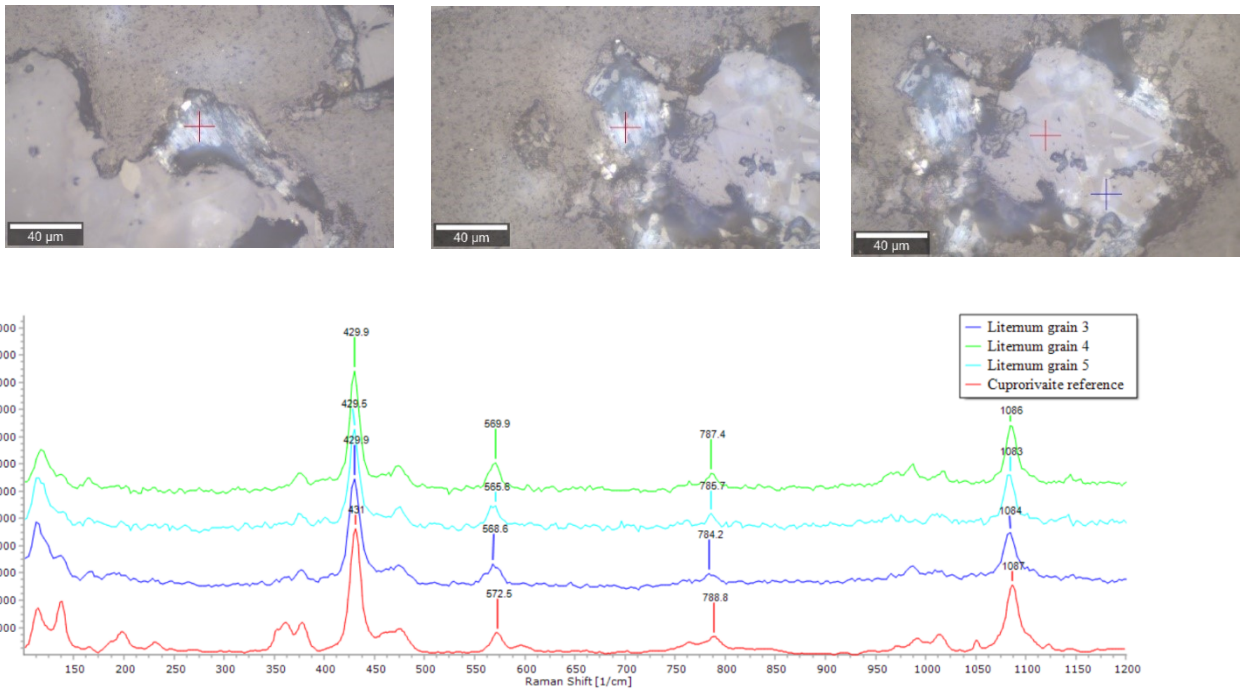

Figure 70 - Above, point analysis made on Literium samples (from the left grain 3, grain 4 blue cross and grain 5); below, comparison between Raman spectrum of that grains and relative cuprorivaite reference spectrum.

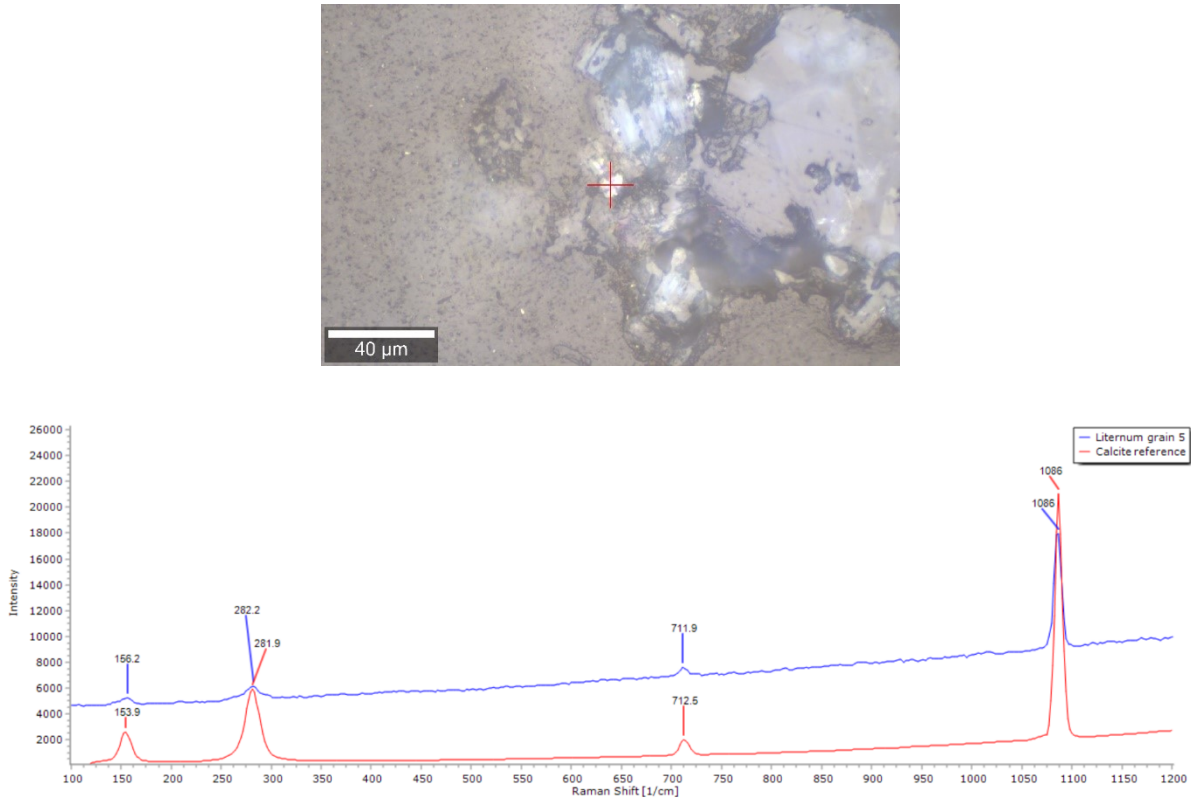

Figure 71 - Above, point analysis made on Literium sample; below, comparison between Raman spectrum of that grain and relative calcite reference spectrum.

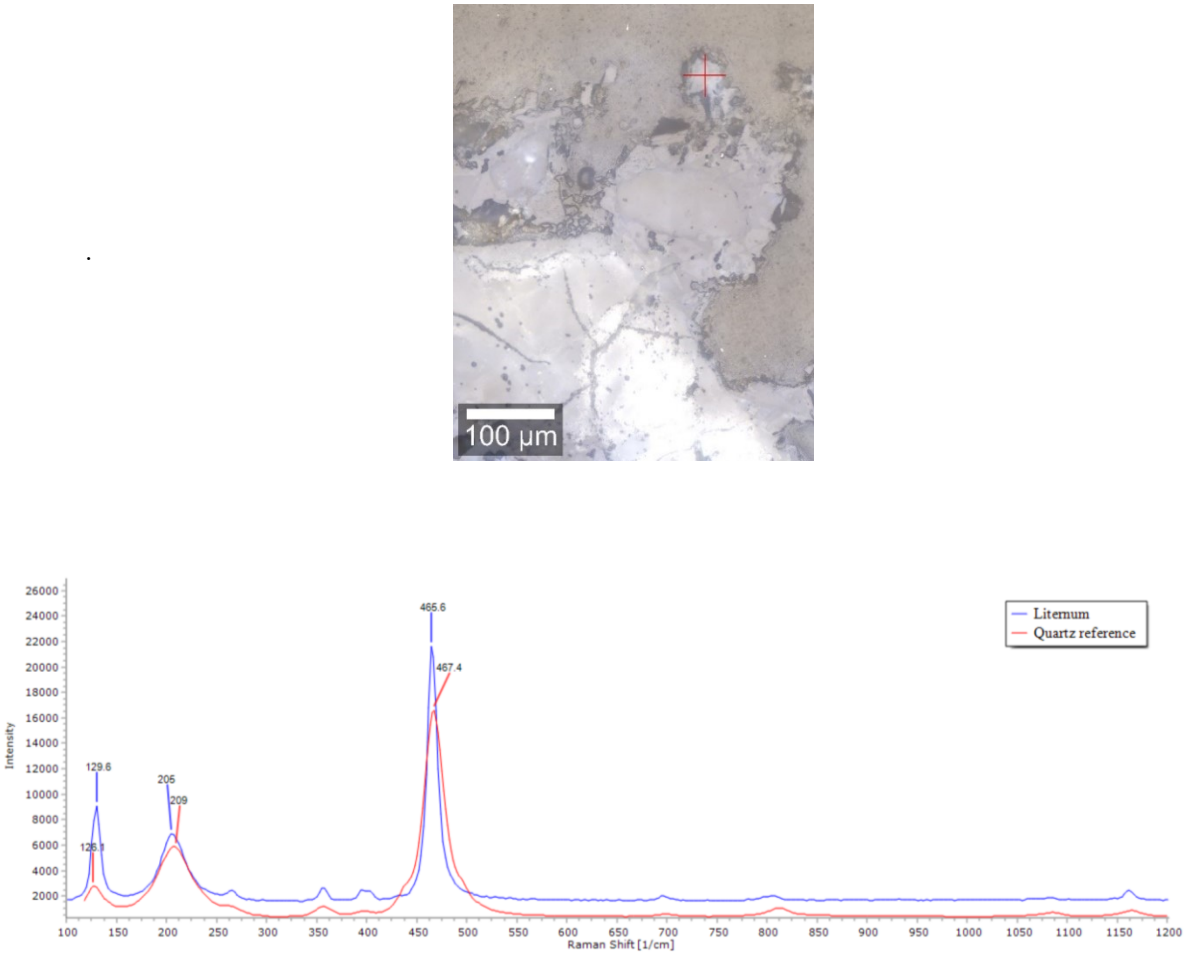

Figure 72 - Above, point analysis made on Liternum sample; below, comparison between Raman spectrum of that grain and relative quartz reference spectrum.

From the visible light photographs taken with Raman incorporated microscope the structure of the synthered conglomerate constituting EB is not so evident but with a careful look is possible to see that cuprorivaite crystals can appear shiny-bright light blue, with a layered structure grey coloured lamellae.

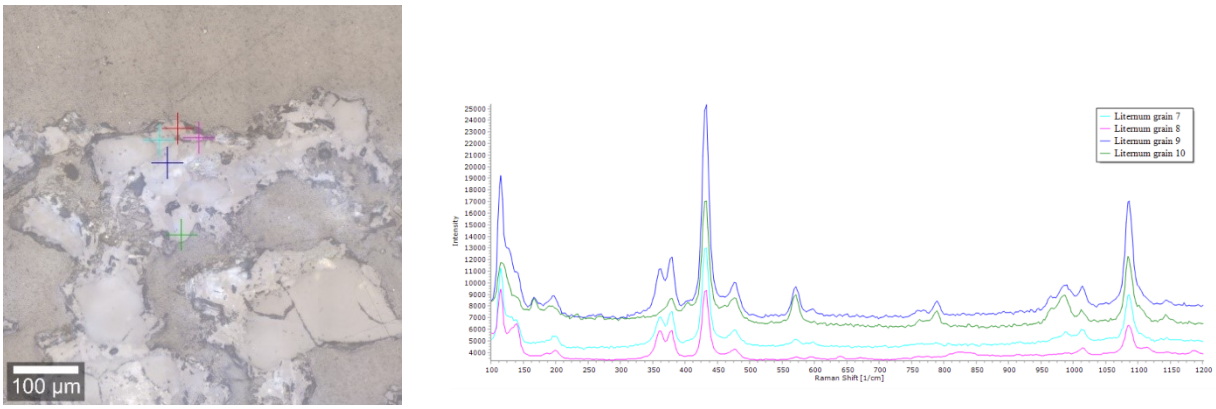

Figure 73 - Another area of the sample with a high concentration of cuprorivaite crystals. (colour of spectra correspond to colours of point analysis, red cross spectrum is missing).

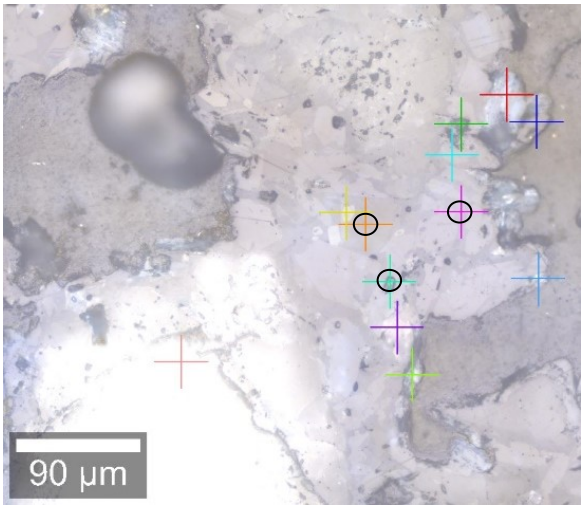

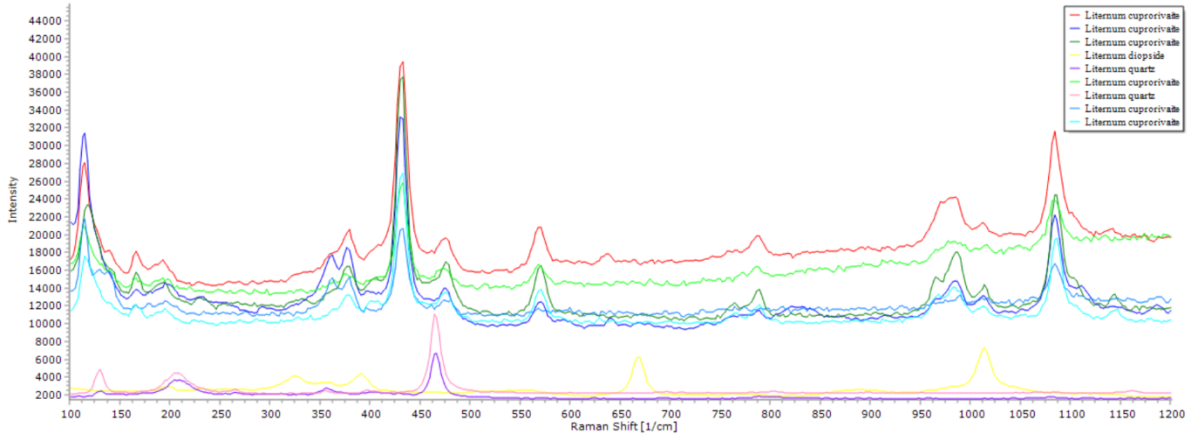

Figure 74 - The circle points are missing spectra because of pour signal.

6.1.5.1 LITERNUM SAMPLE RAMAN MAP

After many points analysis all over the sample, a significative area was selected to perform a Raman map in order to better visualize front reaction, texture and various mineralogical phases.

Apart from a dark shadow area in which the minerals are less visible thanks to the Raman false colour map it is possible to visualize the distribution of the crystals of cuprorivaite, quartz, diopside and tridymite.

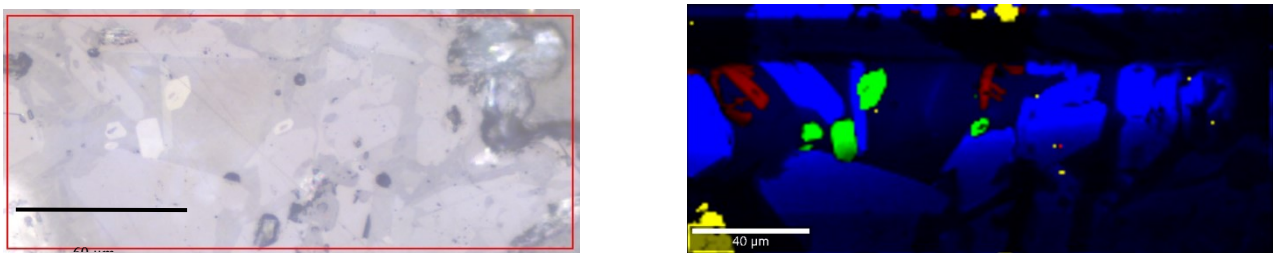

Figure 75 - Detail of the area of Liternum sample chosen to make the Raman map and the correspondence Raman map in false colours with EB in blue, quartz in yellow, diopside in green and trydimite in red.

6.2 MICRO-FTIR ANALYSIS

On the sample of Ortolano's painting there is optical evidence of a surface varnish. Since from the point of view of identifying organic parts, Raman spectroscopy induces fluorescence and has poor signal, it was decided to use micro-FTIR.

In particular, we wanted to understand the type of varnish and siccative oil used by the artist and check what type of substance forms the red particles in the pictorial matrix that Bredal-Jørgensen et al. (BREDAL-JØRGENSEN ET AL. 2011) claimed to be red lacquer.

Since it was not possible to touch the sample, the reflection mode was used, which unfortunately turns out to be less resolving, the spectra obtained was of pour quality and prevented the possibility to interpret them in a resolutive way.

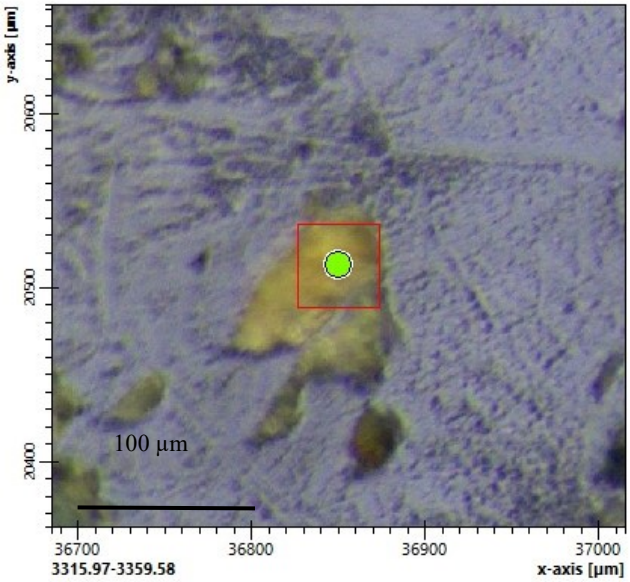

Figure 76 - Small fragment of Ortolano sample fragmented.

In only one case ATR analysis was tried, on a small isolated yellowish fragment Figure 77 of the same nature as the imprimitura.

The spectra (Figure 78) obtained was compared with the ones present in literature, showing that the main component of the fragment is gypsum (Figure 79) but the organic binder was not identified.

The FTIR spectra of the small fragment present also two peaks at 2900 cm^{-1} probably due to asymmetrical C-H stretching while the doublet at 1389-1410 cm^{-1} can correspond to C-H and C-O vibrations.

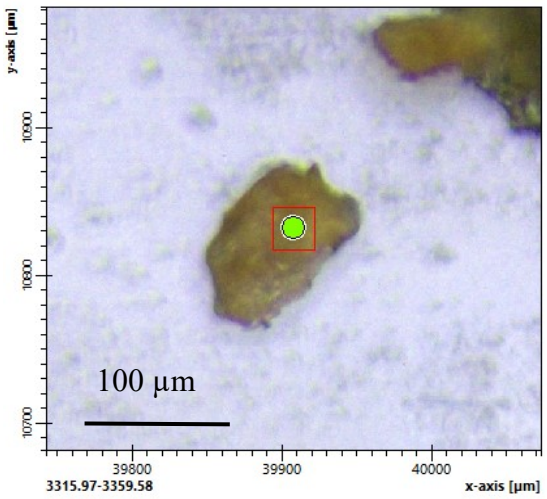

Figure 77 - Small fragment of ground layer of Ortolano entire sample.

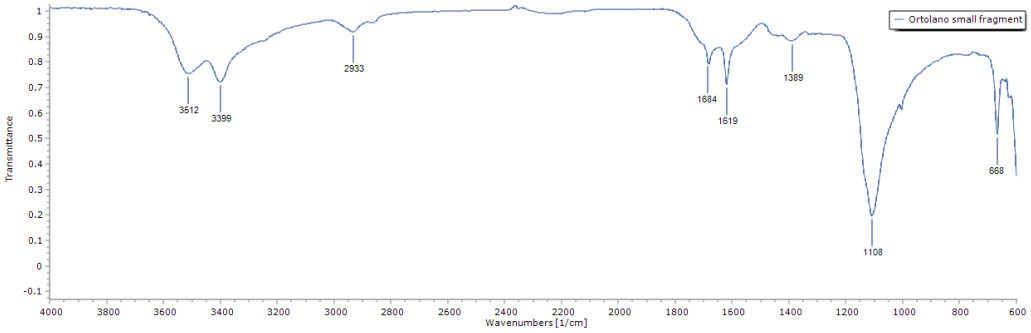

Figure 78 - ATR-FTIR spectra of Ortolano small fragment.

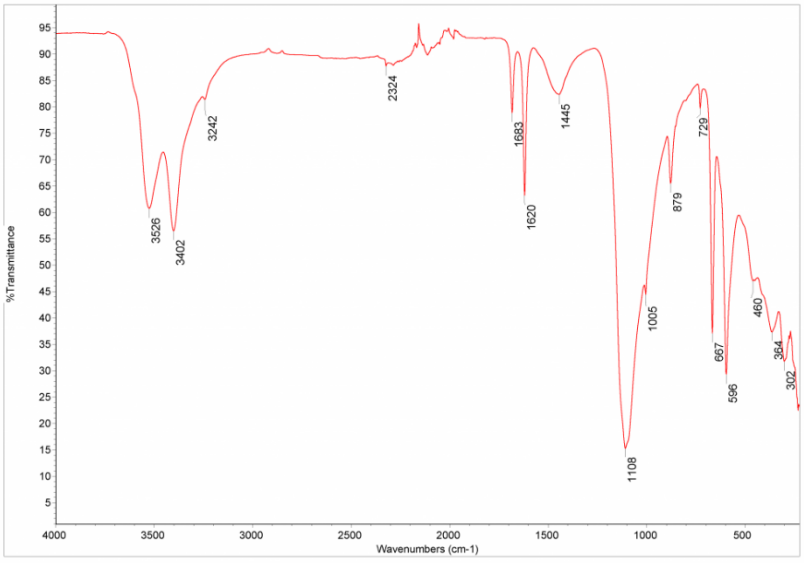

Figure 79 - ATR-FTIR spectra of gypsum. (Source: https://spectra.chem.ut.ee/paint/fillers/gypsum/)

6.3 SEM ANALYSIS

Once the Egyptian blue grains and some of the minerals in the samples were identified, SEM-EDS analyses were performed to confirm the spectroscopic analyses, to understand if the chemical composition of EB in the specimens is comparable to the standard composition of cuprorivaite and which types of trace elements correlated with it were present.

Thanks to the electron beam, the electron backscattered images of the samples are of much higher quality than the optical ones, allowing better identification of the single grains of minerals and in some cases allowing the internal texture of the grain to be appreciated.

To guarantee a certain degree of statistics, several analysis points were carried out for each selected EB grain to obtain an average cuprorivaite composition in the four samples.

Since it was decided not to use the coating on the sample, ESEM in low vacuum mode was used for the elemental analyses.

The EDS detector permitted to know the elemental composition of the single point spectra acquired. It was decided to present the data both in weight percentage of elements and in oxides, by reporting just the values in excess of 0.1 wt%, given that lower values are comparable to the instrument's detection limit, and therefore unreliable.

The elemental data are reported in the Appendix C.

6.3.1 ORTOLANO SAMPLE

Initially an attempt of SEM analysis was done on the not embedded sample position on the fragmented sample on stub (No.3). To make the sample conductive it was coated with the help of a sputter coater to deposit a layer of graphiite with 15-20 nm of thickness on the Ortolano sample n.3 with a pressure of $5x10^{-3}$ mbar with $3x10^{-3}$ ms of evaporation.

Figure 80 - Sputter Coater EmiTech K950X at the Geoscience department of the University of Padua.

Since the samples are not embedded in resin the EDS map in false colours (Figure 81) turns out to be of poor quality with the various elements not always easily distinguishable.

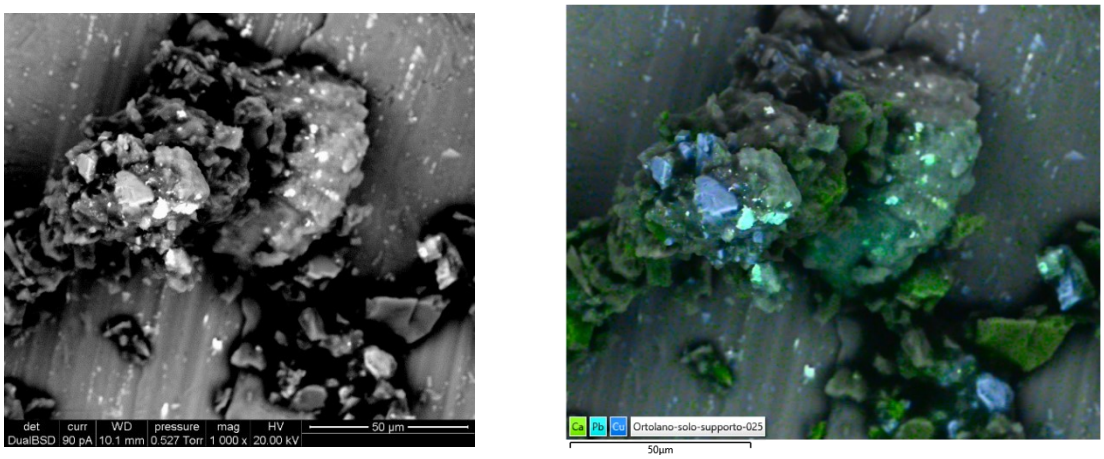

Figure 81 - SEM backscattered electrons image (left) and the false colour map with Ca in green, Pb in turquoise and Cu in blue enhanced.

Verified the poor quality of the results obtainable on the unembedded sample it was decided to perform ESEM analysis on the embedded sample of Ortolano.

In the case of the Ortolano sample in particular, the use of ESEM was very helpful in distinguishing the multitude of different mineral grains (Figure 82), not easily identified by optical imaging.

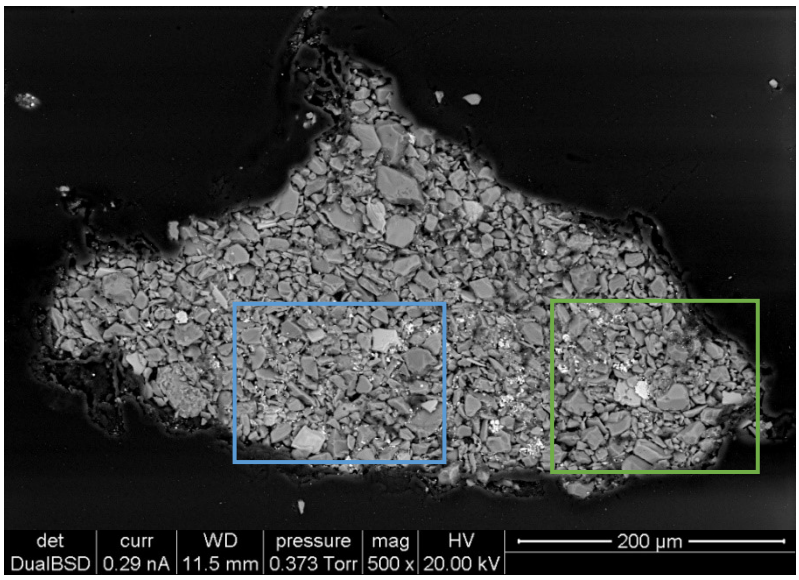

Figure 82 - Backscattered electrons image of the entire sample of Ortolano where the heavy elements appear lighter than the small atomic number ones, the two coloured squares show the parts selected for EDS analysis.

For the subsequent compositional analysis, two areas of interest with a high concentration of cuprorivaite grains were selected (Figure 83) and both the maps of elements and various point analyses were carried out, the compositions and some spectra of which are reported below.

The maps of elements in false colours permit to fast visualize where the grains of different minerals are located understanding their distribution, sizes and shapes (Figure 84).

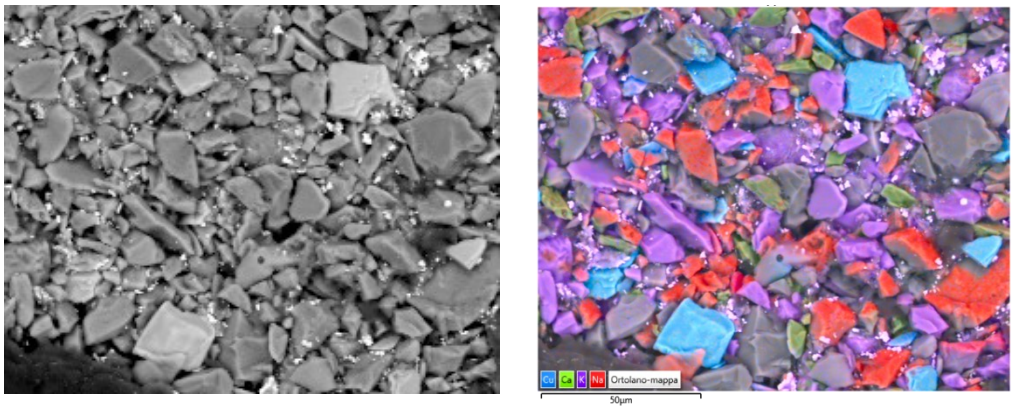

Figure 83 - Part of Ortolano's sample (light blue square of Fig.) false coloured SEM image of copper (Cu=blue), calcium (Ca=green), potassium (K=purple), sodium (Na=red).

In our case it was selected to enhance the presence of EB grains assigning the colour blue to the copper (Cu) which constitute a marker since that the other blue pigment lacks this element. The presence of lazurite, one of the principal components of lapis lazuli instead is highlighted in the coloured maps by sodium (Na) coloured in red.

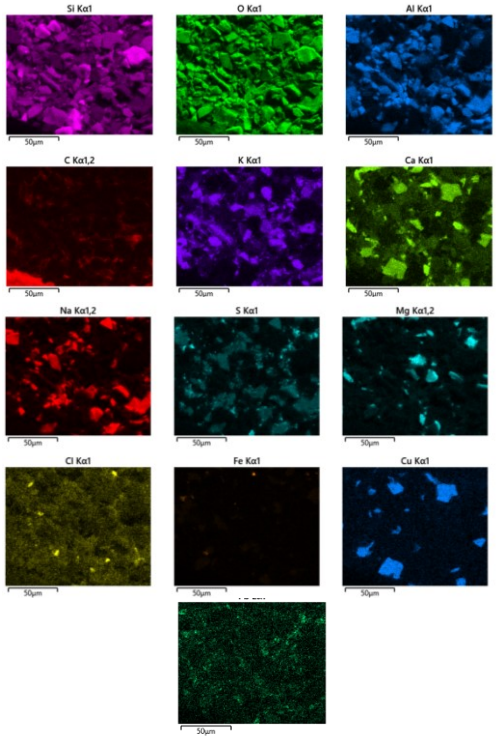

Figure 84 - Single elements maps in false colours of Na, S, Mg, Cl, Fe, Cu, Si, O, Al, C, K, Ca, Pb showing the areas most rich in that element.

The green and violet areas are respectively rich of calcium (Ca) and potassium (K) which are probably indicative of calcium carbonate and k-feldspars, the small white particles spread over the surface of the other phases are rich in lead, so probably they are white lead pigment.

The single elements maps showed the omnipresence of silicon (Si) and oxygen (O) mainly due to the two blue pigments silicate based, the quartz grains are visible instead in grey tones in the general map.

The same procedure was performed in the other area of the sample indicated with green square in Figure 82.

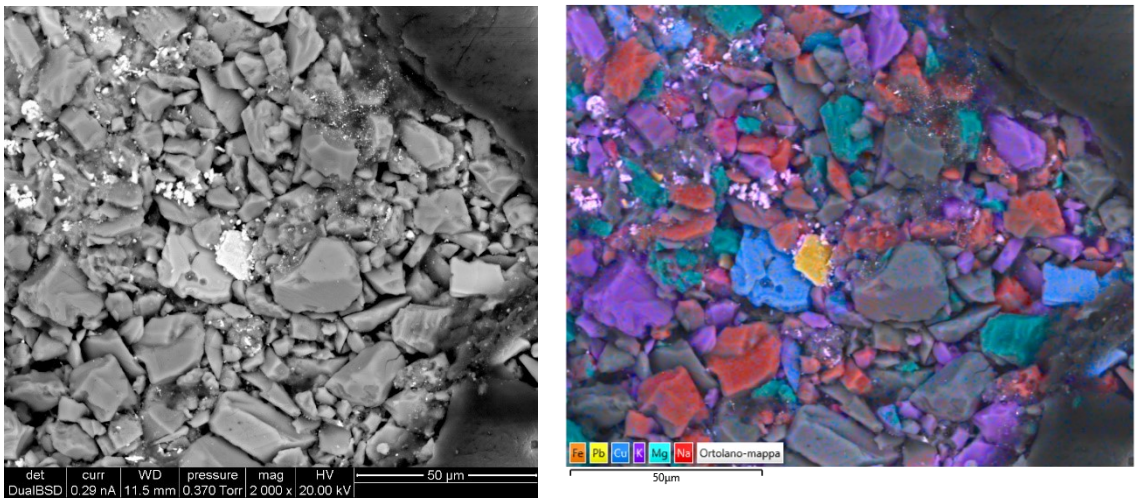

Figure 83 - Part of Ortolano's sample (green square of Fig.) false coloured SEM image of iron (Fe), lead (Pb), copper (Cu), potassium (K), magnesium (Mg) and sodium (Na).

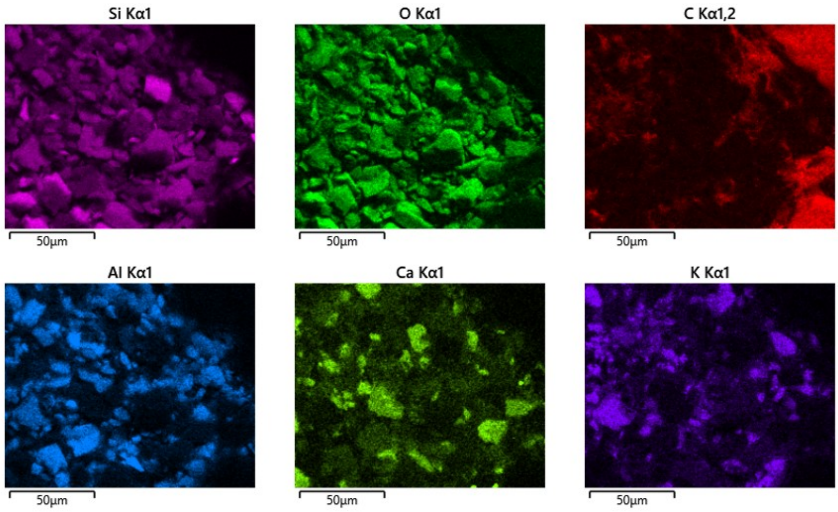

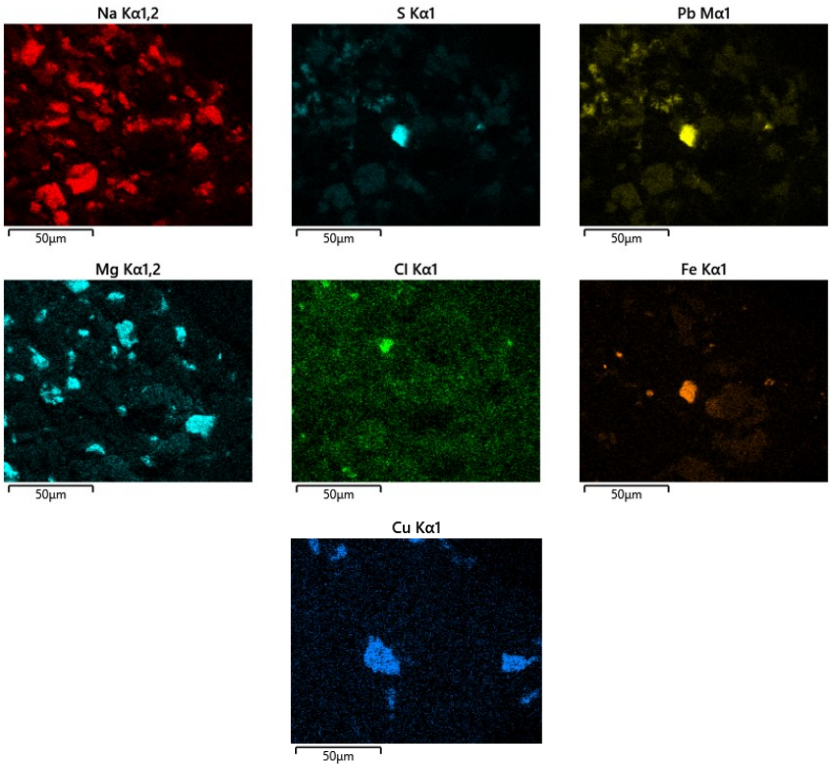

Figure 84 - Single elements maps in false colours of Si, O, C, Al, Ca, K, Na, S, Pb, Mg, Cl, Fe, Cu showing the areas most rich in that element.

The grain with a high percentage of Fe and S is a pyrite grain that could be due to lazurite presence given that pyrite is a minor component of natural occurring lapis lazuli. (BERKE ET AL. 2010)

To obtain a semiquantitative analysis of cuprorivaite grains some point analysis (Figure 85) were performed on the grains containing Cu and the results expressed in oxides are reported in a table with also the average value and the standard deviation calculated for all and each grain.

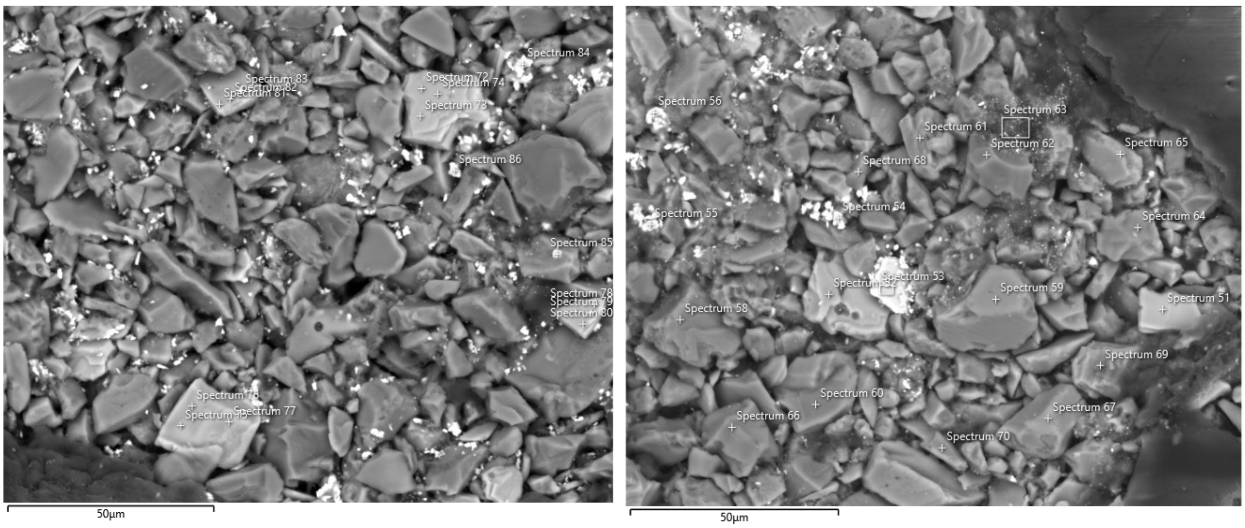

Figure 85 – Point analysis on the two selected areas of Ortolano sample.

The initial data were acquired in elements already normalized and then transformed into oxides resulting in not normalized data anymore with resulting sums of not always 100 so data were normalized again.

An EDS spectrum for each cuprorivaite grain was selected and reported in the Figure 86.

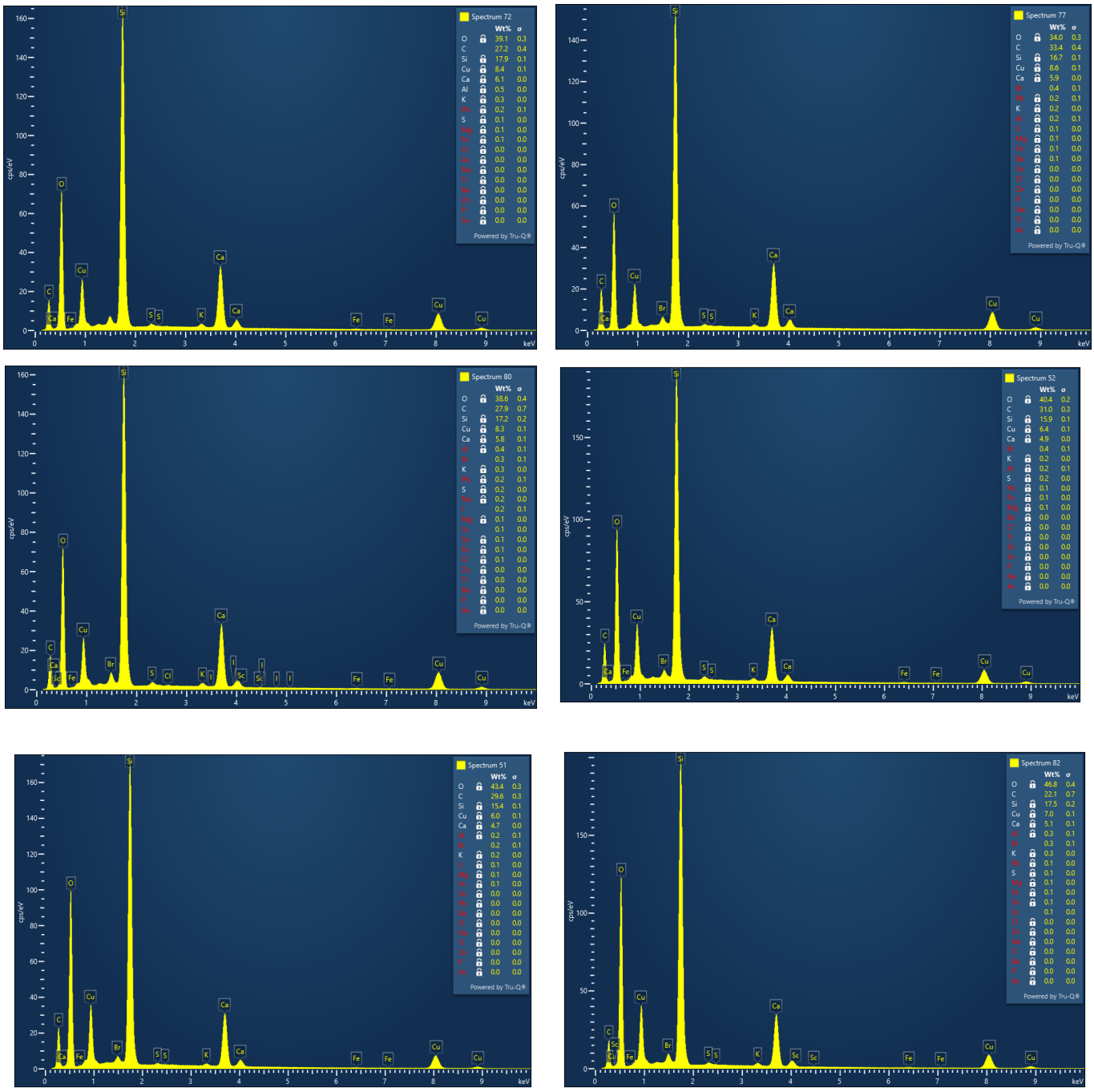

Figure 86 – EDS spectra of cuprorivaite grains of Ortolano sample.

6.3.2 RAPHAEL SAMPLE

The same procedure was applied to Raphael sample (Figure 87).

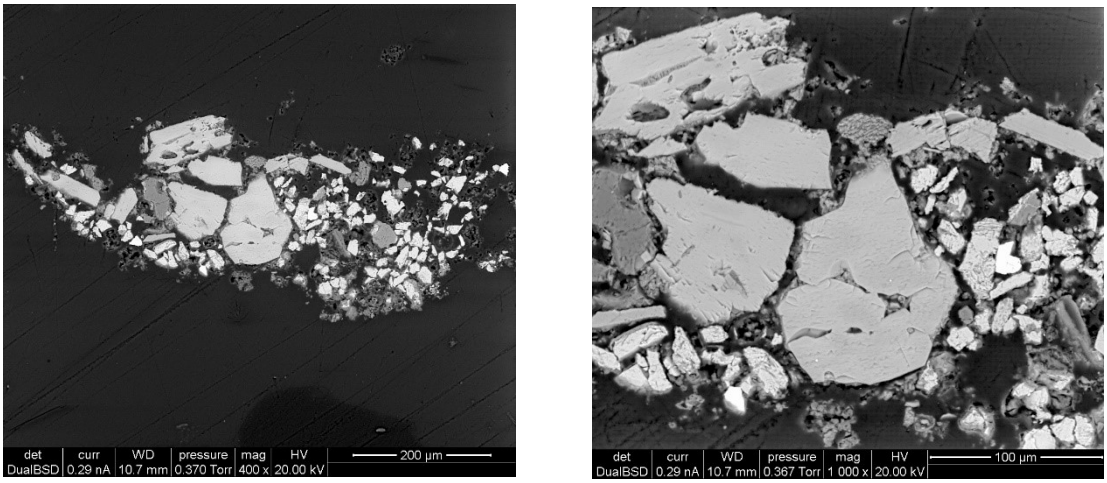

Figure 87 - SEM map of Raphael sample on the left and its magnification on the right.

The observation of the fragment under the OM and the confocal microscope already highlighted the bigger granulometry of EB grains respect to the AZ ones as already noticed by previous analysis (SIDOTI ET AL. 2018)

The maps in false colours have confirmed the presence and location of EB and azurite grains (Figure 88).

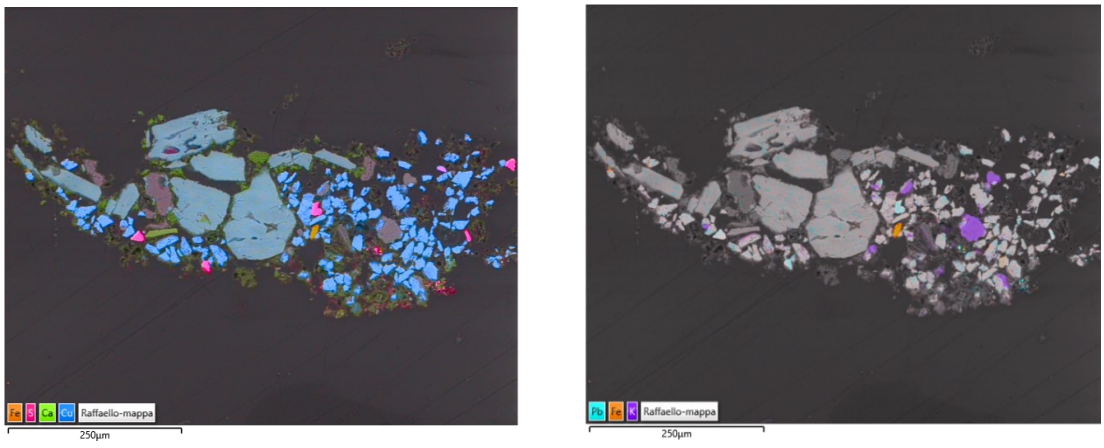

Figure 88 - False colours maps of Raphael sample and point analysis.

Also for this sample many points analysis were performed (Figure 89).

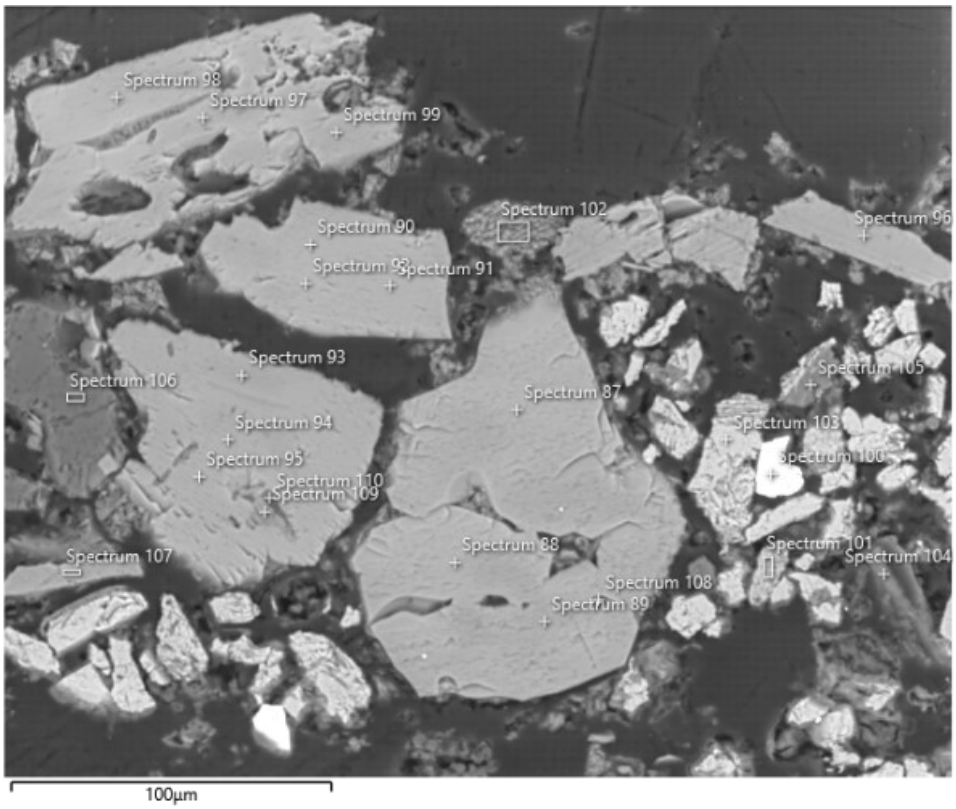

Figure 89 - Point analysis made on Raphael sample

The point analysis 100 (magenta colour in the false colours map) it is probably barite while spectrum 101 is goethite and 105 orthoclase.

Also in this case just one spectrum each cuprorivaite grain is reported.

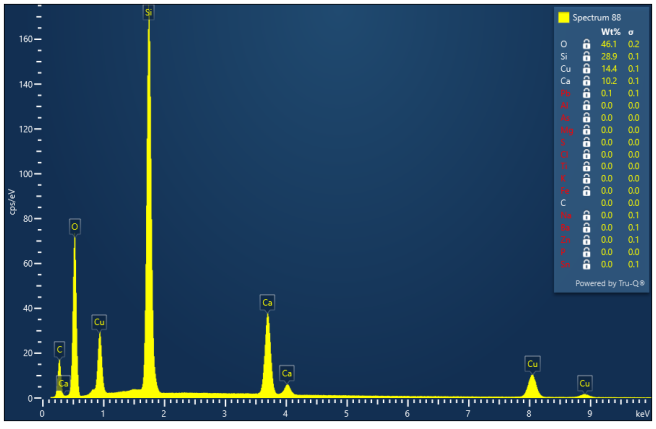

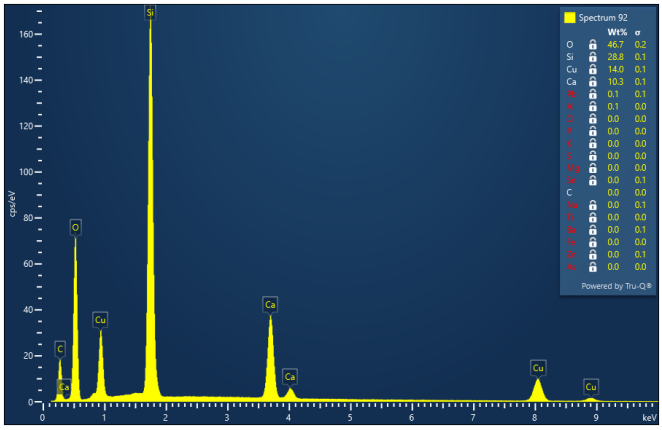

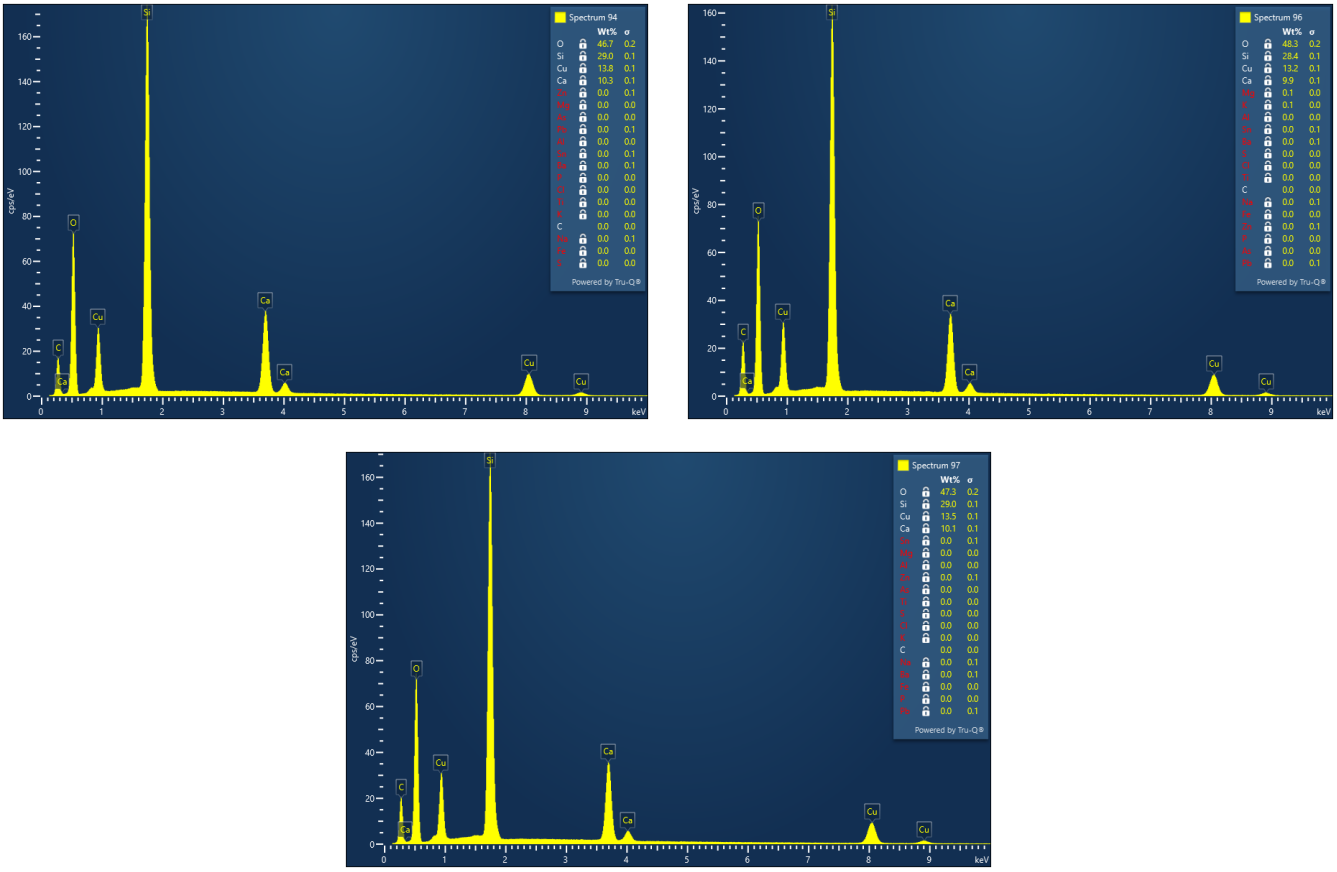

6.3.3 OSTIA SAMPLE

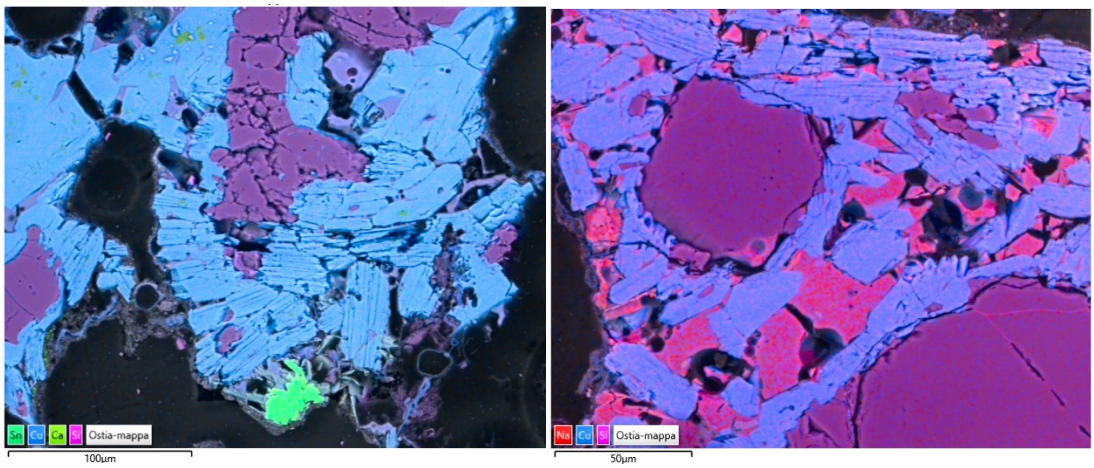

Figure 90 - Ostia sample SEM false colour maps

In the Ostia sample the blue areas with a high concentration of Cu indicate the presence of cuprorivaite, the Si rich areas instead form the matrix, while the Na rich areas form the glassy interface. In the left map, the Ca predominated area is constituted by malayaite and cassiterite minerals. It is noticeable how the lamellar texture of cuprorivaite is evident thanks to ESEM photograph.

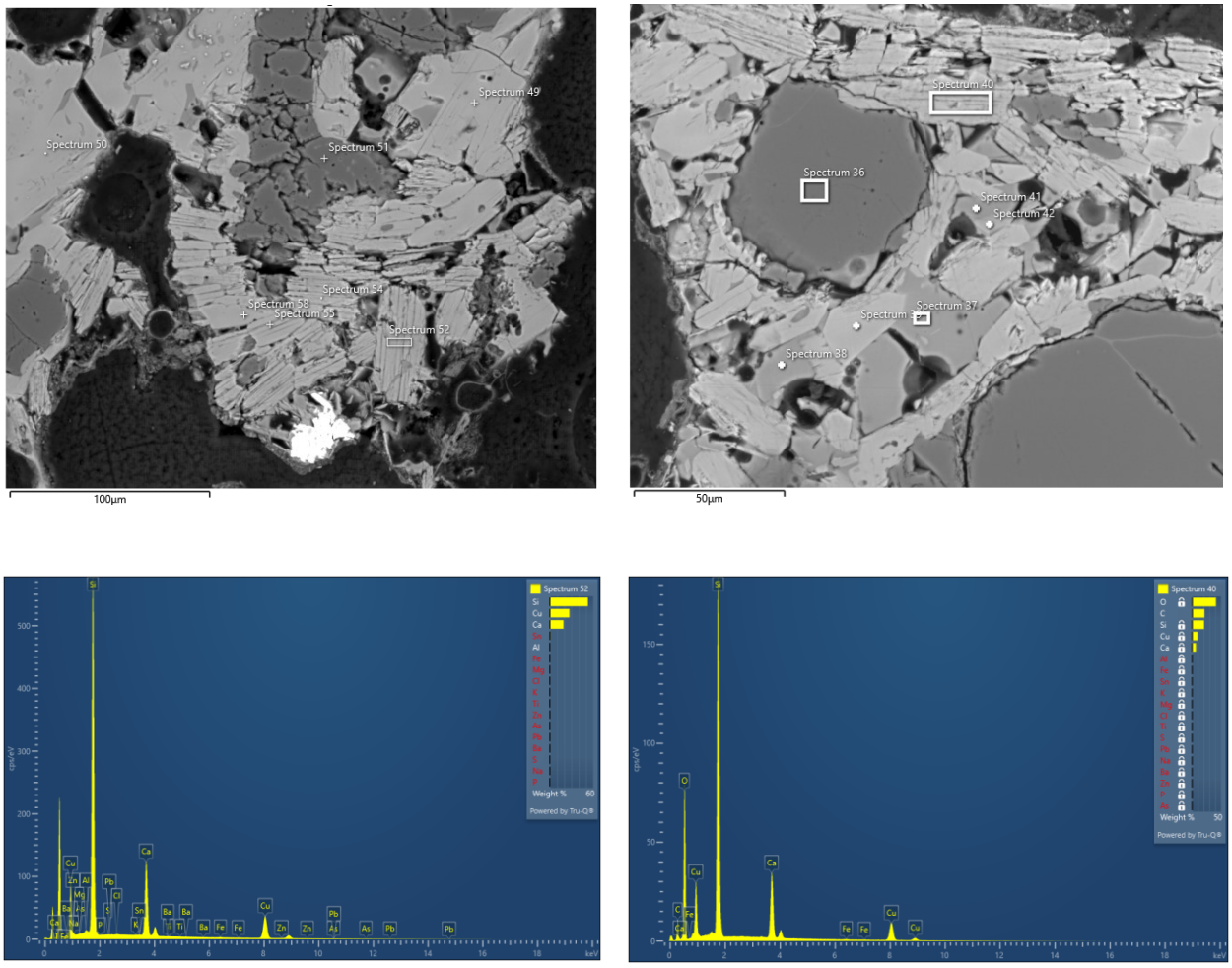

Figure 91 - Point analysis made on Ostia sample with an example of cuprorivaite spectra obtained from the two areas.

6.3.4 LITERNUM SAMPLE

Liternum sample present many grains of Egyptian blue oriented in different directions, showing a smooth or lamellar texture. They are embedded in a glassy matrix carachterized by the presence of Na and globular quartz grains. Like for the other samples false colour maps, point analysis and spectra are reported.

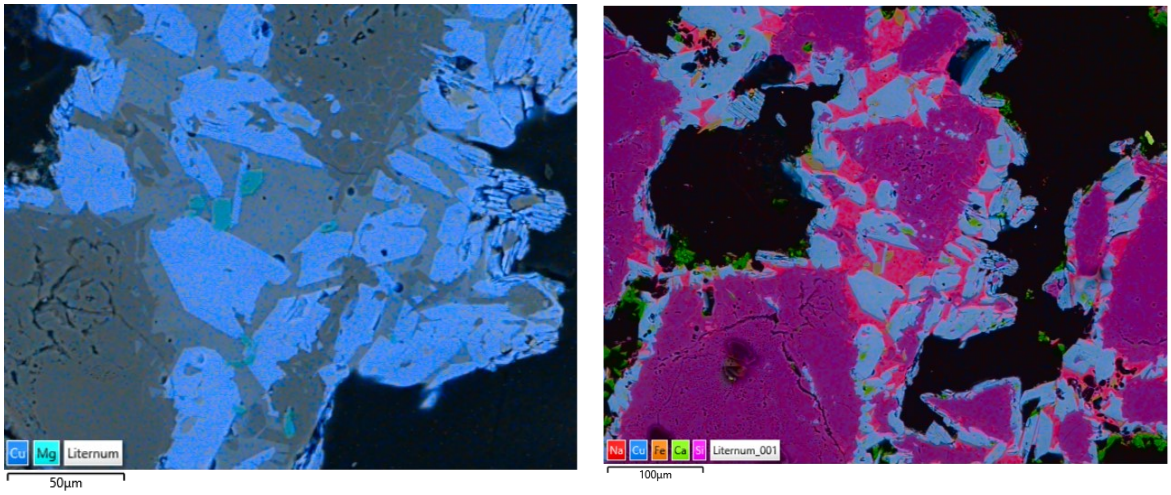

Figure 92 - SEM false colours maps of Liternum sample.

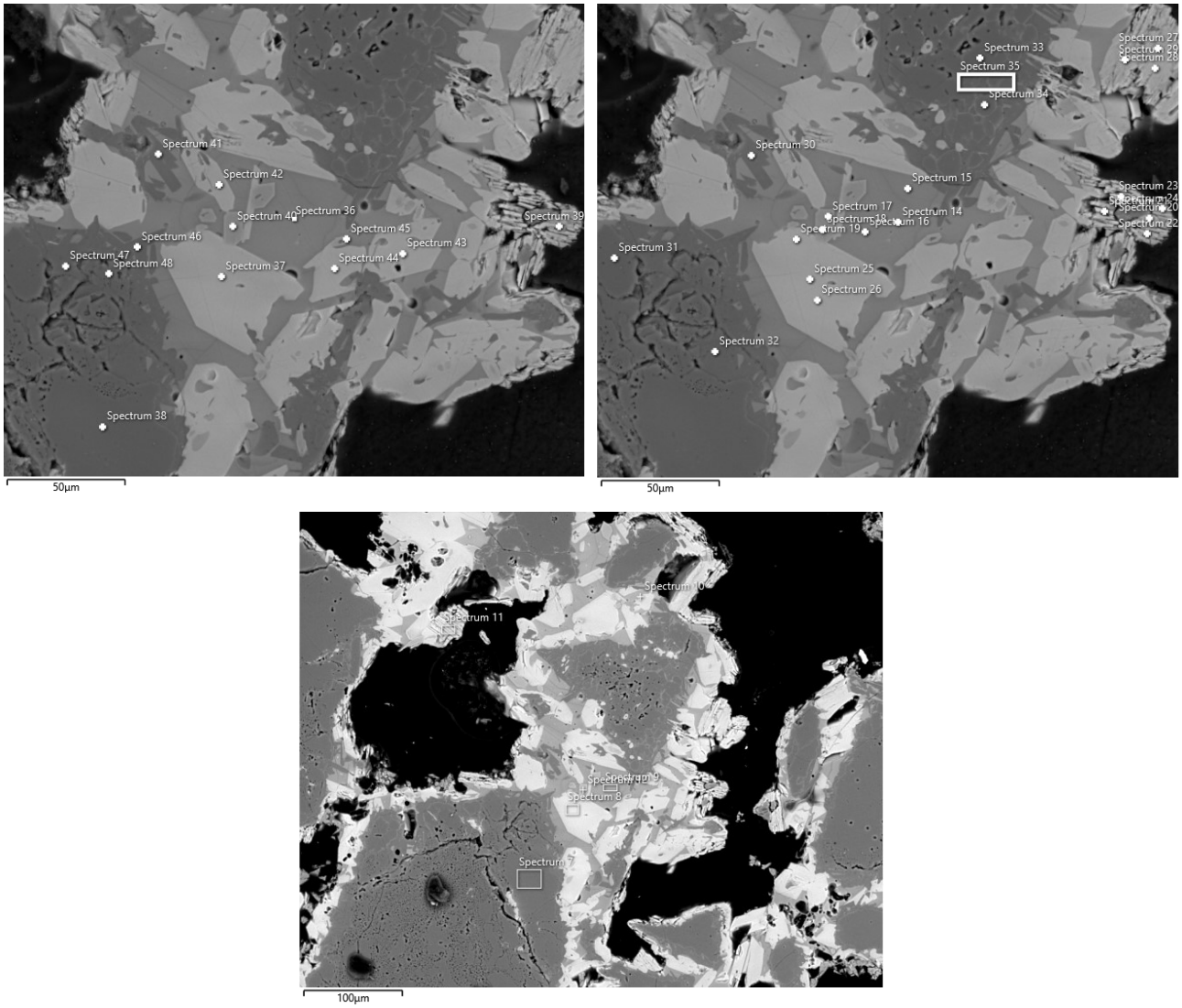

Figure 93 - Point analysis of Liternum sample.

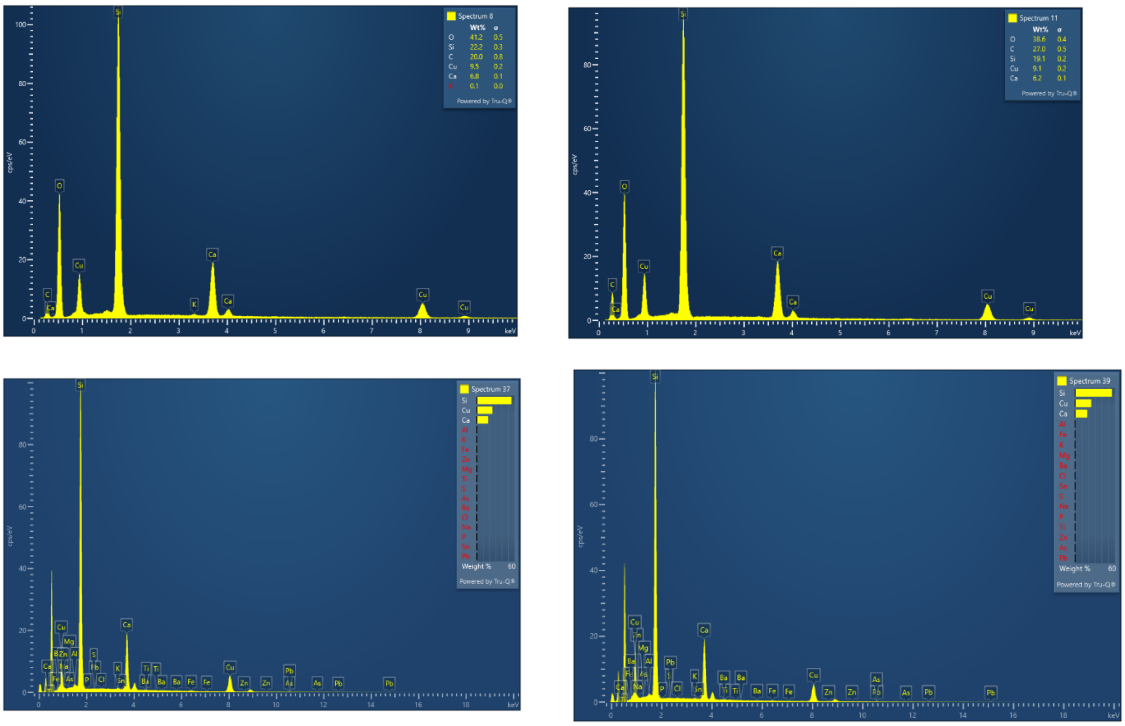

Figure 94 - Cuprorivaite spectra of Liternum sample.

6.3.5 COMPARISONS BETWEEN THE SAMPLES

The averages values of SEM-EDS previously calculated concerning the three oxides (SiO_2, CaO, CuO) composing crystal of cuprorivaite of the samples of Raphael and Ortolano were normalized and compared in a ternary plot (Figure 95) to establish their variability and enhance similarities and differences between them and with the stochiometrical composition of cuprorivaite. To obtain the mean value of each grain the outlier values were removed. The values highlighted in yellow are the ones more distant and this depend on the location of point analysis, i.e. whether the SEM electron beam also invested the area outside the cuprorivaite.

	SiO_2	CaO	CuO
Raph 1	65.6	15.2	19.2
Raph 2	65.9	15.4	18.6
Raph 3	66.1	15.4	18.5
Raph 4	66.6	15.2	18.2
Raph 5	66.8	15.2	18.0
Orto 1	68.0	14.6	17.4
Orto 2	65.3	15.4	19.2
Orto 3	68.0	14.6	17.4
Orto 4	71.0	13.8	15.3
Orto 5	70.5	13.3	16.2
Cupro	63.9	14.9	21.2

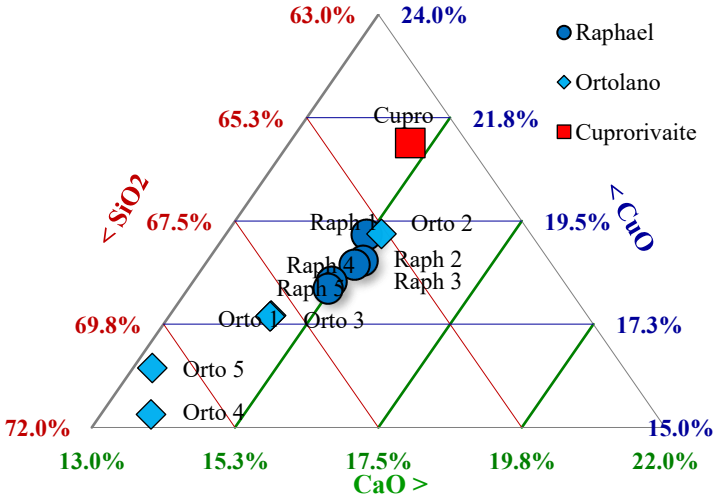

Figure 95 - Ternary plot of the average values of EB grains in Raphael and Ortolano samples compared to cuprorivaite.

Ostia and Liternum samples were compared too in a ternary plot (Figure 96).

	SiO_2	CaO	CuO
Ost 1	66.1	14.1	19.8
Ost 2	67.0	14.7	18.3
Ost 3	66.5	13.7	19.8
Ost 4	68.3	14.0	17.7
Ost 5	68.7	13.9	17.4
Ost 6	74.4	9.7	15.9
Ost 7	66.0	14.0	20.0
Ost 8	64.8	14.9	20.3
Ost 9	65.0	14.8	20.3
Ost 10	65.8	14.5	19.7
Ost 11	64.6	13.4	22.0
Ost 12	65.5	14.6	19.9
Lit 1	69.0	13.8	17.2
Lit 2	69.2	13.8	17.0
Lit 3	70.5	13.0	16.4
Lit 4	71.9	12.4	15.7
Lit 5	68.1	14.3	17.6
Lit 6	67.9	13.8	18.3
Lit 7	67.9	14.1	17.9
Lit 8	69.3	13.7	17.0
Lit 9	68.1	14.0	17.9
Lit 10	68.7	13.7	17.7
Cupro	63.9	14.9	21.2

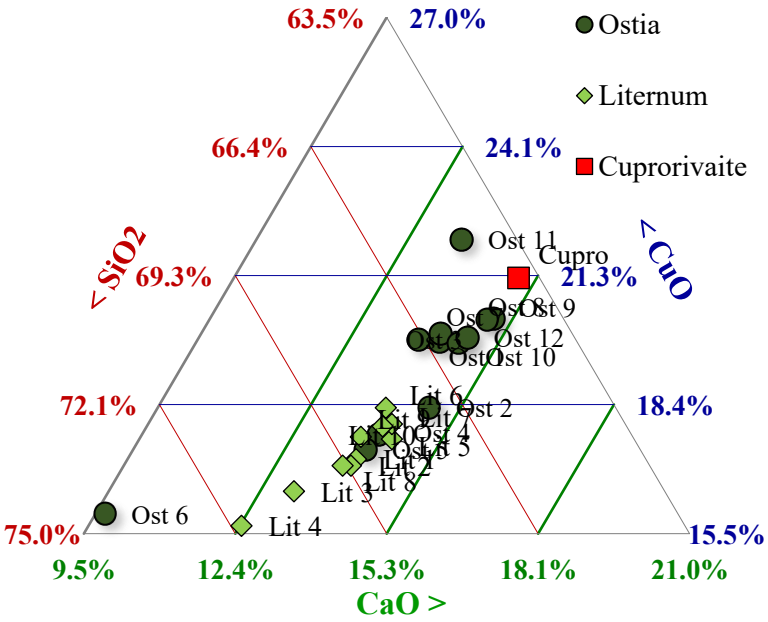

Figure 96 - Ternary plot of the average values of EB grains in Ostia and Liternum samples compared to standard composition of cuprorivaite.

The third ternary plot (Figure 97) show the comparison between all the samples.

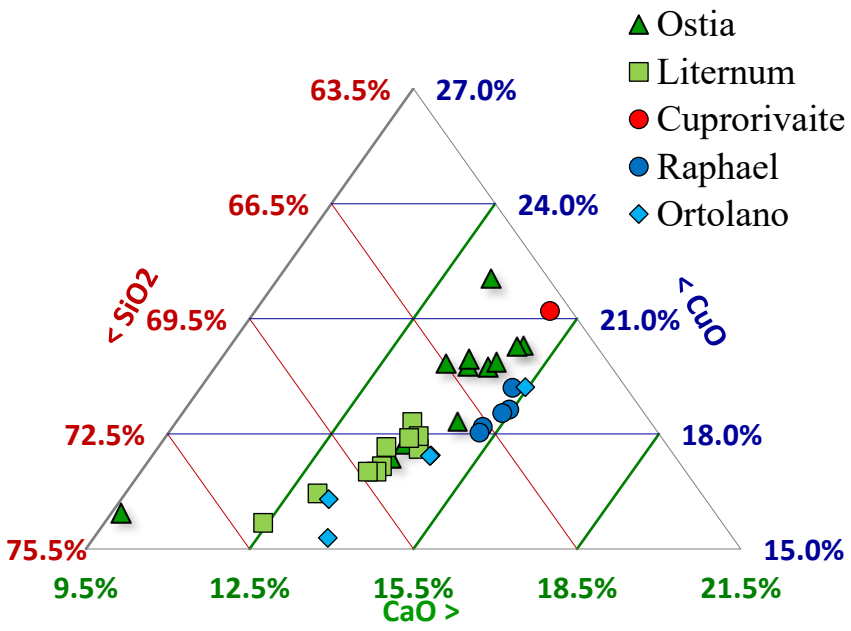

Figure 97 – Ternary plot of the average values of EB grains in Rpahael, Ortolano, Ostia and Liternum samples compared to standard composition of cuprorivaite.

From ternary diagrams, it is difficult to understand a compositional trend as the points used on the graph are the product of average on grains and of several necessary normalisations.

Below are comparisons between Raman maps and SEM maps of the Ostia and Liternum samples.

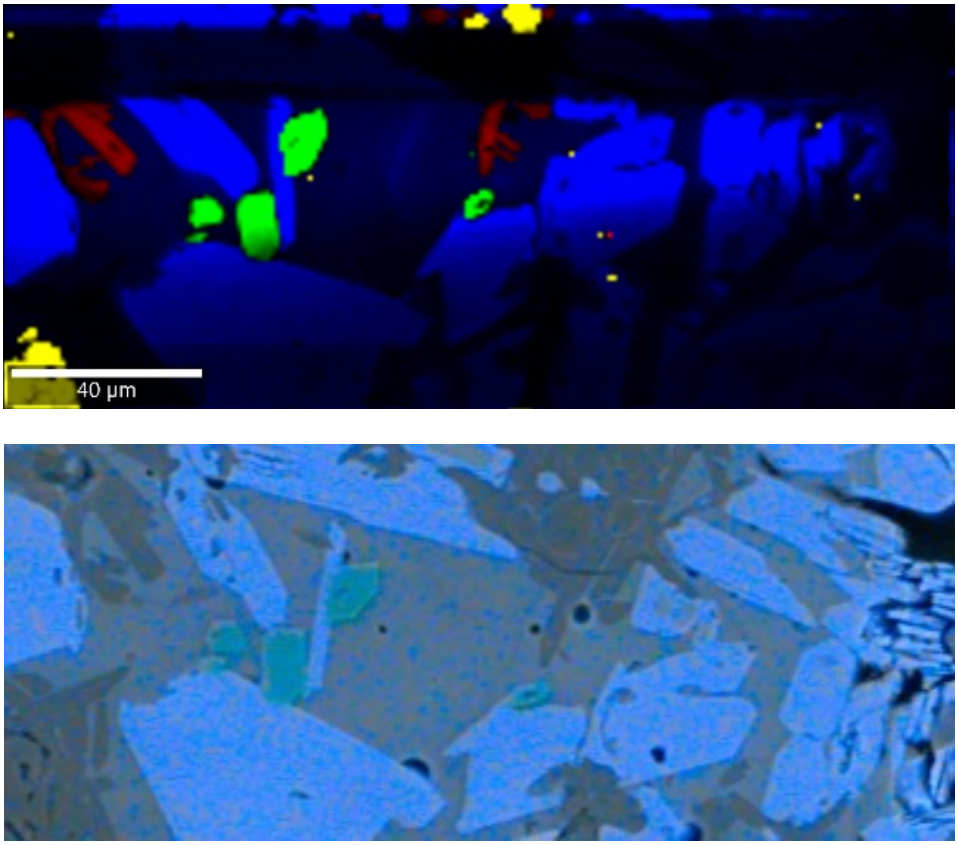

Figure 98 - Raman map of Liternum sample compared with SEM false colours maps.

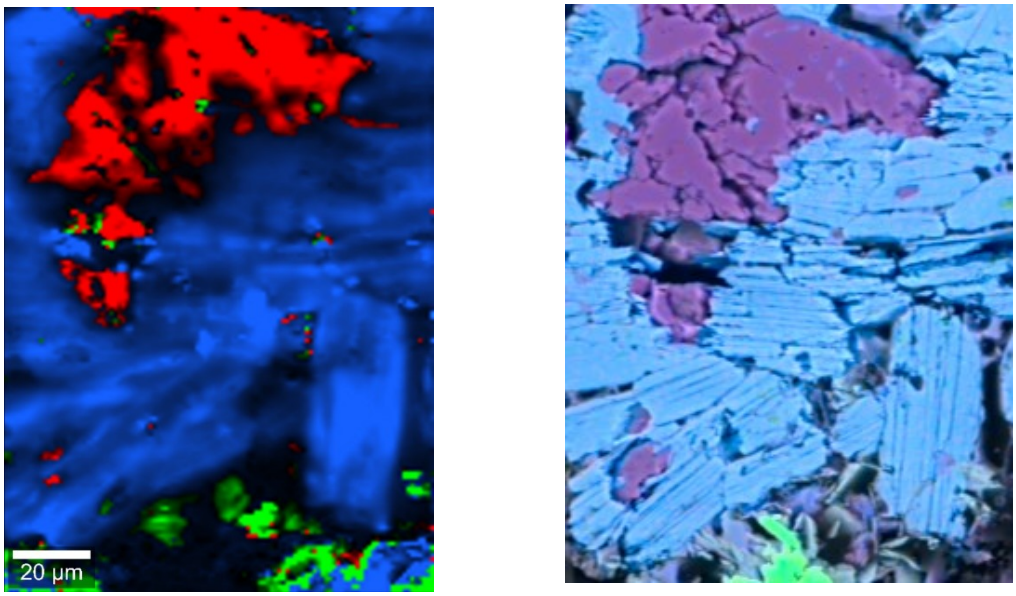

Figure 99 - Raman map of Ostia sample compared with SEM false colours maps.

7. PRINCIPAL COMPONENT ANALYSIS (PCA)

In order to try to answer to the main question of this research, which is about the origin of the pigment used in Renaissance time by Raffaello, Garofalo and Ortolano, and in view of the impossibility of performing the originally planned Pb-isotope analysis, it was decided to make a comparison between the chemical SEM analyses performed on our samples, with the ones present in literature selected from available scientific papers (PAGÈS-CAMAGNA, COLINART 2003; HATTON, G.D 2005; SHORTLAND 2006; PANAGIOTAKI ET AL. 2008; INGO ET AL. 2013; DE VIVO ET AL. 2019). Dott. Alexandra Rodler kindly provided the assembled data, they are summarized in a table available in Appendix C of this thesis. The geographical location of the sites analysed is at the end of this paragraph. (Figure 108)

Usually in the literature it is possible to found the terminology “cakes” or “pellets” for primary workshop raw material according to shape and size of the material, sometimes the more generic term “ingot” is used to enhance the fact that is a reworked material but with not finished shape. (KOVALEV ET AL. 2023)

7.1 PCA 1

First of all, it was done an analysis with all the samples available and all the elements to understand the trend of data based on age, geographical provenance and different typology of samples.

SiO2	CaO	CuO	Na2O	K2O	MgO	Al2O3
Min. :56.18	Min. : 6.30	Min. : 4.40	Min. :0.000	Min. :0.0000	Min. :0.0000	Min. :0.0000
1st Qu.:64.78	1st Qu.: 8.95	1st Qu.:11.40	1st Qu.:1.210	1st Qu.:0.1000	1st Qu.:0.3125	1st Qu.:0.3700
Median :68.70	Median :11.00	Median :13.60	Median :1.900	Median :0.2101	Median :0.6000	Median :0.5500
Mean :68.77	Mean :11.35	Mean :13.36	Mean :2.108	Mean :0.2662	Mean :0.9727	Mean :0.6595
3rd Qu.:72.53	3rd Qu.:13.71	3rd Qu.:15.98	3rd Qu.:2.900	3rd Qu.:0.4100	3rd Qu.:1.1000	3rd Qu.:0.9000
Max. :79.20	Max. :19.25	Max. :19.84	Max. :5.700	Max. :1.1000	Max. :6.3000	Max. :2.8000

FeO	SnO2	PbO	TiO2
Min. :0.0000	Min. :0.0000	Min. :0.0000	Min. :0.00000
1st Qu.:0.3000	1st Qu.:0.1039	1st Qu.:0.0000	1st Qu.:0.00000
Median :0.5000	Median :0.4500	Median :0.1000	Median :0.10000
Mean :0.7692	Mean :0.5982	Mean :0.8409	Mean :0.06667
3rd Qu.:0.7825	3rd Qu.:0.9000	3rd Qu.:0.3000	3rd Qu.:0.10000
Max. :3.2000	Max. :3.1000	Max. :6.0000	Max. :0.20000
	NA's :5	NA's :10	NA's :15

As it is possible to see from the table above the analyses are very heterogeneous., In some samples not all elements were not measured; in particular in 5 samples tin, in 10 samples lead and in 15 samples titanium data are missing (red square on the table).

The data with 11 variables represented by the elements (expressed in oxides) of the samples were reduced by the algorithm of the software in 5 components with the percentages of 27.47% 23.50% 14.34% 11.41% and 8.58% which explained 85,3% of variance.

Component 1 is plotted with *Component 2* showing the trend of sample with various geographical provenance and different age. To better visualize sample names and chemical components the graph was split in score plot and loading plot (Figure 100). The same analysis was done considering the different sample types. (Figure 101)

The LBA and Hellenistic/Roman samples have a broader distribution with more variability while Iron Age samples (apart from a Nimrud sample) are more similar between each other, and also the Renaissance ones. Cu, Ca and Si represent discriminating elements between the samples, possibly related to the reagent proportions (i.e. silica vs lime + copper). Sn, Pb and Fe also have a great variability among samples (i.e. they are discriminating elements), potentially related to the metal source), while the content of K, Mg, Al and Na is less variable.

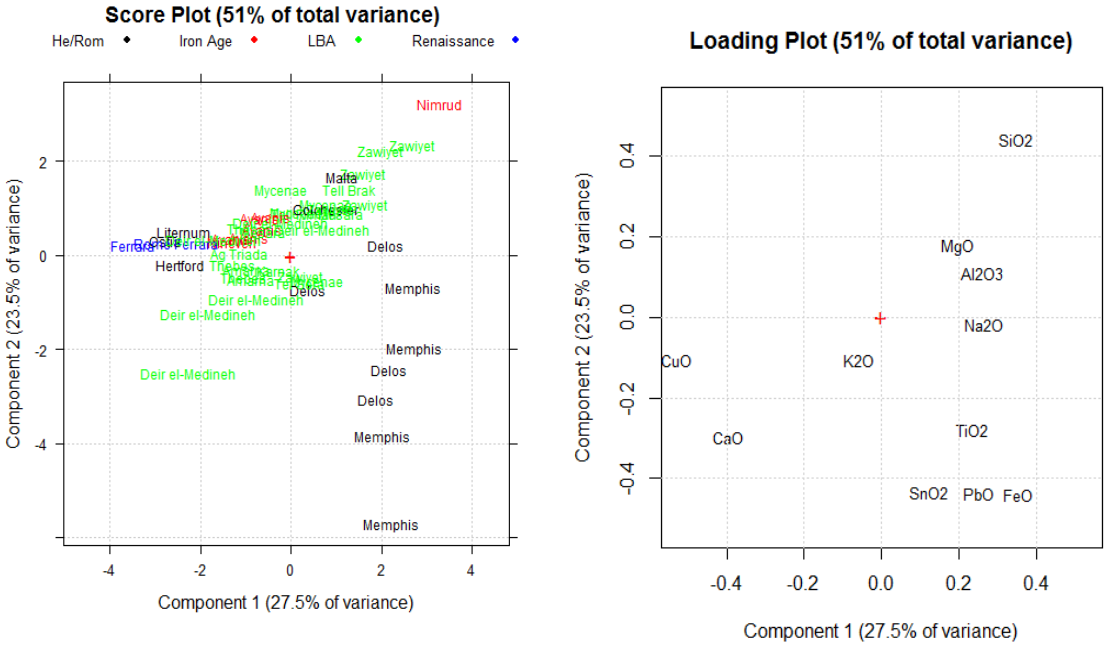

Figure 100 - PCA 1 analysis of EB samples according to different ages, Hellenistic/Roman (He/Rom), Iron Age, Late Bronze Age (LBA), Renaissance and various archaeological sites.

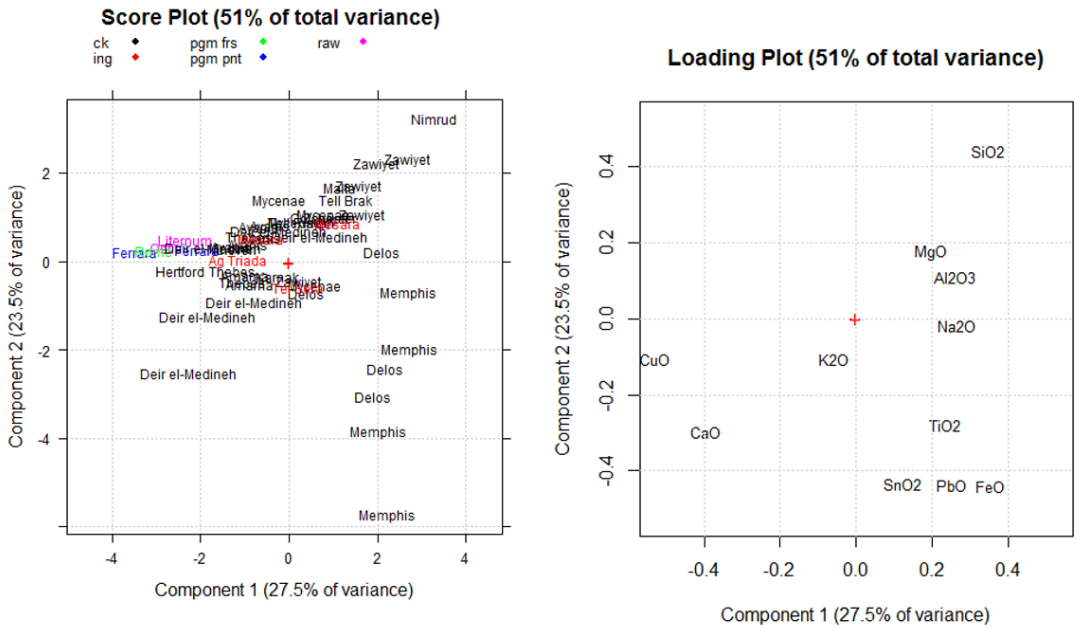

Figure 101 - PCA 1 analysis of EB samples according to different types of samples: cakes (ck), ingots (ing), fresco pigment (pgm frs), painting pigment (pgm pnt), our Roman age EB fragments are labelled as raw to better distinguish them.

Pb, Fe and Sn are correlated and they seem more typical of Egyptian and Aegean Hellenistic/Roman materials; Ostia and Literum samples despite been Roman age are separated respect to the ones of the same period and are more similar to the Renaissance ones. Egyptian/Aegean materials of LBA period have a completely different distribution (Figure 102).

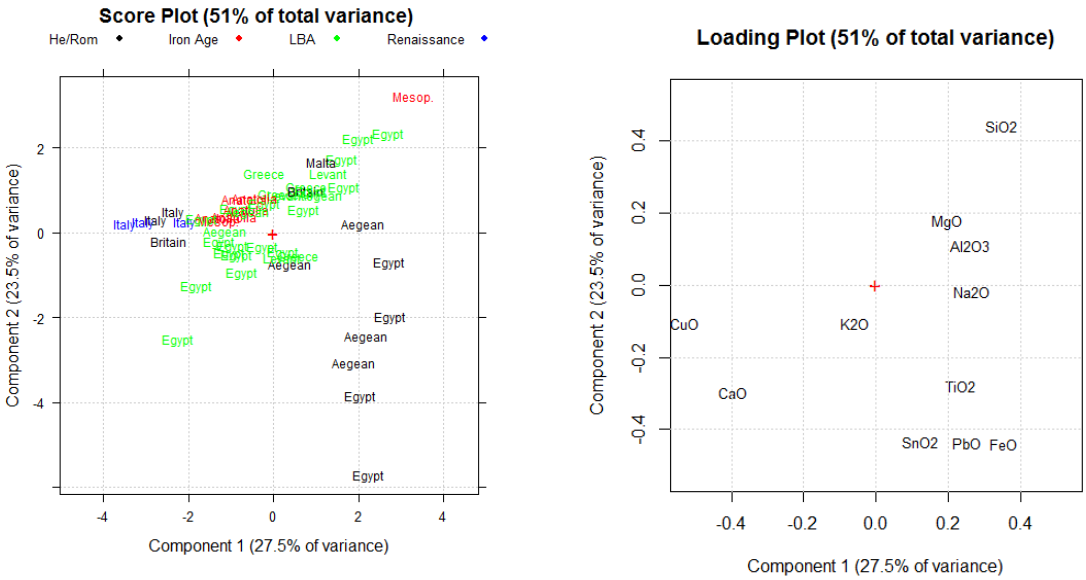

Figure 102 - PCA 1 analysis of EB samples according to different geographical regions.

The same procedure was performed plotting also Component 2 with Component 3 resulting in no new or further considerations.

7.2 PCA 2

Having a set of samples with elements not analysed may create bias in the interpretation. Therefore, it was decided to perform again the PCA analysis by removing the samples missing the Sn, Pb and Ti data, in order to understand their impact on the results.

SiO2	CaO	CuO	Na2O	K2O	MgO	Al2O3
Min. :58.40	Min. : 6.30	Min. : 4.40	Min. :0.000	Min. :0.0000	Min. :0.000	Min. :0.0000
1st Qu.:64.82	1st Qu.: 8.85	1st Qu.:10.50	1st Qu.:1.400	1st Qu.:0.1000	1st Qu.:0.475	1st Qu.:0.3980
Median :68.20	Median :11.25	Median :12.40	Median :2.000	Median :0.2000	Median :0.600	Median :0.6000
Mean :69.08	Mean :11.14	Mean :12.57	Mean :2.128	Mean :0.2511	Mean :1.130	Mean :0.7382
3rd Qu.:73.28	3rd Qu.:13.70	3rd Qu.:15.25	3rd Qu.:2.900	3rd Qu.:0.4000	3rd Qu.:1.125	3rd Qu.:1.0000
Max. :79.20	Max. :17.40	Max. :19.82	Max. :5.700	Max. :1.1000	Max. :6.300	Max. :2.8000

FeO	SnO2	PbO	TiO2
Min. :0.000	Min. :0.0000	Min. :0.0000	Min. :0.00000
1st Qu.:0.300	1st Qu.:0.1789	1st Qu.:0.1000	1st Qu.:0.00000
Median :0.500	Median :0.5000	Median :0.1633	Median :0.10000
Mean :0.858	Mean :0.6060	Mean :0.9535	Mean :0.06667
3rd Qu.:0.950	3rd Qu.:0.9000	3rd Qu.:0.3351	3rd Qu.:0.10000
Max. :3.200	Max. :3.1000	Max. :6.0000	Max. :0.20000

In this case the 5 components of PCA explain the 87.33% and each component represent 29.48%, 25.28%, 12.98%, 10.87% and 8.72% of variance.

PCA 2 plotting Component 1 and Component 3 (Figure 103) shows in a clearer way the similarity between the Ostia, Liternum, Raphael and Garofalo samples, while the Ortolano sample (Ferrara blue and green writings in the graphs) is somehow distinct.

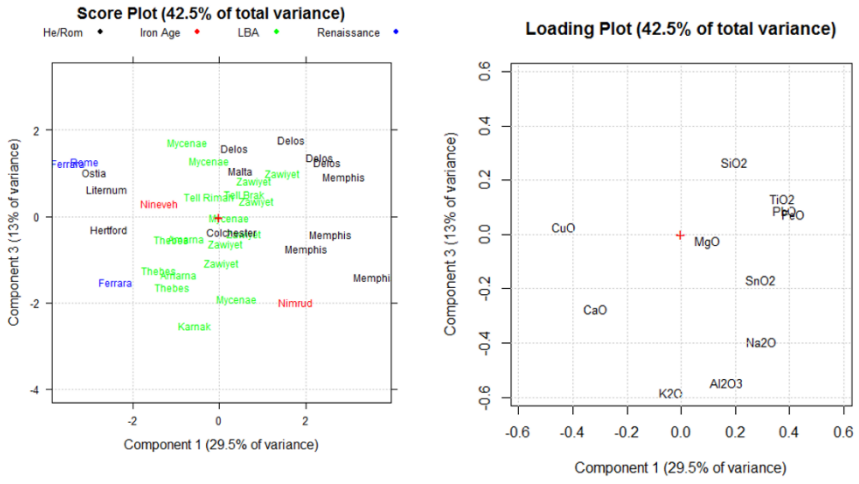

Figure 103 - PCA 2 analysis of EB samples according to different ages, Hellenistic/Roman, Iron Age, Late Bronze Age, Renaissance and various archaeological sites.

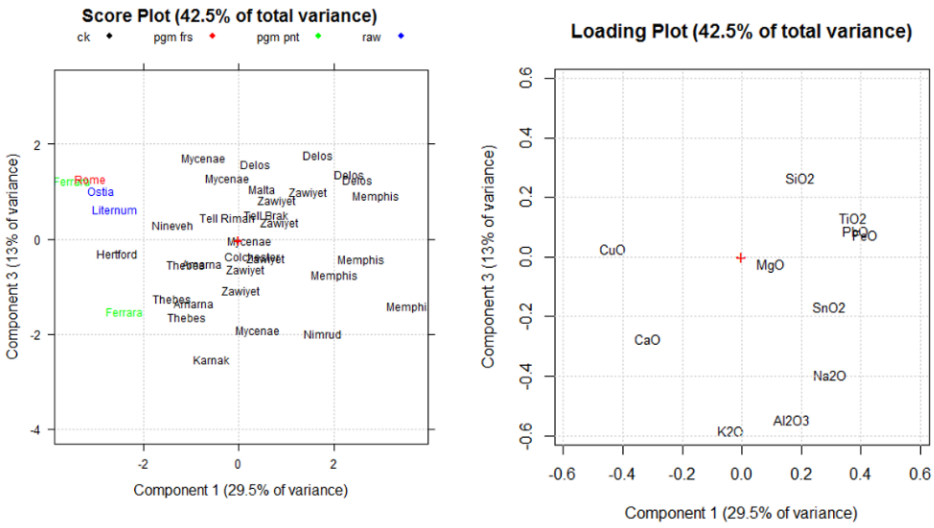

Figure 104 - PCA 2 analysis of EB samples according to different types of samples: cakes, ingots, fresco pigment, painting pigment, our Roman age EB fragments are labelled as raw to better distinguish them.

In this case the data result in statistically less significant results, but the distribution is more visible and shows the relevance of the content of Cu in the samples analysed in this thesis respect to the other samples from the literature. This new PCA shows how Ti, Pb and Fe are correlated between them.

7.3 PCA 3

```
     SiO2            CaO             CuO            Na2O             K2O              MgO            Al2O3
Min.   :56.18   Min.   : 6.30   Min.   : 4.40   Min.   :0.000   Min.   :0.0000   Min.   :0.0000   Min.   :0.0000
1st Qu.:64.78   1st Qu.: 8.95   1st Qu.:11.40   1st Qu.:1.210   1st Qu.:0.1000   1st Qu.:0.3125   1st Qu.:0.3700
Median :68.70   Median :11.00   Median :13.60   Median :1.900   Median :0.2101   Median :0.6000   Median :0.5500
Mean   :68.77   Mean   :11.35   Mean   :13.36   Mean   :2.108   Mean   :0.2662   Mean   :0.9727   Mean   :0.6595
3rd Qu.:72.53   3rd Qu.:13.71   3rd Qu.:15.98   3rd Qu.:2.900   3rd Qu.:0.4100   3rd Qu.:1.1000   3rd Qu.:0.9000
Max.   :79.20   Max.   :19.25   Max.   :19.84   Max.   :5.700   Max.   :1.1000   Max.   :6.3000   Max.   :2.8000
      FeO
Min.   :0.0000
1st Qu.:0.3000
Median :0.5000
Mean   :0.7692
3rd Qu.:0.7825
Max.   :3.2000
```

For the PCA 3 the data set was done keeping all the samples but removing all the sample analyses where Sn, Pb, Ti were not measured or detected.. With this new data set the variance explained is of 88.89% with the 5 components explaining 33.88%, 18.11%, 14.76%, 13.69% and 8,44% of variance.

As it is possible to notice from the plots of PCA 3 without the omitted elements (Figure 105) the samples of LBA and He/Rom period are less differentiated and more widespread. While the Iron Age samples are characterized by a higher amount of Cu resulting to be in general closer to each other. Also with this data set the Italian and Renaissance samples are grouped and present a relevant Cu content.

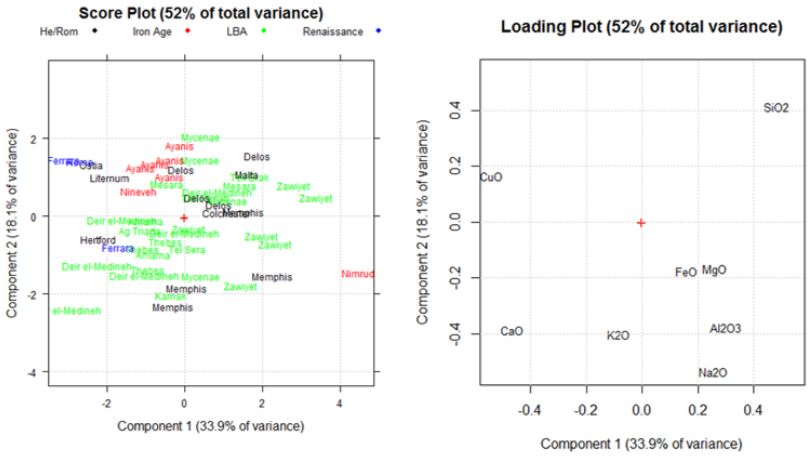

Figure 105 - PCA 3 analysis of EB samples according to different ages, Hellenistic/Roman, Iron Age, Late Bronze Age, Renaissance and various archaeological sites.

But it has to be considered that the painting/fresco samples have just the main elements corresponding to pure cuprorivaite (Cu, Ca and Si) with only Ortolano that have a more articulated composition.

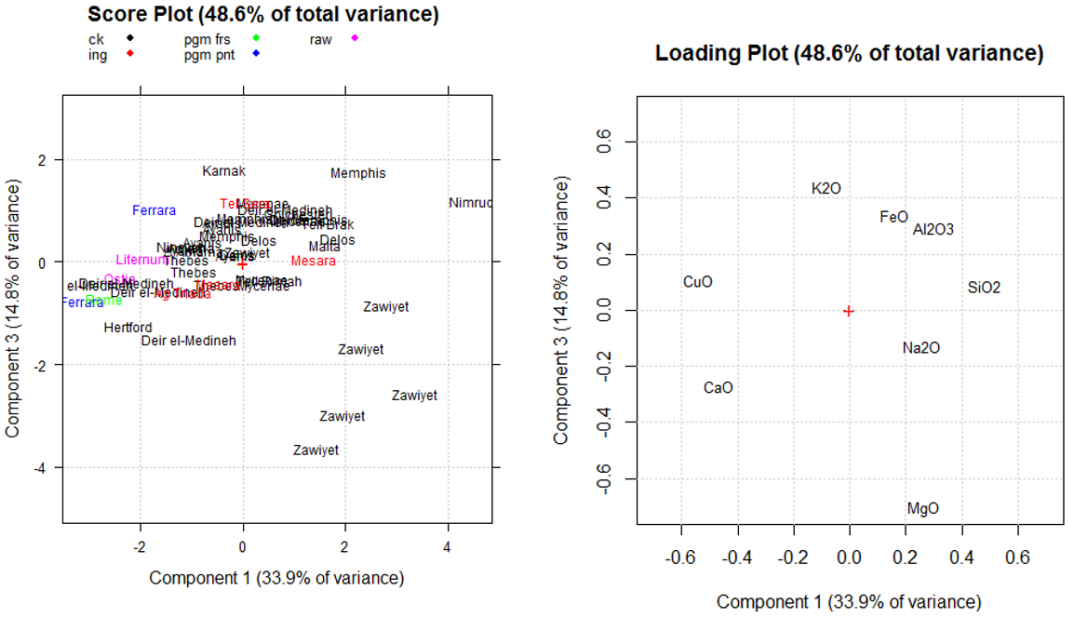

Figure 106 - PCA 3 analysis of EB samples according to different types of samples: cakes, ingots, fresco pigment, painting pigment, our Roman age EB fragments are labelled as raw to better distinguish them.

In conclusion each of the three PCA enhanced specific peculiarities of the data set. In PCA 1 with complete data set, the algorithm should complete the missing elements resulting in a not accurate analysis, while PCA 2 is more reliable enhancing the difference between Hellenistic/Roman and Egyptian/Aegean EB samples from Roman and Italian ones appearing really similar and close to each other. PCA 3 confirmed the already explained trend showing also the similarities between Iron Age Anatolia/Mesopotamia samples. In the end, the most clear indications may derive from the PCA plot in Figure 107, which excludes the samples with missing analyses, and shows the clear differences between the group of samples.

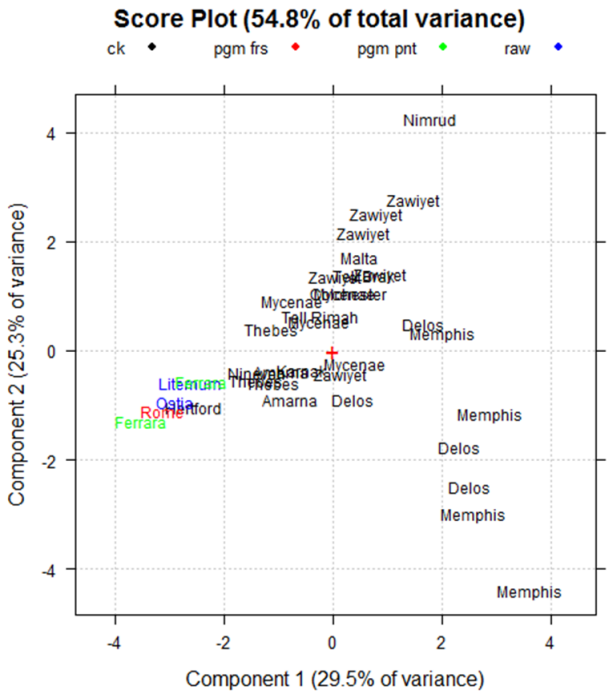

Figure 107 – PCA 2 plot according to different types of samples: cakes, ingots, fresco pigment, painting pigment, our Roman age EB fragments are labelled as raw to better distinguish them.

The mentioned consideration has however some limitations. It is useful to remind that SEM analyses are semiquantitative, the quantity of some elements is near the limit of detection, have been done by different research groups with different methodologies that may have introduced systematic errors and on heterogeneous samples, i.e. raw samples such as cakes, ingots or refined, cleaned samples embedded in a painting matrix such as those found in works of art such as oil paintings and frescoes.

However, it is possible to say that (1) the samples from Roman Italy (i.e. Ostia, Liternum) are clearly distinguished from the ancient EB samples of different regions, including Greece, the Aegean, Egypt, and Mesopotamia), (2) the major chemical distinction is the CuO/SiO_2 ratio, that is they are richer in Cu and poorer in silica, and (3) the Renaissance sample plot very close to the ancient Roman Italian samples, showing a striking chemical similarity. This suggests that the Egyptian blue pigment used by Renaissance artists was potentially obtained from archaeological sources in the Italian area although it appears to have been purified and/or treated for painting.

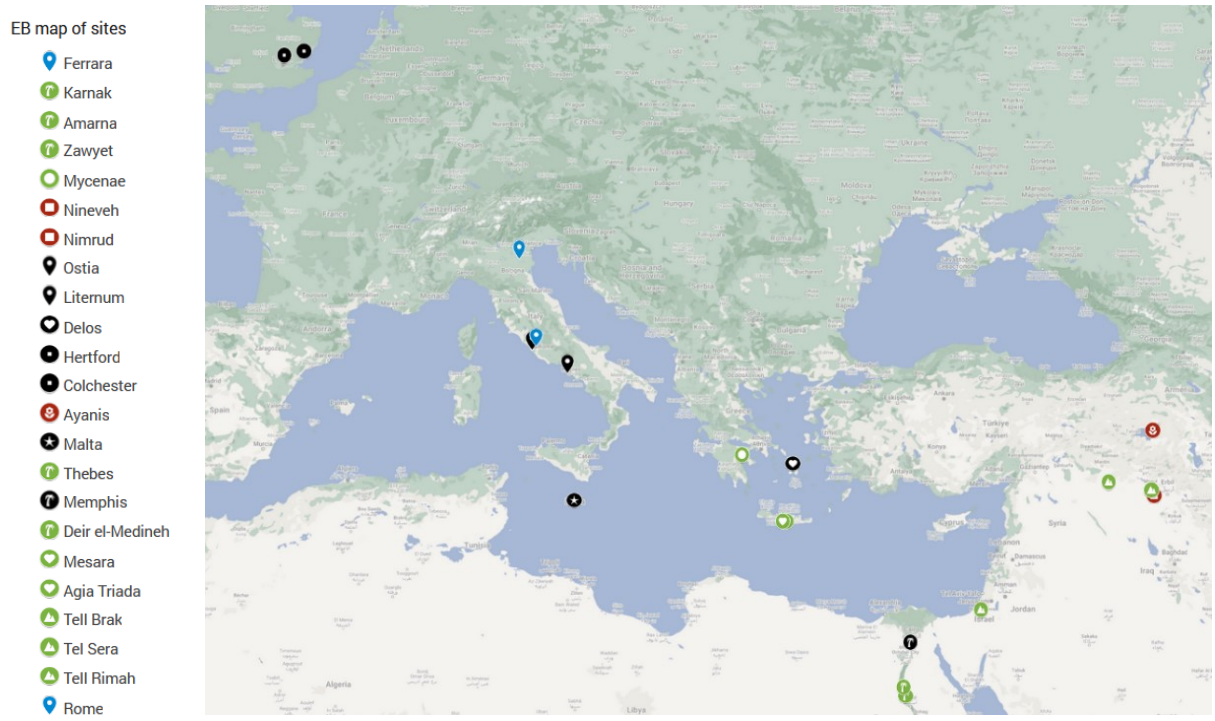

Figure 108 - Geographical places have different symbols, whereas the different ages are identified by different colours.

8. Discussion and conclusions

The analysis performed on such tiny heterogenous fragments have represented a challenge for the instruments employed. The difficulties encountered were also due to the fact that non-invasive analyses had to be used so that the samples could also be re-analysed using other techniques. In particular the pictorial samples characterised by a heterogeneous matrix represent always a demanding task to analyse. Moreover, the comparison between archaeological samples of raw pigment with refined Egyptian blue grains in pictorial matrixes must be taken with due care being samples from heterogeneous sources.

The use of SEM - EDS to identify the trace elements must be taken with due caution, as it is a semi-quantitative technique. PCA analysis have revealed how the Renaissance samples fall near the Roman Age ones as visible in the score plot below from PCA 2.

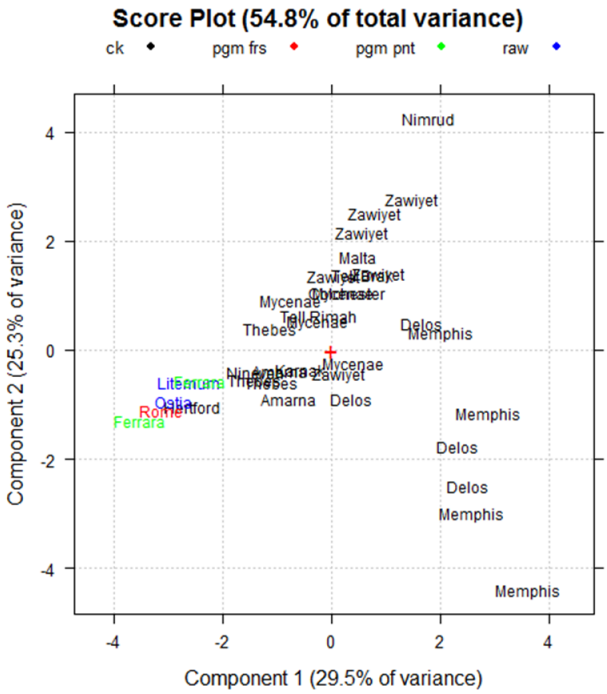

Figure 109 – PCA 2 plot according to different types of samples: cakes, ingots, fresco pigment, painting pigment, our Roman age EB fragments are labelled as raw to better distinguish them.

The pictorial Renaissance samples however result to be more pure and refined respect to the Ostia and Liternum samples.

The PCA seems to convey the idea of a reuse of ancient yet refined pigment. In addition, there are no notable chemical elements that would suggest the precise origin of the pigment.

However, the extensive use of the pigment, especially in the frescoed vault of the Villa Farnesina, shows a massive and systematic use of Egyptian blue that could suggest its production in the Renaissance period, even though neither literary sources nor archaeological production sites

from the Renaissance period are known to date that could confirm this second hypothesis.
In addition, as we have seen the specific stratigraphy made by artists with the Egyptian blue mixed with lapislazuli while red organic dye mixed with azurite in one case and in the other with EB separated by azurite could suggest and intentional use by the artists to convey specific colour and shade final effects to the paintings.

We should also notice that the EB is always very diluted and used in conjunction with other blue pigments, so that indeed a re-use of a substantial but limited quantity of a refined archaeological materials is possible.

In conclusion, it was not possible with the techniques used to conclusively settle the issue. Although the strong chemical similarity between the Renaissance samples and the EB produced in Central-Southern Itali in Roman times may be a strong indication of re-use.

The use of lead isotope analysis (LIA) in the copper of the pigment could resolve the question of the origin of the pigment used in Renaissance times.

Further and more detailed quantitative analyses could be precious to compare different samples of various geographical areas and different ages.

A synergetic work between scientists already started with the BLUENET project is of paramount importance for the study of a large scale of sample to permit having a big database of all the occurrences which in this thesis was limited to some of the available ones.

The invention of the night goggles system constitutes a new frontier for the rapid and certain detection of Egyptian blue pigment in a large number of artworks in a totally non-invasive manner that can be really helpful to have a general screening of all the artworks at least of Renaissance painters in the circle of Raphael.

A more general and exhaustive screening of the use of EB in the 16^{th} century would also provide indication of the availability of the pigment in this period.

In conclusion, future research should expand the use of analytical techniques, from visual inspection to complex chemical analyses, to deepen the understanding of technology transfer and variations in raw material choices to understand the evolution of production techniques over time.

References

ACCORSI G., VERRI G., BOLOGNESI M., ARMAROLI N., CLEMENTI C., MILIANI C., ROMANI A. 2009. *The Exceptional Near-Infrared Luminescence Properties of Cuprorivaite (Egyptian Blue)*. "Chemical Communications", no. 23, 3392–94.

ANSELMI C., VAGNINI M., SECCARONI C., AZZARELLI M., FRIZZI T., ALBERTI R., FALCIONI M., SGAMELLOTTI A. 2020. *Imaging the Antique: Unexpected Egyptian Blue in Raphael's Galatea by Non-Invasive Mapping.* "Rendiconti Lincei. Scienze Fisiche e Naturali" 31 (4): 913–17. https://doi.org/10.1007/s12210-020-00960-4.

ARTIOLI G. 2010. *Scientific Methods and Cultural Heritage: An Introduction to the Application of Materials Science to Archaeometry and Conservation Science*, 42–46, 66–68. Oxford University Press.

AUSILI A., SÁNCHEZ M., GÓMEZ-FERNÁNDEZ J. 2015. *Attenuated Total Reflectance Infrared Spectroscopy: A Powerful Method for the Simultaneous Study of Structure and Spatial Orientation of Lipids and Membrane Proteins*. "Biomedical Spectroscopy and Imaging" 4 (April):159–70. https://doi.org/10.3233/BSI-150104.

BALDASSINI G. 2021. *Giovan Battista Benvenuti - L'Ortolano. Pittore ferrarese.* Thesis. https://etd.adm.unipi.it/t/etd-03212021-115517/.

BARUFFALDI G. 1844. *Vite de' Pittori e Scultori Ferraresi*. Ferrara: Domenico Taddei.

BECK J. H. 1994. *Raphael*. New York: Harry N. Abrams, Inc.

BECKER H. 2022. *Pigment Nomenclature in the Ancient Near East, Greece, and Rome.* "Archaeological and Anthropological Sciences" 14 (1): 20.

BELLINI M. 2023. *Il Blu Egizio e Il Simbolo. Una Nota.* "Materiali Di Estetica." Terza Serie, no. 10.1. https://riviste.unimi.it/index.php/MdE/article/view/20617.

BERKE H., PORTMANN A., BOUHEROUR S. ET AL. 2010. *The Development of Ancient Synthetic Copper-Based Blue and Purple Pigments.* In "Conservation of Ancient Sites on the Silk Road: Proceedings of the Second International Conference on the Conservation of Grotto Sites, Mogao Grottoes, Dunhuang, People's Repubblic of China". June 28–July 3, *2004.*, The Getty Conservation Institute, 225–33. Los Angeles: Neville Agnew.

BERKE, H. 2007. *The Invention of Blue and Purple Pigments in Ancient Times*. "Chemical Society Reviews" 36 (1): 15–30.

BERTHOMIEU C., HIENERWADEL R. 2009. *Fourier Transform Infrared (FTIR) Spectroscopy.* "Photosynthesis Research" 101 (2): 157–70. https://doi.org/10.1007/s11120-009-9439-x.

BINET E. 1622. *Essay des merveilles de nature, et des plus nobles artifices. Piece tres-necessaire à tous ceux qui font profession de'eloquence, par René François [pseud.].* I. Osmont.

BOSCHETTI C. 2011. *Vitreous Materials in Early Mosaics in Italy: Faience, Egyptian Blue, and Glass*. "Journal of Glass Studies" 59–91.

BREDAL-JØRGENSEN J., SANYOVA J., RASK V., SARGENT M.L., HOBERG THERKILDSEN R. 2011. *Striking Presence of Egyptian Blue Identified in a Painting by Giovanni Battista Benvenuto from 1524*. "Analytical and Bioanalytical Chemistry" 401 (4): 1433–39. https://doi.org/10.1007/s00216-011-5140-y.

BUSATTA S. 2014. T*he Perception of Color and The Meaning of Brilliance Among Archaic and Ancient Populations and Its Reflections on Language.* "Antrocom: Online Journal of Anthropology" 10 (2).

LADERCHI C. 1856. *La Pittura Ferrarese. Memorie*. Ferrara: Abram Servadio Editore.

CAMPANELLA B., PALLESCHI V., LEGNAIOLI S. 2021. *Introduction to Vibrational Spectroscopies.* "ChemTexts" 7 (1): 5. https://doi.org/10.1007/s40828-020-00129-4.

Confocal Microscope. 2024. In "Encyclopedia Britannica". https://www.britannica.com/technology/microscope/Stereoscopic-microscopes.

DARIZ P., SCHMID T. 2021. *Trace Compounds in Early Medieval Egyptian Blue Carry Information on Provenance, Manufacture, Application, and Ageing*. "Scientific Reports" 11 (1): 11296.

DAVIDSON, M.W., ABRAMOWITZ M. 2002. *Optical Microscopy.* "Encyclopedia of Imaging Science and Technology" 2 (1106–1141): 120.

NIKOLAS D., JOKINIEMI E. 2008. *Dictionary of Architecture and Building Construction*. In "Dictionary of Architecture and Building Construction", 131. Routledge.

DE VIVO G.,VAN LOON A., NOBLE P., HIRAYAMA A., ABE Y., NAKAI I., BULL D. 2019. *An Unusual Pigment in 16th-Century Ferrara: "Egyptian Blue" in Garofalo's "Adoration of the Magi" and Ortolano's "St Margaret"*. In "Trading Paintings and Painters' Materials 1550-1800".

DOMÉNECH-CARBÓ M., OC L. 2016. *Another Beauty of Analytical Chemistry: Chemical Analysis of Inorganic Pigments of Art and Archaeological Objects*. "ChemTexts 2" (August). https://doi.org/10.1007/s40828-016-0033-5.

EASTAUGH N. ET AL. 2004. *Egyptian blue.* In "The Pigment Compendium: A Dictionary of Historical Pigments". Part I.147-148. Elsevier.

EASTAUGH N. ET AL. 2004. *Calcium Copper Silicate, Cuprorivaite Type*. In "The Pigment Compendium. Optical Microscopy of Historical Pigments ", Part II. 26–27. Elsevier.

ELLIOTT A. D. 2020. *Confocal Microscopy: Principles and Modern Practices*. "Current Protocols in Cytometry" 92 (1): e68. https://doi.org/10.1002/cpcy.68.

GERLINI E. 2007. *Villa Farnesina Alla Lungara, Roma*. Istituto Poligrafico e Zecca dello Stato.

FRABETTI G. 1966. *L'Ortolano*. Milano: Amilcare Pizzi.

FRANZ F. 2018. *Disvelando Pale, Effigi e Panneggi.* "MDCCC 1800" 7:95–126.

TALIER G. 1704. In *Nuovo Plico d'ogni Sorte Di Tinture, Arricchito Di Rari, e Bellissimi Segreti per Colorire Animali, Vegetabili, e Minerali; Raccolti Da Gallipidio Talier e Dati in Luce Dal Medesimo à Beneficio Comune. Consecrato al Molt'Illustre Signor Kav. Sebastiano Bombelli Pittore Eccellentissimo*, 134. Venezia: Lorenzo Baseggio.

GARCÍA-FERNÁNDEZ P., MORENO M., ARAMBURU J.A. 2015. *Origin of the Exotic Blue Color of Copper-Containing Historical Pigments*. "Inorganic Chemistry" 54 (1): 192–99. https://doi.org/10.1021/ic502420j.

SIDOTI G., SECCARONI C., SANTOPADRE P. 2018. *Il Blu Egiziano Nelle Sezioni Stratigrafiche Dei Dipinti Di Raffaello Nella Villa Farnesina Di Roma*. In "Bollettino ICR. Istituto Centrale per Il Restauro", 6–23. Nuova Serie 37. Firenze: Nardini Editore.

MALAFARINA G. ed. 2003. *La Villa Farnesina a Roma*. "Mirabilia Italiae". Franco Cosimo Panini.

MANCINI G., PENNY N. 2016. *The Sixteenth Century Italian Paintings*. Vol. III Bologna and Ferrara. Yale University Press.

GUARINI M. 1621. *Compendio Historico Dell'origine, Accrescimento, e Prerogatiue Delle Chiese, e Luoghi Pij Della Città, e Diocesi Di Ferrara, e Delle Memorie Di Que' Personaggi Di Pregio, Che in Esse Son Sepelliti*. Ferrara: Eredi Vittorio Baldini.

HAMMOND C., EVENNETT P. J. 2005. *MICROSCOPY TECHNIQUES | Light Microscopy*. In "Encyclopedia of Analytical Science (Second Edition)", edited by Paul Worsfold, Alan Townshend, and Colin Poole, 100–106. Oxford: Elsevier. https://doi.org/10.1016/B0-12-369397-7/00378-2.

HATTON, G.D. 2005. *The Technology of Egyptian Blue*. Doctoral dissertation, Oxford, UK.: University of Oxford.

HOLIK, A. S. 2001. *Optical Microscopy*. In "Encyclopedia of Materials: Science and Technology", edited by K. H. Jürgen Buschow, Robert W. Cahn, Merton C. Flemings, Bernhard Ilschner, Edward J. Kramer, Subhash Mahajan, and Patrick Veyssière, 6458–63. Oxford: Elsevier. https://doi.org/10.1016/B0-08-043152-6/01142-6.

INGO G.M., ÇILINGIROĞLU A., DI CARLO G., BATMAZ A., DE CARO T., RICCUCCI C., PARISI E. I., FARALDI F. 2013. *Egyptian Blue Cakes from the Ayanis Fortress (Eastern Anatolia, Turkey): Micro-Chemical and-Structural Investigations for the Identification of Manufacturing Process and Provenance*. "Journal of Archaeological Science" 40 (12): 4283–90.

CROWE J.A., CAVALCASELLE G.B. 1871. *A History of Painting in North Italy*. Londra 1912. Londra: Borenius.

J.D. PASSAVAN. 1882. *Raffaello d'Urbino e Il Padre Suo, Giovanni Santi*. Le Monnier. Firenze.

XI J., HIGUCHI T., JINNAI H. 2019. *Scanning Electron Microscopy.* In "Molecular Soft-Interface Science: Principles, Molecular Design, Characterization and Application″, edited by Mizuo Maeda, Atsushi Takahara, Hiromi Kitano, Tetsuji Yamaoka, and Yoshiko Miura, 141–46. Tokyo: Springer Japan. https://doi.org/10.1007/978-4-431-56877-3_9.

RIEDERER J. 1997. *Egyptian Blue*. In "Artists' Pigments. A Handbook of Their History and Characteristics", 3:23–40. Elisabeth West FitzHugh.

KAISER, J. W. 1881. *Beschrijving Der Schilderijen van Het Rijksmuseum Te Amsterdam.* Algemeene Landsdrukkerij.

TRINDER K. 2018. *An Atlas of Rare & Familiar Colour: The Harvard Art Museums' Forbes Pigment Collection*. Atelier Éditions.

KOVALEV I., RODLER A. S., BRØNS C., REHREN TH. 2023. *Making and Working Egyptian Blue–a Review of the Archaeological Evidence*. "Journal of Archaeological Science" 153:105772.

LE BRUN P. 1849. *Recueil Des Essaies Des Merveilles de La Peinture 1635*. In "Original Treatises: Dating from the XIIth to XVIIIth Centuries on the Arts of Painting, in Oil, Miniature, Mosaic, and on Glass; of Gilding, Dyeing, and the Preparation of Colours and Artificial Gems; Preceded by a General Introduction; with Translations, Prefaces, and Notes", by Mary Philadelphia Merrifield. J. Murray.

MERRIFIELD M.P. 1849. *Original Treatises: Dating from the XIIth to XVIIIth Centuries on the Arts of Painting, in Oil, Miniature, Mosaic, and on Glass; of Gilding, Dyeing, and the Preparation of Colours and Artificial Gems; Preceded by a General Introduction; with Translations, Prefaces, and Notes*. 2 vols. J. Murray.

MAZZOCCHIN G.A., RUDELLO D., BRAGATO C., AGNOLI F. 2004. *A Short Note on Egyptian Blue*. "Journal of Cultural Heritage" 5 (1): 129–33.

MEZZETTI A., LEIBL W. 2017. *Time-Resolved Infrared Spectroscopy in the Study of Photosynthetic Systems*. "Photosynthesis Research″ 131 (February). https://doi.org/10.1007/s11120-016-0305-3.

MORELLI G. (IVAN LERMOLIEFF) 1897. *Della Pittura Italiana. Studii Storico Critici. Le Gallerie Borghese e Doria-Pamphili in Roma*. Milano: Fratelli Treves.

NICOLA M., GOBETTO R., BAZZACCO A., ANSELMI C., FERRARIS E., RUSSO A., MASIC A., SGAMELLOTTI A. 2024. *Real-Time Identification and Visualization of Egyptian Blue Using Modified Night Vision Goggles*. "Rendiconti Lincei. Scienze Fisiche e Naturali" 35 (2): 495–512. https://doi.org/10.1007/s12210-024-01245-w.

NICOLA M., GOBETTO R., MASIC A. 2023. *Egyptian Blue, Chinese Blue, and Related Two-Dimensional Silicates: From Antiquity to Future Technologies. Part A: General Properties and Historical Uses*. "Rendiconti Lincei. Scienze Fisiche e Naturali" 34 (2): 369–413. https://doi.org/10.1007/s12210-023-01153-5.

NICOLA M., SEYMOUR L.M., ACETO M., PRIOLA E., GOBETTO R., MASIC A. 2019. *Late Production of Egyptian Blue: Synthesis from Brass and Its Characteristics*. "Archaeological and Anthropological Sciences" 11 (10): 5377–92. https://doi.org/10.1007/s12520-019-00873-w.

ORNA M.V., LOW M. J. D., BAER N. S. 1980. *Synthetic Blue Pigments: Ninth to Sixteenth Centuries. I. Literature*. "Studies in Conservation" 25 (2): 53–63. https://doi.org/10.2307/1505860.

PABST A. 1959. *Structures of Some Tetragonal Sheet Silicates*. "Acta Crystallographica" 12 (10): 733–39. https://doi.org/10.1107/S0365110X5900216X.

PAGÈS-CAMAGNA S., COLINART S. 2003. *The Egyptian Green Pigment: Its Manufacturing Process and Links to Egyptian Blue*. "Archaeometry" 45 (4): 637–58.

PANAGIOTAKI M., TITE M., MANIATIS Y. 2008. *Egyptian Blue in Egypt and beyond: The Aegean and the Near East*. In "Proceedings of the Tenth International Congress of Egyptologists", University of the Aegean, Rhodes, 2:1769–89.

PANDEY D. K., KAGDADA H. L., SANCHORA P., SINGH D. K. 2021. *Overview of Raman Spectroscopy: Fundamental to Applications.* In "Modern Techniques of Spectroscopy: Basics, Instrumentation, and Applications", edited by Dheeraj Kumar Singh, Manik Pradhan, and Arnulf Materny, 145–84. Singapore: Springer. https://doi.org/10.1007/978-981-33-6084-6_6.

HATTON G.D., TITE M. S., SHORTLAND A. J. *Production of Egyptian Blue and Green Frits*. 2008. In "Production Technology of Faience and Related Early Vitreous Materials" 147–85. Oxford University School of Archaeology.

RAGAI J. 1986. *Colour: Its Significance and Production in Ancient Egypt*. "Endeavour" 10 (2): 74–79.

GETTENS R. J., STOUT G.L. 1966. *Egyptian Blue*. In "Painting Materials. A Short Encyclopedia", 112–13. New York: Dover Publications, Inc.

SGAMELLOTTI A., ANSELMI C. 2022. *An Evergreen Blue. Spectroscopic Properties of Egyptian Blue from Pyramids to Raphael, and Beyond*. "Inorganica Chimica Acta" 530 (January):120699. https://doi.org/10.1016/j.ica.2021.120699.

SGARZINI G. 2006. *Raphael*. ATS Italia Editrice.

SHORTLAND, A. J. 2006. A*pplication of lead isotope analysis to a wide range of late bronze age egyptian materials*. "Archaeometry″ 48 (4): 657–69. https://doi.org/10.1111/j.1475-4754.2006.00279.x.

SPRING M., BILLINGE R., VERRI G. 2019. *A Note on an Occurrence of Egyptian Blue in Garofalo's "The Holy Family with Saints Elizabeth, Zacharias, John the Baptist (and Francis?)"*. National Gallery Technical Bulletin 40:74–85.

SUPERBI A. 1620. *Apparato de Gli Huomini Illustri Della Città Di Ferrara, i Quali Nelle Lettere, & in Altre Nobili Virtù Fiorirono*. Ferrara: Francesco Suzzi.

KUSTODIEVA T., LUCCO M. eds. 2008. *Garofalo: Pittore Della Ferrara Estense*. Skira.

THAVAPALAN S., STENGER J., SNOW C. 2016. *Color and Meaning in Ancient Mesopotamia: The Case of Egyptian Blue*. "Zeitschrift Für Assyriologie Und Vorderasiatische Archäologie" 106 (2): 198–214. https://doi.org/10.1515/za-2016-0014.

ULLRICH D. 1987. *Egyptian Blue and Green Frit: Characterization, History and Occurrence, Synthesis.* Edited by François Delamanre, Tony Hackens, and Bruno Helly. "Pact: Journal of European Study Group on Physical, Chemical, Biological and Mathematical Techniques Applied to Archaeology" 17 (II.3.1): 323–32.

VERRI G. 2009. *The Spatially Resolved Characterisation of Egyptian Blue, Han Blue and Han Purple by Photo-Induced Luminescence Digital Imaging.* "Analytical and Bioanalytical Chemistry" 394 (4): 1011–21.

WIEDEMANN H.G., BAYER G. 1997. *Formation and Stability of Chinese Barium Copper-Silicate Pigments*. In "Conservation of Ancient Sites on the Silk Road: Proceedings of an International Conference on the Conservation of Grotto Sites" The Getty Conservation Institute, 379–87. Los Angeles: Neville Agnew.

Sitography

https://www.pinacotecabologna.beniculturali.it/it/content_page/item/291-estasi-di-santa-cecilia-fra-i-santi-paolo-giovanni-evangelista-agostino-e-maria-maddalena

https://theframeblog.com/2015/08/

https://vcg.isti.cnr.it/farnesina/loggia/

https://closer.colasantiaste.com/2016/09/05/in-dettaglio-villa-farnesina-iconografia-botanica-della-loggia-di-amore-e-psiche/

https://www.cultweek.com/morbelli/

https://artinvestment.ru/en/news/auctnews/20200721_shishkin.html

Databases of minerals and pigments

https://rruff.info/

https://www.chem.ucl.ac.uk/resources/raman/

https://chsopensource.org/pigments-checker/

https://chsopensource.org/raman-1064-nm/

https://lithotheque.ens-lyon.fr/Raman/raman.php

https://spectra.chem.ut.ee/

Softwares

F. Menges "Spectragryph - optical spectroscopy software", Version 1.2.15, 2024

Oxford EDS AZtec

Appendices

Appendix A

Paintings

Ortolano, *Saint Margaret*, 1524. Oil on poplar panel, Statens Museum for Kunst, Copenhagen, Denmark

Raphael, *The Ecstasy of Saint Cecilia*, 1514-1517, oil transferred from panel to canvas, Pinacoteca Nazionale, Bologna, Italy

Giovanni Paolo Pannini, *Interior of a picture gallery with the collection of Cardinal Silvio Valenti Gonzaga*, 1749, oil on canvas, The Ella Gallup Sumner & Mary Catlin Sumner Collection Fund, Wadsworth Atheneum, Hartford, Connecticut, USA

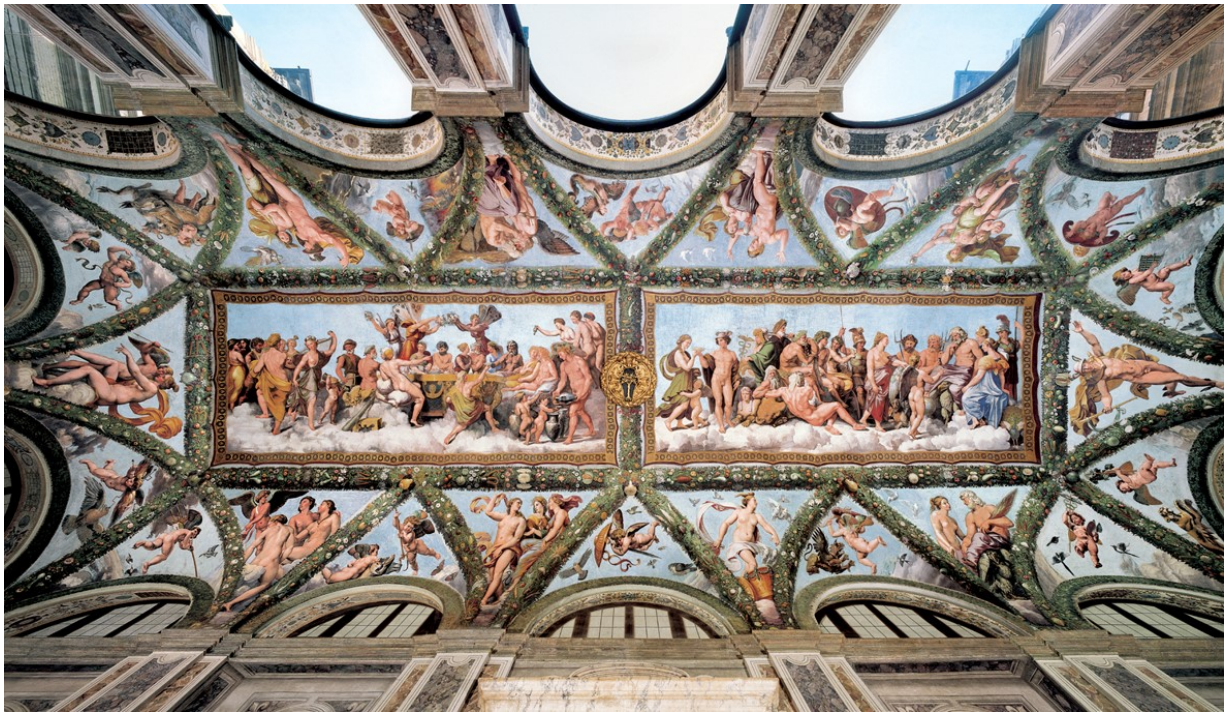

Raphael and his workshop, *The Loggia of Cupid and Psyche,* 1518, fresco, Loggia of Cupid and Psyche in Villa Farnesina, Rome, Italy

Raphael, *The triumph of Galatea*, 1512, fresco, The Loggia of Galatea in Villa Farnesina, Rome, Italy

Garofalo, *Adoration of the Magi*, 1530s, oil on panel, Rijksmuseum, Amsterdam, Netherlands

Garofalo, *Resurrection of Lazarus*, 1532, oil on panel, Pinacoteca Nazionale, Ferrara, Italy

Garofalo, *Identification of the True Cross*, 1536, oil on panel, Pinacoteca Nazionale, Ferrara, Italy

Garofalo, *Madonna of the veil*, 1500 / 1550, oil on wood, Louvre, Paris, France

Garofalo, *The Holy Family with Saints Elizabeth, Zacharias, John the Baptist (and Francis?)*,1520-35, oil on canvas, transferred from panel, The National Gallery, London, United Kingdom

Raffaello and workshop, *Holy Family of Francis I*, 1518, oil on canvas transferred from wood, Louvre, Paris, France

Garofalo*, The Virgin Mary venerating the Christ Child with angels presenting the instruments of the Passion,* 1517, oil on canvas transferred from wood, Gemäldegalerie Alte Meister, Dresden, Germany

Garofalo, *Slaughter of the innocents*, 1519, oil on panel, Pinacoteca Nazionale, Ferrara, Italy

Garofalo, *Holy Family with Saints John and Elizabeth*, 1524, oil on canvas, Musei Civici, Padova, Italy

Garofalo, *A Pagan Sacrifice,* 1526, oil on canvas, The National Gallery, London, United Kingdom

Angelo Morbelli, *Happy dawn*, 1892-1893, Oil on canvas, private collection, Milan, Italy.

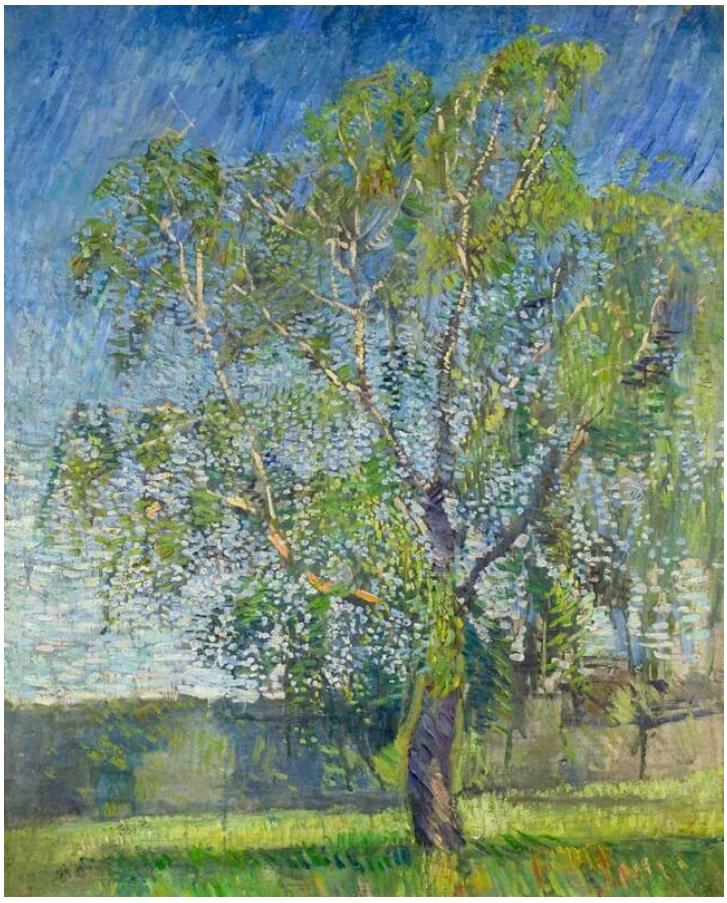

Robert Falk. *Birch. Spring.* 1907. Oil on canvas. private collection.

Appendix B

EB historical occurrences

Occurrences of Egyptian blue in works made from the 5th century A.D.

Period	Location	Work/Monument
432-440 CE	Rome, S. Sabina, counter-façade	fields on bedding mortar of the mosaic
5th cent.	Rome, S. Sabina, esonarthex	wall paintings: fake opus sectile
5th-6th cent.	Rome, S. Maria Antiqua, choir	wall paintings
5th-6th cent.	Quarazze/Gratsch (Merano), S. Pietro	wall paintings
late 5th-early 6th cent.	Vouneuil-sous-Biard (Vienne), priory	painted stucco
5th-7th cent.	Ravenna, S. Agata Maggiore	fields on bedding mortar of the mosaic
5th-7th cent.	Ravenna, S. Croce	fields on bedding mortar of the mosaic
early 6th cent.	Vicenza, Basilica of SS. Felice e Fortunato, chapel	wall paintings
6th cent.	Negev Desert (Israel), Byzantine church in Shivta	wall paintings: Transfiguration
6th cent.	Kilisebükü (Turkey), Baptistery	wall paintings
6th cent.	Rome, S. Maria Antiqua, palimpsest wall and presbytery	wall paintings: palimpsest wall Beautiful Angel, right wall of the presbytery panel with St. Anne
6th-7th cent.	Tavşan Adası (Turkey), south nave	wall paintings: II phase
6th-7th cent.	Rome, S. Maria Antiqua, presbytery	wall paintings: right wall of the presbytery Christological cycle II phase
second half of 7th cent.	old Dongola (Sudan) Cruciform Building	wall paintings
7th-9th cent.	Canterbury, St Augustine	Anglo-Saxon era capital
705-707 CE	Rome, S. Maria Antiqua, triumphal arch	wall paintings: Adoration of the Cross
first half of 8th cent.	Rome, S. Saba	wall paintings: Healing of the paralytic, St. Peter saved from the waters
late 8th cent.	Rome, S. Susanna	wall paintings: Agnus Dei, Madonna enthroned with Child, two saints and five saints
late 8th-early 9th cent.	Rome, S. Sabina	window stucco transennae
8th-9th cent.	Barete (AQ), S. Paolo	limestone transenna
around 800 CE	Mals/Malles, S. Benedetto	wall paintings
8th-9th cent.	S. Vincenzo al Volturno, assembly hall (or prophets)	wall paintings
817-842 CE	S. Vincenzo al Volturno, refectory of esteemed guests	painted decorations
9th cent.	S. Vincenzo al Volturno, crypt of Joshua	wall paintings
mid-9th cent.	Rome, S. Maria Antiqua, atrium	wall paintings
843-1204 CE	Hierapolis (Turkey), S. Filippo	wall paintings

847-855 CE	Rome, S. Clemente, lower basilica	wall paintings: Ascension
around 850 CE	Auxerre, Saint-Germain, crypt, oratory of S. Stefano	fake Carolingian era capital
9th cent.	Müstair (Canton of Grisons, Switzerland), chapel of the Holy Cross	wall paintings
9th-10th cent.	Müstair (Canton of Grisons, Switzerland), church of S. Giovanni	wall paintings
9th-10th cent.	Castelseprio, S. Maria foris portas	wall paintings
9th-11th cent.	Saranda (Albania), basilica of the Forty Martyrs	wall paintings
10th cent.	San Vittore (Canton of Grisons, Switzerland), Carolingian rotunda of S. Lucio	wall paintings
10th-11th cent.	Fossacaprara (Cremona), parish church	wall paintings
11th cent.	Terrassa (Spain), Sant Pere	stone altar
first half of 11th cent.	Faras (Sudan), cathedral (Warsaw, National Museum)	detached wall paintings
1078-1084 CE	Rome, S. Clemente, central nave of the lower basilica	wall paintings: Mass of St. Clement, Legend of St. Alexius
1151-1166 CE	St Albans (Hertfordshire)	stuccos of the chapter house
late 12th cent.	Vatican Museums (from the oratory of S. Gregory Nazianzen)	Nicolò and Giovanni, Last Judgment, tempera on wood
1276-1277 CE	Treviso, Loggia dei Cavalieri	fresco decoration
late 13th cent.	Genoa, Cathedral, central portal lunette	polychrome stone reliefs
14th cent.	Auxerre, Saint-Germain, crypt, oratory of S. Stefano	'entrelacs peint'
1512 CE	Rome, Villa Farnesina	Raphael, Triumph of Galatea,
1518 CE	Rome, Villa Farnesina	Raphael, Loggia of Cupid and Psyche
1524 CE	Copenhagen, Staatens Museum	Ortolano, Santa Margherita
1520-1535 CE	London, National Gallery	Garofalo (attr.), Holy Family and saints
1530-1540 CE	Amsterdam, Rijksmuseum	Garofalo, Adoration of the Magi
16th cent.	Bologna	wall paintings
first half of 17th cent.	Private collection	Alessandro Algardi (studio), Magdalene, papier-mâché
first half of 17th cent.	Vatican City, Governor's Chapel	Alessandro Algardi, Crucifix in polychrome raw clay

Table 7 – Table modified after (SIDOTI G. ET AL. 2018), see also (NICOLA M. ET AL. 2023).

Occurrences of Egyptian blue in manuscripts

Period	Library / Code / Place of production
550-600 CE	Vienna, Nationalbibliothek / MS. theol. gr. 31 (Vienna Genesis) / Syria (Antioch)
around 600 CE	Paris, Bibliothèque Nationale de France / MS. NAL 2334 (Ashburnham Pentateuch) / Spain (or North Africa, Syria or Italy)
781-783 CE	Paris, Bibliothèque Nationale de France / MS. lat.1203 (Godescalc Evangelistary) / Germany (Aachen)
around 810 CE	Cambridge, Trinity College / MS. B.16.3 (Rabano Mauro) / Germany (Fulda) or England
10th cent.	Paris, Bibliothèque Nationale de France / MS. lat. 987 (Pontifical) / England (Winchester)
10th cent.	Orléans, Médiathèque / MS. 127 (Winchcombe Sacramentary) / England (Ramsey?)
10th cent.	Cambridge, Trinity College / MS. B.10.4 / England (Peterborough?)
around 925-950 CE	Cambridge, Trinity College / MS. B.11.2 / Scriptorium of Canterbury
around 1000 CE	Cambridge, Corpus Christi College / MS. 411 / Scriptorium of Canterbury?
around 1100 CE	Durham Cathedral Library / MS. B.II.16 / Scriptorium of Canterbury
around 1100 CE	Cambridge, Trinity College / MS. B.3.9 / Scriptorium of Canterbury

Table 8 – Table modified after (SIDOTI G. ET AL. 2018), see also (NICOLA M. ET AL. 2023).

Appendix C

SEM data

Raphael

	SiO_2	CaO	CuO		SiO_2	CaO	CuO	
Spectrum 87	65.7	15.2	19.1					
Spectrum 88	65.6	15.2	19.1	**AVERAGE**	65.6	15.2	19.2	**Raph 1**
Spectrum 89	65.4	15.3	19.3					
Spectrum 90	66.1	15.4	18.5					
Spectrum 91	65.7	15.5	18.7	**AVERAGE**	65.9	15.4	18.6	**Raph 2**
Spectrum 92	65.9	15.4	18.7					
Spectrum 93	66.6	15.1	18.2					
Spectrum 94	66.1	15.4	18.4	**AVERAGE**	66.1	15.4	18.5	**Raph 3**
Spectrum 95	65.5	15.5	19.0					
Spectrum 96	66.6	15.2	18.2		66.6	15.2	18.2	**Raph 4**
Spectrum 97	66.7	15.2	18.1					
Spectrum 98	67.1	15.1	17.8	**AVERAGE**	66.8	15.2	18.0	**Raph 5**
Spectrum 99	66.5	15.3	18.1					

Table 8 – SEM-EDS data of cuprorivaite in Raphael sample.

Ortolano

	SiO2	CaO	CuO		SiO2	CaO	CuO	
Spectrum 51	71.1	13.8	15.0	**AVERAGE**	71.0	13.8	15.3	**Orto 4**
Spectrum 52	70.8	13.7	15.5					
Spectrum 72	68.0	14.6	17.3					
Spectrum 73	68.2	14.6	17.2	**AVERAGE**	68.0	14.6	17.4	**Orto 1**
Spectrum 74	67.6	14.6	17.7					
Spectrum 75	66.6	15.1	18.3					
Spectrum 76	62.7	16.4	21.0	**AVERAGE**	65.3	15.4	19.2	**Orto 2**
Spectrum 77	66.8	14.9	18.4					
Spectrum 79	68.3	14.6	17.1	**AVERAGE**	68.0	14.6	17.4	**Orto 3**
Spectrum 80	67.6	14.6	17.8					
Spectrum 81	70.0	13.2	16.8					
Spectrum 82	70.9	13.4	15.7	**AVERAGE**	70.5	13.3	16.2	**Orto 5**
Spectrum 83	70.8	13.3	15.9					

Table 9 – SEM-EDS data of cuprorivaite in Ortolano sample.

Ostia

	SiO_2	CaO	CuO	
Spectrum 21	66.1	14.1	19.8	Ost 1
Spectrum 22	67.0	14.7	18.3	Ost 2
Spectrum 23	66.5	13.7	19.8	Ost 3
Spectrum 39	68.3	14.0	17.7	Ost 4
Spectrum 40	68.7	13.9	17.4	Ost 5
Spectrum 42	74.4	9.7	15.9	Ost 6
Spectrum 49	66.0	14.0	20.0	Ost 7
Spectrum 50	64.8	14.9	20.3	Ost 8
Spectrum 52	65.0	14.8	20.3	Ost 9
Spectrum 54	65.8	14.5	19.7	Ost 10
Spectrum 55	64.6	13.4	22.0	Ost 11
Spectrum 58	65.5	14.6	19.9	Ost 12

Table 10 - SEM-EDS data of cuprorivaite in Ostia sample.

Liternum

	SiO_2	CaO	CuO		SiO_2	CaO	CuO	
Spectrum 8	69.7	13.7	16.6	AVERAGE	69.0	13.8	17.2	Lit 1
Spectrum 11	68.3	14.0	17.7					
Spectrum 19	69.9	13.7	16.5	AVERAGE	69.2	13.8	17.0	Lit 2
Spectrum 25	68.9	13.8	17.2					
Spectrum 26	68.7	13.9	17.4					
Spectrum 20	72.3	12.2	15.5	AVERAGE	70.5	13.0	16.4	Lit 3
Spectrum 21	69.4	13.4	17.2					
Spectrum 22	69.9	13.5	16.7					
Spectrum 23	67.1	14.2	18.7	AVERAGE	71.9	12.4	15.7	Lit 4
Spectrum 24	76.7	10.6	12.6					
Spectrum 27	67.4	14.4	18.2	AVERAGE	68.1	14.3	17.6	Lit 5
Spectrum 28	68.2	14.4	17.4					
Spectrum 29	68.7	14.2	17.2					
Spectrum 37	67.9	13.8	18.3		67.9	13.8	18.3	Lit 6
Spectrum 39	67.9	14.1	17.9		67.9	14.1	17.9	Lit 7
Spectrum 42	69.3	13.7	17.0		69.3	13.7	17.0	Lit 8
Spectrum 43	68.1	14.0	17.9		68.1	14.0	17.9	Lit 9
Spectrum 44	68.7	13.7	17.7		68.7	13.7	17.7	Lit 10

Table 11 - SEM-EDS data of cuprorivaite in Liternum sample.

SEM EDS data for PCA

Sample №	Object	Site	Region	Age	Period	Source	SiO_2	CaO	CuO	Na_2O	K_2O	MgO	Al_2O_3	FeO	SnO_2	PbO	TiO_2
Garofalo	pgm pnt	Ferrara	Italy	Renaissance	16 CE	De Vivo et al.2019	64.23	15.93	19.83	0.00	0.00	0.00	0.00	0.00	0.00	0.00	0.00
23178	ck	Kamak	Egypt	LBA	16-11 BCE	Hatton 2005	68.30	13.90	11.80	1.40	1.10	0.90	1.20	0.90	0.30	0.10	0.10
23183	ck	Thebes	Egypt	LBA	16-11 BCE	Hatton 2005	65.30	15.20	12.90	2.90	0.50	0.80	0.60	0.30	1.10	0.30	0.00
23185	ck	Thebes	Egypt	LBA	16-11 BCE	Hatton 2005	66.10	14.60	13.80	2.10	0.50	0.70	0.60	0.30	0.90	0.20	0.00
23187	ck	Thebes	Egypt	LBA	16-11 BCE	Hatton 2005	67.10	11.90	14.80	4.60	0.30	0.40	0.10	0.20	0.20	0.20	0.00
HH65	ck	Tell Brak	Levant	LBA	15 BCE	Hatton 2005	77.10	7.50	10.60	1.20	0.40	1.10	0.90	0.60	0.50	0.10	0.10
TR4747A	ck	Tell Rimah	Levant	LBA	15 BCE	Hatton 2005	70.00	8.60	15.00	1.40	0.30	2.50	0.80	0.70	0.20	0.30	0.10
24684	ck	Amama	Egypt	LBA	14 BCE	Hatton 2005	65.60	12.00	15.70	3.70	0.50	0.50	0.40	0.40	0.10	0.10	0.00
25153a	ck	Amama	Egypt	LBA	14 BCE	Hatton 2005	64.70	11.60	18.20	1.70	0.20	0.70	1.20	0.50	1.10	0.10	0.10
ZURM1S311	ck	Zawiyet	Egypt	LBA	13 BCE	Hatton 2005	78.40	8.20	6.70	2.30	0.10	2.40	0.80	0.70	0.40	0.20	0.00
ZURM1S415	ck	Zawiyet	Egypt	LBA	13 BCE	Hatton 2005	71.90	10.20	8.80	3.80	0.00	3.20	1.30	0.50	0.50	0.10	0.00
Columns	ck	Mycenae	Greece	LBA	13 BCE	Hatton 2005	74.50	9.00	13.10	1.40	0.00	0.60	0.10	0.30	0.60	0.20	0.00
Citadel	ck	Mycenae	Greece	LBA	13 BCE	Hatton 2005	74.30	8.90	11.70	1.90	0.40	0.60	1.00	0.50	0.40	0.00	0.10
Sample 7	ck	Mycenae	Greece	LBA	13 BCE	Hatton 2005	73.20	8.90	13.60	1.40	0.20	1.30	0.20	0.40	0.50	0.20	0.10
Artisan	ck	Mycenae	Greece	LBA	13 BCE	Hatton 2005	66.80	11.00	13.50	2.30	0.60	1.20	1.60	1.10	1.10	0.10	0.10
13712	ck	Nineveh	Mesop.	Iron Age	8 BCE	Hatton 2005	69.40	11.80	15.90	1.20	0.50	0.50	0.10	0.20	0.20	0.20	0.10
14123	ck	Nimrud	Mesop.	Iron Age	8 BCE	Hatton 2005	79.20	6.30	5.70	0.50	0.20	0.20	2.80	0.00	0.00	0.00	0.00
Mem16	ck	Memphis	Egypt	He/Rom	3 BCE-3 CE	Hatton 2005	71.80	9.40	8.50	2.30	0.20	0.50	0.50	2.50	1.20	2.90	0.20
UC47305b	ck	Memphis	Egypt	He/Rom	3 BCE-3 CE	Hatton 2005	68.90	9.20	9.80	3.70	0.10	0.10	2.00	3.00	0.00	3.30	0.00
UC47310	ck	Memphis	Egypt	He/Rom	3 BCE-3 CE	Hatton 2005	58.40	13.70	10.70	3.60	0.30	0.50	0.80	2.50	3.10	6.00	0.20
UC47311	ck	Memphis	Egypt	He/Rom	3 BCE-3 CE	Hatton 2005	62.10	13.80	10.20	2.70	0.30	0.50	0.90	2.90	0.70	5.60	0.20
EB1	ck	Delos	Aegean	He/Rom	2 BCE	Hatton 2005	68.70	9.40	15.10	1.30	0.00	0.60	0.40	1.50	0.50	2.40	0.10
EB2	ck	Delos	Aegean	He/Rom	2 BCE	Hatton 2005	68.00	8.70	11.60	2.00	0.10	0.70	0.30	3.20	0.90	4.40	0.10
EB3	ck	Delos	Aegean	He/Rom	2 BCE	Hatton 2005	67.80	10.40	11.20	1.60	0.10	0.50	0.20	2.40	1.80	3.70	0.20
EB4	ck	Delos	Aegean	He/Rom	2 BCE	Hatton 2005	76.90	7.60	8.50	1.50	0.10	0.50	0.40	1.40	0.60	2.50	0.10
14121	ck	Malta	Malta	He/Rom	2 BCE	Hatton 2005	76.70	7.40	11.80	3.30	0.10	0.10	0.60	0.50	0.00	0.00	0.10
13982	ck	Hertford	Britain	He/Rom	Roman	Hatton 2005	61.70	17.40	16.70	2.00	0.10	1.10	0.40	0.40	0.10	0.10	0.00
2708	ck	Colchester	Britain	He/Rom	1 CE	Hatton 2005	73.50	8.40	11.90	2.50	0.50	0.50	0.90	0.40	0.40	0.10	0.10
ZURG7EZ	ck	Zawiyet	Egypt	LBA	13 BCE	Hatton2005; Shortland2006	68.10	11.50	13.70	1.80	0.30	1.20	1.10	1.40	0.00	0.40	0.10
ZURM124	ck	Zawiyet	Egypt	LBA	13 BCE	Hatton2005; Shortland2006	72.10	12.50	6.20	2.90	0.10	4.70	0.40	0.50	0.60	0.20	0.10
ZURM1S32	ck	Zawiyet	Egypt	LBA	13 BCE	Hatton2005; Shortland2006	78.20	8.70	4.40	2.40	0.10	4.80	0.60	0.30	0.40	0.10	0.10
ZURM1S411	ck	Zawiyet	Egypt	LBA	13 BCE	Hatton2005; Shortland2006	64.50	12.20	10.80	3.70	0.10	6.30	1.00	0.40	0.90	0.00	0.00
Ayanis 1	ck	Ayanis	Anatolia	Iron Age	7 BCE	Ingo et al. 2013	68.25	10.56	18.14	1.07	0.16	0.23	0.39	0.50		0.00	
Ayanis 2	ck	Ayanis	Anatolia	Iron Age	7 BCE	Ingo et al. 2013	72.64	9.72	15.23	1.16	0.00	0.00	0.43	0.50		0.00	
Ayanis 3	ck	Ayanis	Anatolia	Iron Age	7 BCE	Ingo et al. 2013	70.35	10.76	16.23	0.56	0.22	0.31	0.41	0.63		0.15	
Ayanis 4	ck	Ayanis	Anatolia	Iron Age	7 BCE	Ingo et al. 2013	72.43	9.19	15.43	0.45	0.42	0.40	0.35	0.39		0.00	
Ayanis 5	ck	Ayanis	Anatolia	Iron Age	7 BCE	Ingo et al. 2013	70.72	9.33	16.06	1.22	0.36	0.42	0.42	0.56		0.00	0.00
Liternum	raw	Liternum	Italy	He/Rom	1 CE	Our analysis	64.85	13.13	16.52	0.00	0.21	0.12	0.39	0.25	0.00	0.00	0.00
Ostia	raw	Ostia	Italy	He/Rom	1 BCE-1 CE	Our analysis	63.79	13.72	18.86	0.00	0.00	0.06	0.42	0.20	0.12	0.06	0.00
Raphael	pgm frs	Rome	Italy	Renaissance	16 CE	Our analysis	62.43	14.44	17.53	0.00	0.00	0.00	0.00	0.00	0.00	0.13	0.00
Ortolano	pgm pnt	Ferrara	Italy	Renaissance	16 CE	Our analysis	62.37	13.92	16.92	0.32	0.53	0.32	1.56	0.14	0.00	0.44	0.00
P5	ck	Deir el-Medineh	Egypt	LBA	16-11 BCE	Pages, Colinart 2003	69.10	9.20	15.40	3.86	0.49	0.00	0.61	0.18	0.00		
P7	ck	Deir el-Medineh	Egypt	LBA	16-11 BCE	Pages, Colinart 2003	63.90	14.10	17.90	2.87	0.00	0.00	0.70	0.00	0.00		
P10	ck	Deir el-Medineh	Egypt	LBA	16-11 BCE	Pages, Colinart 2003	74.20	7.55	12.50	2.84	0.50	0.20	0.00	1.17	0.00		
P11	ck	Deir el-Medineh	Egypt	LBA	16-11 BCE	Pages, Colinart 2003	64.20	16.92	11.73	3.93	0.31	1.46	0.00	0.41	0.97		
P12	ck	Deir el-Medineh	Egypt	LBA	16-11 BCE	Pages, Colinart 2003	58.73	13.42	19.84	3.90	0.40	0.89	0.00	0.77	0.78		
P6	ck	Deir el-Medineh	Egypt	LBA	16-11 BCE	Page, Colinart 2003	56.18	19.25	17.23	3.02	0.48	0.61	0.55	0.53	1.95		
Mesara 1	ing	Mesara	Aegean	LBA	18-14 BCE	Panagiotaki et al. 2008	69.20	11.70	15.20	1.20	0.10	1.10	0.60	0.50	0.30		
Mesara 2	ing	Mesara	Aegean	LBA	18-14 BCE	Panagiotaki et al. 2008	74.00	8.50	12.10	1.90	0.10	1.30	1.00	0.90	0.30		
Ag Triada 2	ing	Ag Triada	Aegean	LBA	18-14 BCE	Panagiotaki et al. 2008	66.80	15.50	13.70	1.90	0.30	1.00	0.30	0.60	0.00		
Tel Sera	ing	Tel Sera	Levant	LBA	12 BCE	Panagiotaki et al. 2008	69.40	12.10	12.30	1.00	0.70	1.00	1.30	0.70	1.40		